

Novel Gold Nanoparticles for Dipeptide Recognition in Water

dem Fachbereich Chemie der Universität Kaiserslautern
zur Erlangung des akademischen Grades "Doktor der Naturwissenschaften"
eingereichte Dissertation

D 386



Datum der wissenschaftlichen Aussprache: 13.09.2016

vorgelegt von

Serap Yapar

Betreuer: Prof. Dr. Stefan Kubik

Kaiserslautern 2016

Die vorliegende Arbeit wurde unter der Leitung von Prof. Dr. Stefan Kubik im Zeitraum von September 2011 bis September 2015 im Fachbereich Chemie der Technischen Universität Kaiserslautern angefertigt.

Betreuer: Prof. Dr. S. Kubik

Prüfungskommission

Vorsitzender: Prof. Dr. Werner Thiel

1. Gutachter: Prof. Dr. Stefan Kubik

2. Gutachter: Jr. Prof. Dr. Frederic Patureau

Hiermit versichere ich, dass ich die vorliegende Arbeit selbstständig verfasst und keine anderen als die angegebenen Quellen und Hilfsmittel verwendet, sowie Literaturzitate kenntlich gemacht wurden.

Ich erkläre außerdem, dass diese Dissertation weder in gleicher, noch in anderer Form bereits in einem anderen Prüfungsverfahren vorlag.

Kaiserslautern, den 02.09.2016

Serap Yapar

Teile dieser Arbeit wurden bereits veröffentlicht:

S. Yapar, M. Oikonomou, A. H. Velders and S. Kubik,

"Dipeptide recognition in water mediated by mixed monolayer protected gold nanoparticles",
Chem. Commun., **2015**, 51, 14247-14250.

Acknowledgments

First and foremost, I would like to express my gratitude to Prof. Dr. Stefan Kubik for giving me the chance to join his research group, and for his continuous support during this Ph.D. process. I very much enjoyed being a part of the welcoming working environment and was able to learn a lot about chemistry. Lastly, thank you for our enlightening discussions about my project and for always motivating me to perform at my best.

Secondly, I want to thank Prof. Dr. Werner Thiel and Prof. Dr. Frederic Patureau for their kind help with the revision of my thesis.

I would also like to thank the people who made lab work and coffee breaks more enjoyable. My first lab mates Laura, Michael, Astrid, Alexander, Fabian, Arnold, Luzian and Christian who made me feel welcome in Kaiserslautern and Disha, Michaela, Steffi, Ligia, Julia, Steffen and Björn for making this place a home.

I also want to mention my professors and friends from DYNAMOL network. Maria, Rui, Piotr, Laura and the others, you made my experience as an ESR fun and informative. I believe that I made friends for life in this network.

Furthermore, I am expressing my deep gratitude to Prof. Dr. Aldrik Velders from WUR, who was always helpful and friendly during my visits to Wageningen, and I always felt like a part of his group. I cannot thank Maria enough for our long DOSY-NMR measurements and of course for her friendship. I enjoyed the discussions and dinners with Rui and Jeroen after long work days. I also should not forget Jan Bart, who measured TEM for me and was fun to chat to during the 'group meetings'.

I would like to extend my thanks to Dr. Herald Kelm and Dr. Christiana Müller for the NMR measurements. I am also thankful to Prof. Dr. Sandro Keller and Abraham Olusegun Oluwole, who helped me to perform DLS measurements.

I also want to acknowledge the kind members of our Chemistry Department; Susanna Zeigner, Ludwig Napast, Jürgen Rahm and Frank Schröer for being always helpful and cheerful.

I also want to mention my friends in Kaiserslautern, Martina, Luis, Jenny, and Mayur for the fun we had together at Salsa parties and the delicious food we shared.

Not to forget, my first Turkish friend in Germany, Ezgi. I always appreciate your friendship. I am sure we will share more adventures and celebrate more successes together in the future.

My long time friend Tugba, I am just thankful to have you as a friend, 'sister' and support in my life. My sweet friend Merve, you are the kindest person I know. Thank you girls for being always with me, although we are kilometers away. My lovely friends Kanykei, Oyuntuya, Sezin and Duygu, with whom we started this Chemistry journey together. We were never separated, and I know we will always be traveling overseas to visit each other.

My lovely partner Yannic, I can never thank you enough for your understanding and support during this thesis period, you should get a trophy for that :) I am just too lucky to have you in my life, and you are my family in Germany.

Last but not least, my sweet mother Asuman. You believe in me and support me in every step of my life, you are my hero. My father, thank you for supporting me all this time. And my siblings Selcuk, Merve and Fatma, you are my best friends and partners in crime. I am blessed to have you guys on my side...

Table of Contents

| | |
|---|-----|
| Table of Contents | I |
| Abbreviations | III |
| 1 Introduction | 1 |
| 1.1 Nanoparticle-Based Self-Assembly Systems | 1 |
| 1.2 Gold Nanoparticles | 4 |
| 1.2.1 Ligand Exchange Reactions of Gold Nanoparticles | 7 |
| 1.2.2 Gold Nanoparticles as Molecular Receptors | 10 |
| 1.2.3 Determination of Surface Structure of Gold Nanoparticles and their Interactions with Substrate Molecules | 15 |
| 2 Scope of the Project | 17 |
| 3 Results and Discussions | 21 |
| 3.1 Ligand Syntheses | 21 |
| 3.2 Syntheses of the Mixed Monolayer Protected Gold Nanoparticles | 25 |
| 3.3 Nanoparticle Characterization | 32 |
| 3.3.1 ¹ H-NMR Spectroscopy | 32 |
| 3.3.2 UV-Vis Spectroscopy | 33 |
| 3.3.3 Transition Electron Microscopy | 34 |
| 3.3.4 Dynamic Light Scattering | 37 |
| 3.3.5 DOSY-NMR Spectroscopy | 39 |
| 3.3.6 Iodine Decomposition | 41 |
| 3.3.7 Discussion | 44 |
| 3.4 Binding Studies | 51 |
| 3.4.1 ¹ H-NMR Spectroscopy | 51 |
| 3.4.2 DOSY-NMR Spectroscopy | 53 |

| | |
|--|-----|
| 3.4.3 Fluorescence Spectroscopy | 57 |
| 3.4.4 Discussion | 65 |
| 4 Summary and Outlook | 71 |
| 5 Experimental Part | 75 |
| 5.1 Materials | 75 |
| 5.2 Analytical Methods | 75 |
| 5.3 Ligand Syntheses | 78 |
| 5.4 Nanoparticle Syntheses..... | 91 |
| 5.5 General Procedure for Iodine Decomposition | 94 |
| 5.6 DOSY-NMR Spectroscopy and Titrations | 95 |
| 5.7 Fluorescence Titration Experiments | 100 |
| 6. References | 106 |
| 7. Appendix | 113 |

Abbreviations

| | |
|----------------|--|
| a.u. | Arbitrary units |
| AuNPs | Gold nanoparticles |
| calcd. | calculated |
| d | day |
| DCC | <i>N,N'</i> -dicyclohexylcarbodiimide |
| DLS | Dynamic light scattering |
| DOSY | Diffusion-ordered spectroscopy |
| D_{bound} | Diffusion constants of the nanoparticles |
| D_{free} | Diffusion constants of the peptides |
| D_{obs} | Observed diffusion constants of peptides in complexes with AuNPs |
| DIEA | <i>N,N</i> -Diisopropylethylamine |
| DMAP | 4-Dimethylaminopyridine |
| DMSO | Dimethyl sulfoxide |
| DMF | <i>N,N</i> -Dimethylformamid |
| eq | equivalents |
| FFT | Fast Fourier transformation |
| FT-IR | Fourier transform infrared spectroscopy |
| <i>Gly-Gly</i> | Glycylglycine |
| <i>Gly-Phe</i> | Glycyl-L-phenylalanine |
| <i>Gly-Trp</i> | Glycyltryptophane |
| h | hour |
| HPLC | High performance liquid chromatography |
| <i>Hz</i> | Hertz |
| ITC | Isothermal titration calorimetry |
| ILT | Inverse Laplace transformation |
| MALDI-TOF MS | Matrix-assisted laser desorption/ionization mass spectroscopy |
| Mp | Melting point |

Abbreviations

| | |
|---------|--|
| NMR | Nuclear magnetic resonance spectroscopy |
| MPA | Mercaptopropionic acid |
| PGSE | Pulsed-field gradient spin-echo measurements |
| SAM | Self-assembled monolayer |
| SPR | Surface plasmon resonance |
| ppm | Parts per million |
| TEM | Transmission electron microscopy |
| THF | Tetrahydrofuran |
| TLC | Thin Layer Chromatography |
| Tyr | Tyrosine |
| UV-Vis | Ultraviolet–visible spectroscopy |
| v/v | Volume to volume |
| Z-group | Carboxybenzyl protecting group |

1. Introduction

1.1 Nanoparticle-Based Self-Assembly Systems

Supramolecular chemistry studies the interactions between molecules through recognition and assembly on the molecular level. It thus provides a platform for biological and material science applications, such as the design of receptors that can be used for the the delivery of drug molecules or the mimicking of biomolecules. Binding partners in supramolecular receptors communicate through noncovalent forces such as hydrogen bonds, hydrophobic, aromatic, electrostatic, or van-der-Waals interactions and metal-ligand bonds. These interactions usually motivate supramolecular structures to self-assemble spontaneously due to the interactions of the complementary recognition units. Self-assembly is an appealing approach to synthesize complex systems because equilibrium is reached via a fast and self-correcting process under thermodynamic control.¹

Cooperativity is a key concept in the realization of supramolecular self-assembling systems and is achieved by two or more interactions that behave different together than individually. Thus, novel collective properties of a system are achieved that are not observed in the individual components. Depending on the nature of the cooperativity, whether interactions favor or disfavor each other, the terms positive or negative cooperativity are used.

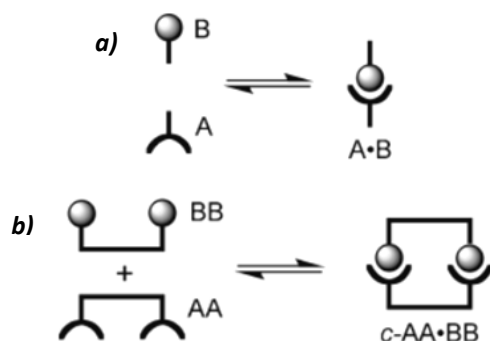


Figure 1.1 Complexation equilibria of *a)* molecules with single binding site, *b)* molecules with more than one binding site "Reprinted with permission from; C. A. Hunter and H. L. Anderson, *Angew. Chem. Int. Ed.*, 2009, **48**, 7488–7499, Copyright 2009, John Wiley and Sons"

Figure 1.1 depicts the association equilibrium of a receptor and a ligand with single binding sites and the corresponding equilibrium of binding partners with multiple binding sites. If the overall affinity in the latter case is larger than the sum of the individual interactions in terms of ΔG , the two binding sites act with a positive cooperativity. A well-known literature example for positive cooperativity is the binding of oxygen to the subunits of hemoglobin. In this case, binding of oxygen to one site improves affinity of the other sites.² This feature is also observed in the strengthening of the interactions that involve more than one recognition unit assembled on a suitable receptor core and is due to favorable thermodynamics.³⁻⁵ Nanoparticles containing multiple receptor units comprise attractive platforms to realize cooperative binding of individual binding sites to target molecules.^{6,7}

Nanomaterials, which are sub-micrometer scale materials, can be readily manipulated in terms of structure and properties to achieve an application of interest. An important aspect of nanotechnology is functionalizing materials that are initially inert to implant functionalities and potentially also biocompatibility. With multivalent attachment sites for small molecules, nanomaterials have a great potential in biomedical applications due to the enhanced specific binding affinity. Various nanomaterials are available that can be further functionalized, for instance, quantum dots, polymeric nanoparticles, metal nanoparticles and nanotubes. Functionalization can benefit from the spontaneous self-organization of organic molecules on the surface. Examples involve self-assembled monolayers (SAMs) on flat surfaces or on nanoparticles. In contrast to extended flat surfaces, nanoparticles comprise vertexes and edges, resulting in a curvature of the monolayer. Figure 1.2 shows the different arrangements of ligands on flat and curved surfaces as an example, where (a) shows hexadecanethiol molecules in their fully extended conformations adsorbed on a flat Au(111) surface⁸ and (b) shows a cysteine-coated $\text{Au}_{144}(\text{RH})_{60}$ nanocluster⁹.

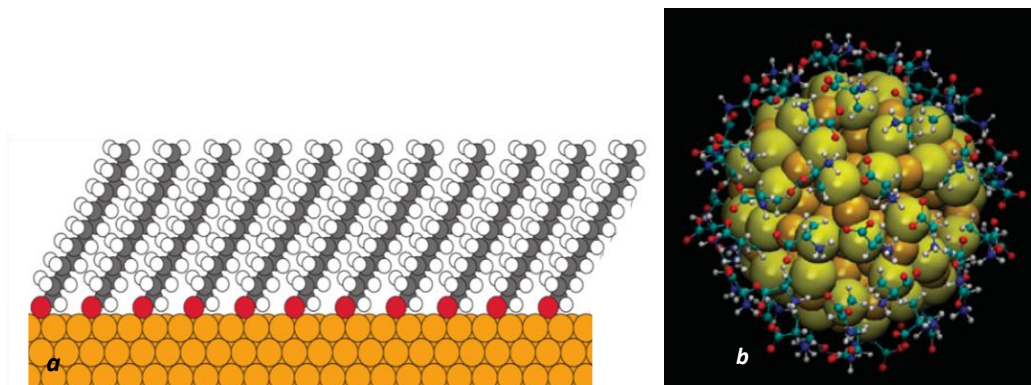


Figure 1.2 Molecular models of *a*) SAM of hexadecanethiol molecules adsorbed on Au(111) surface, *b*) cysteines coated Au₁₄₄(RH)₆₀ nanocluster. The spheres in Figure 1.2-*a* represent gold (orange), sulphur (red), carbon (grey) and hydrogen (white) atoms, and in Figure 1.2-*b* large spheres represent gold (orange) and sulphur (yellow) atoms and the oxygen (red), carbon (cyan), nitrogen (blue) and hydrogen (white) atoms of the ligands are shown as ball-and-stick representations. "Reprinted with permission from; *a*), M. A. Boles, D. Ling, T. Hyeon and D. V. Talapin, *Nat. Mater.*, 2016, **15**, 141-153, Copyright 2016, Nature Publishing Group, *b*) S. A. Alsharif, L. Y. Chen, A. Tlahuice-Flores, R. L. Whetten and M. J. Yacaman, *Phys. Chem. Chem. Phys.*, 2014, **16**, 3909-3913, Copyright 2013, Royal Society of Chemistry"

Nanoparticles most commonly contain a surrounding monolayer and thus display the properties of both their inorganic core and the organic monolayer surrounding it. The inorganic core is not only responsible for the size, shape and physical properties, it also maintains the stability and monodispersity. The organic protecting monolayer, on the other hand, ensures colloidal and chemical stability. In addition, it allows tailoring the solubility and the interactions of the particles with target molecules in various media. Solubility of nanoparticles in aqueous media can, for instance, be achieved by an organic monolayer containing hydrophilic functionalities, such as polyethylene glycol units or ligands containing ionic groups at their termini. These groups also prevent nonspecific adsorption of biomolecules in addition to avoiding nanoparticle precipitation or agglomeration.

Noncovalent interactions mediated by the surface bound functional groups are also used to achieve affinity of the nanomaterials to specific target molecules, including biomolecules.¹⁰ In addition, the surface bound functional groups can also serve other purposes.^{11, 12, 13} They can, for example, catalytically transform a bound substrate or signal its presence by the change of an optical property.^{14, 15} Figure 1.3 shows some applications of functionalized nanoparticles in a schematic fashion.¹⁶

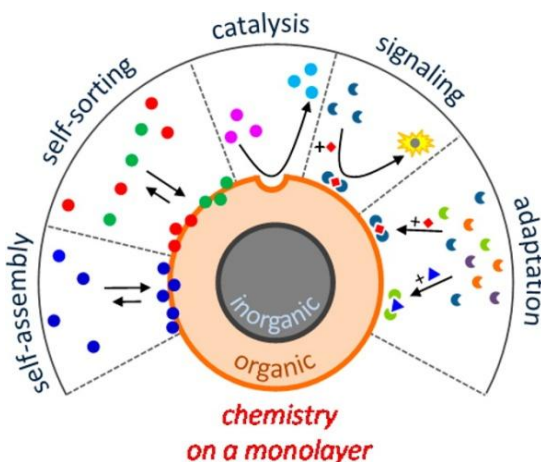


Figure 1.3 Various applications of nanoparticles provided by their functionalized monolayers, "Reprinted with permission from; L. J. Prins, *Acc. Chem. Res.*, 2015, **48**, 1920-1928, Copyright 2015, American Chemical Society"

An attractive feature of using nanoparticles with functionalized surfaces in these applications is that their size can be adapted to be in the same size window of proteins, rendering these systems also relevant for applications in biological contexts.^{17, 18, 19}

1.2 Gold Nanoparticles

Gold nanoparticles (AuNPs) have been used for a long time, especially for the staining of glass. They found wide spread use in nanotechnology only in the last three decades since methods became available of synthesizing stable monolayer protected nanoparticles in a controlled manner. The ease of preparation and functionalization contributes to the attractiveness of such

systems, in addition to their high stability under various conditions.¹⁶ Gold nanoparticles can be stabilized by monolayers of ligands that contain thiol, disulfide, phosphine, or amino groups to interact with the gold atoms. Organic thiols are particularly attractive because they strongly interact with the gold core and their organic residues allow controlling the properties (solubility, reactivity etc.) of the nanoparticles. Figure 1.4 shows the X-ray crystal structure of the $\text{Au}_{102}(\text{p-MBA})_{44}$ nanoparticles to illustrate the three-dimensional structure of such clusters (MPA; mercaptopropionic acid).²⁰

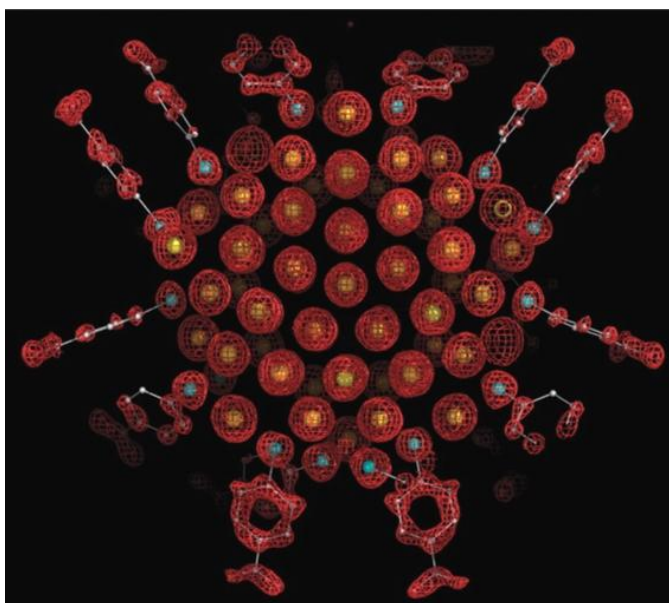


Figure 1.4 X-ray crystal structure of the $\text{Au}_{102}(\text{p-MBA})_{44}$ nanoparticle. The red mesh shows the electron density map with individual atoms denoted as yellow (gold), cyan (sulfur), gray (carbon), and red (oxygen) spheres. "Reprinted with permission from; P. D. Jadzinsky, G. Calero, C. J. Ackerson, D. A. Bushnell and R. D. Kornberg, *Science*, 2007, **318**, 430-433, Copyright 2007, The American Association for the Advancement of Science"

The interactions between the gold surface and the ligand of the monolayer is mediated through the -SH (sulfhydryl) functional group. Formation of a gold-thiolate bond (RS-Au) requires abstraction of a hydrogen atom from the sulfhydryl group and formation of a thiol radical (RS·).

The resulting gold-sulfur bond has a strength close to that of a gold-gold bond, allowing modifications of gold-gold bonding at the gold-sulfur interface. It has been shown that thiols form semi-covalent bonds with gold having a bond strength of ~45 kcal/mol. In comparison, the C-C bond strength is around ~83 kcal/mol.^{21, 22, 23}

A remarkable property of AuNPs is the 'Surface Plasmon Resonance' (SPR), which is an effect resulting from collective oscillations of surface electrons at the interface between the metal core and the monolayer, in resonance with an external electromagnetic field. The ease of tuning the SPR properties of AuNPs by manipulating their size, shape, and structure is attractive for applications in which shifts of the SPR bands are followed that are caused by changes in the size or structure of functionalized AuNPs. The SPR bands of AuNPs can be observed in the visible region of the electromagnetic spectrum.²⁴

Figure 1.5 shows that the SPR band of dodecanethiol protected AuNPs is affected by their size, becoming more intensive and sharper and displaying a slight red shift as the nanoparticle size increases. The SPR band vanishes for particles below ca. 2 nm.²⁵

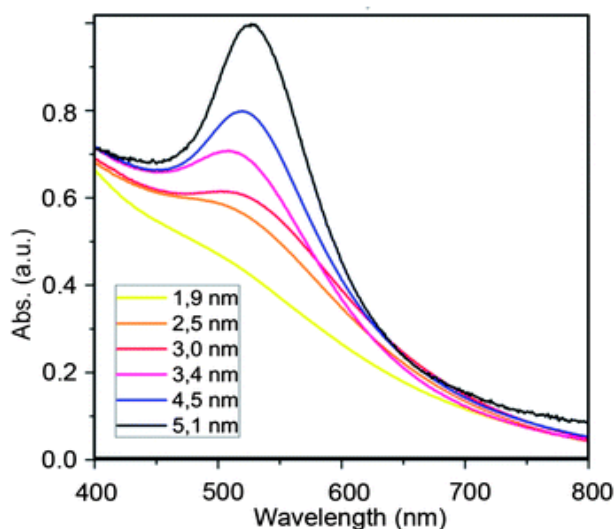


Figure 1.5 UV-Vis absorption spectra of dodecanethiol protected AuNPs of different diameters in DCM "Reprinted with permission from; G. L. Nealon, B. Donnio, R. Greget, J.-P. Kappler, E. Terazzib and J.-L. Gallani, *Nanoscale*, 2012, **4**, 5244-5258, Copyright 2012, Royal Society of Chemistry"

1.2.1 Ligand Exchange Reactions of Gold Nanoparticles

The functional groups of the ligands within the monolayers of AuNPs control the nanoparticle properties.²⁶ To adapt these properties to an application of interest, for instance the binding to a target molecule, it is essential that methods are available to control the presence and ideally also the spatial distribution of functional groups on the nanoparticle surface. In this context, the exchange of surface bound ligands is an effective tool to create functional surfaces. This process is due to adsorption of the incoming ligand and displacement of an existing one on the gold surface.²⁷⁻²⁹ Figure 1.6 illustrates a ligand exchange reaction between thiol-ligands to form mixed monolayer protected nanoparticles.³⁰

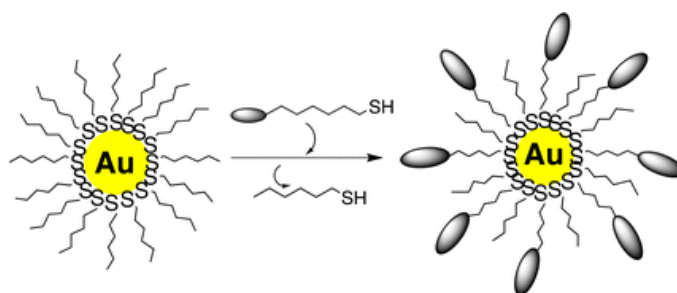


Figure 1.6 Schematic representation of a ligand exchange reaction yielding mixed-monolayer protected AuNPs "Reprinted with permission from; H. K. Bisoyia and S. Kumar, *Chem. Soc. Rev.*, 2011, **40**, 306-319, Copyright 2010, Royal Society of Chemistry"

Ligand exchange reactions are performed by mixing a solution of the precursor nanoparticles with the ligands of interest. This technique also allows the preparation of water soluble nanoparticles by incorporating hydrophilic ligands into the monolayer. Progression of ligand exchange causes the transfer of the particles from the organic phase to the aqueous phase.

Ligand exchange reactions are easy to perform due to the dynamic nature of the interactions between gold nanoparticle surfaces and the ligands.²⁴ They require suitable AuNPs precursors that are sufficiently stable due to a protective layer of suitable ligands. These ligands should also be readily exchanged with other ligands that potentially form more stable bounds to the nanoparticle core.

A number of such precursors are available, for instance, citrate protected AuNPs were introduced by Turkevich³¹ and Frens.³² They are prepared by reduction of a gold salt in the presence of trisodium citrate. These nanoparticles are commonly synthesized with 10-20 nm diameters and have been employed for attaching DNA strands to AuNPs by using the ligand exchange strategy.³³

Thiol protected AuNPs can be prepared by using a method developed by Brust and Schiffrin, which involves reduction of a gold salt in the presence of alkanethiol ligands in a two phase system.³⁴ It involves the reaction of aqueous chloroauric acid solution with sodium borohydride in toluene in the presence of tetraoctylammonium bromide and alkyl thiols. The strong gold-sulfur bonds ensure the stability of the inorganic nanoparticles, even at very low concentrations.¹⁶ The reaction conditions are mild enough to tolerate a wide range of functional groups on the organic ligands. In order to increase the affinity of the ligand to the nanoparticle, multidentate thiols can be used.⁴ The AuNPs obtained by this method usually have a low polydispersity and their diameter can be controlled by the gold salt/reducing agent ratio. They typically have diameters between 0.5-7 nm. Post modifications of the surface layers is possibly by treating the obtained thiol protected nanoparticles with the excess of other thiols, which leads to a ligand exchange.

This method was also used to synthesize stable water soluble nanoparticles with polyethylene glycol units in the monolayer.^{35, 36} In addition, mixed monolayer protected gold nanoparticles are accessible by using a mixture of thiol ligands during the AuNP synthesis. However, this strategy requires careful optimization if a defined surface composition of the different thiols needs to be achieved. Also, all ligands should be stable during the reduction process.

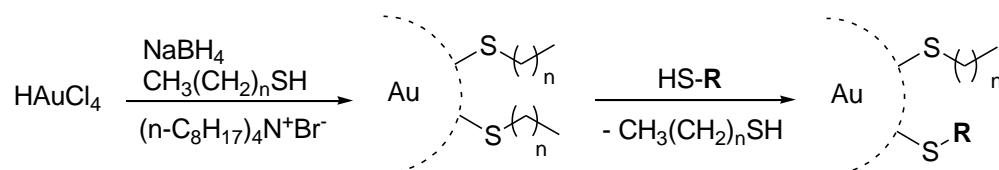


Figure 1.7 Reaction scheme of the Brust-Schiffrin method to synthesize monolayer protected nanoparticles, followed by a ligand exchange reaction

Figure 1.7 illustrates the Brust-Schiffrin method to synthesize nanoparticles, followed by a ligand exchange reaction, resulting in mixed monolayer protected AuNPs.

Finally, a very practical strategy for the synthesis of mixed monolayer protected AuNPs with stable thiols as ligands, including water soluble AuNPs, is to prepare dioctylamine passivated clusters initially, and exchange the weakly bound amine ligands with functionalized alkyl thiols in the next step (Figure 1.8).³⁷ The advantage of this process is that incorporation of the thiols leads to a more stable system, therefore, no large excess of the incoming thiols is required for the ligand exchange. Another advantage of this method is that it allows a better control over the ratio of different ligands in mixed monolayer than when using thiol protected AuNPs as precursors. Equilibrating amine protected AuNPs with a mixture of thiols typically leads to mixed monolayer protected nanoparticles with a ratio of the different surface bound ligands that closely reflects the ratio of the different thiols in the mixture used for the ligand exchange reaction. In contrast, when starting from thiol protected nanoparticles and using a mixture of thiols for ligand exchange, the ratio of surface bound ligands in the products can differ substantially from the one of the reaction mixture, because different ligands are more easily introduced in the nanoparticles than others. The diameters of AuNPs that can be obtained with this method range between 1.5-8 nm, depending on the gold-to-ligand ratio and the amount of the reducing agent used in the synthesis of the precursors.

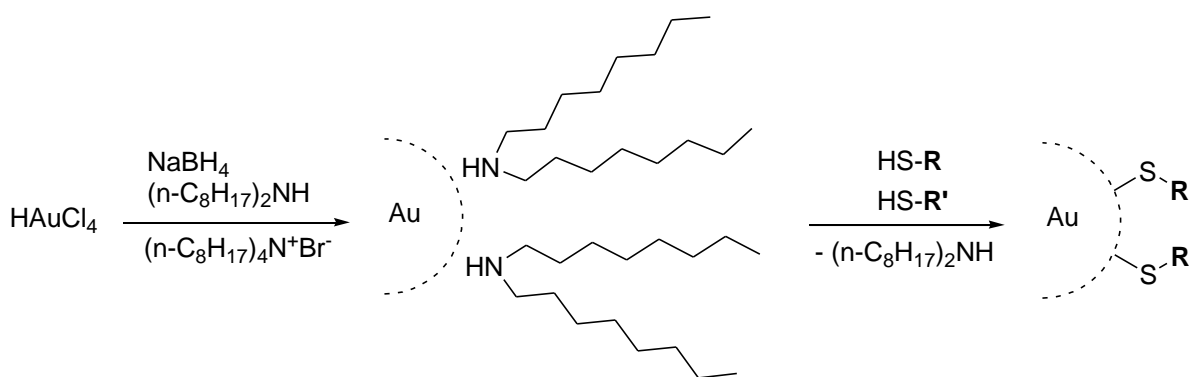


Figure 1.8 Schematic representation of ligand exchange reaction between amine and thiol ligands

Introducing amphiphilic functional thiols into the protective monolayer of AuNPs during the ligand exchange reaction gives rise to water soluble systems whose properties can be further controlled by the functional groups in the ligands. Polyethylene glycol groups, for example, prevent nonspecific adsorption of biomolecules, while ligands with polar terminal groups lead to neutral, anionic and cationic water soluble systems (Figure 1.9).³⁸ Amphiphilic nanoparticles with mixed monolayers containing hydrophobic and hydrophilic ligands have been also shown to behave similar to lipids,³⁹ having water solubility while also being able to penetrate the cell membrane.⁴⁰

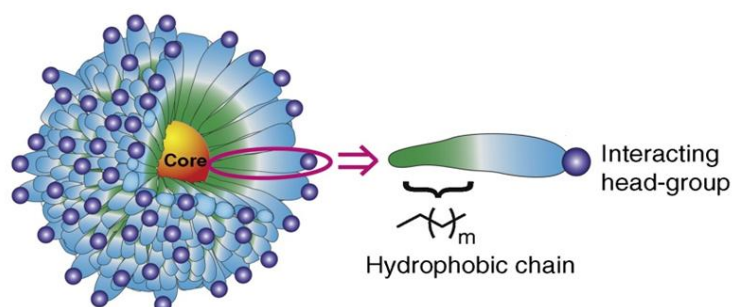


Figure 1.9 Structure of an amphiphilic nanoparticle⁴¹

"Reprinted with permission from; S. Rana, Y.-C. Yeh and V. M. Rotello, *Curr. Opin. Chem. Biol.*, 2010, **14**, 828-834, Copyright 2010, Elsevier"

1.2.2 Gold Nanoparticles as Molecular Receptors

The possibility to cluster functional groups of the same kind or with different structures on the surface of AuNPs renders nanoparticles interesting platforms for the development of nanosize synthetic receptors, which engage in strong and selective interactions with structurally complementary binding partners. Because of the sizes of AuNPs that typically approach those of small biomolecules, work in this area has mainly concentrated on the development of receptors for proteins, nucleotides, or other bio-relevant compounds.

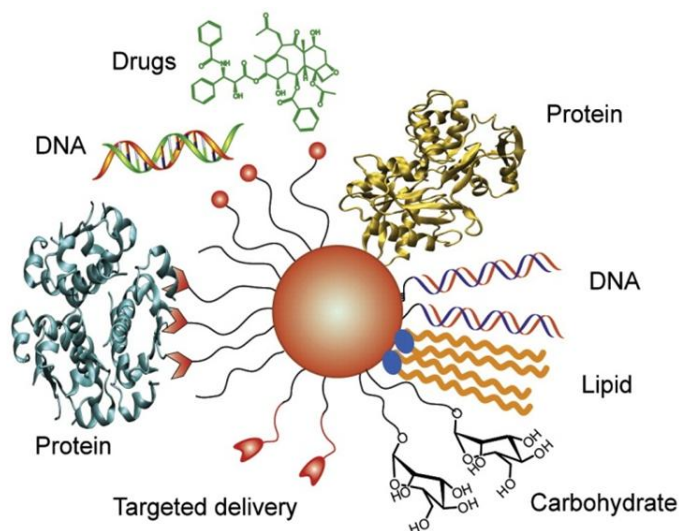


Figure 1.10 Schematic representation of AuNP-surface structures for delivery applications ⁴²

"Reprinted with permission from; S. Rana, A. Bajaja, R. Mouta and V. M. Rotello, *Adv. Drug Deliv. Rev.*, 2012, **2**, 200-216, Copyright 2011, Elsevier"

Figure 1.10 gives an overview of strategies that have been used to access such systems. Nanoparticles with attached DNA strands can, for example, recognize complementary oligonucleotide sequences. Fusing such AuNPs with larger oligonucleotides leads to the crosslinking of the nanoparticles. The resulting nanoparticle aggregation could be visually followed by the pronounced change in the SPR band. AuNPs that are densely functionalized with thiolated oligonucleotides were also attached via double-strand formation to DNA-labeled dye molecules or drugs.⁴³ Additionally, polycationic AuNPs with ligands containing ammonium groups interact with proteins that feature a predominantly negatively charged surface. Rotello's nanoparticle-green fluorescent protein conjugate represents an example of such system.⁴⁴

In contrast, there are significantly fewer examples in the literature of surface functionalized AuNPs that specifically interact with small molecules.⁴⁵⁻⁵¹ Scrimin's AuNP-based catalyst for trans-phosphorylation is one example. This system comprises AuNPs containing triazacyclononane-Zn(II) complexes on their surfaces. These nanoparticles interact with small nucleotides and mediate effective cleavage of phosphate diesters as shown in Figure 1.11. These AuNPs were therefore named 'nanozymes'.⁵²⁻⁵⁵

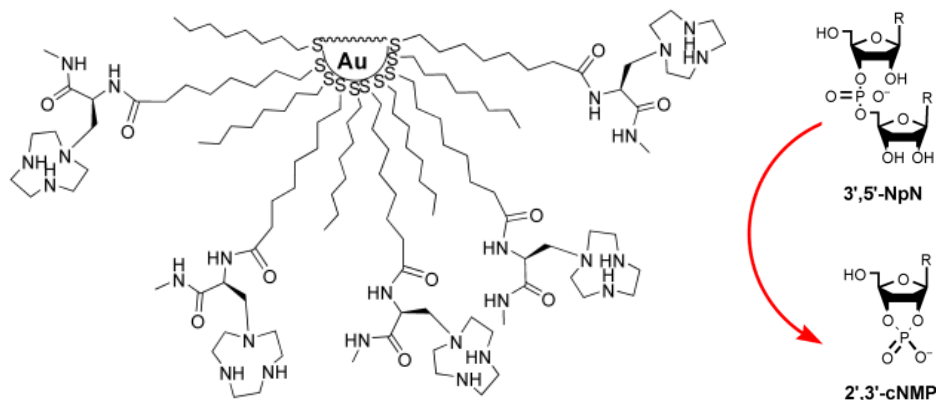


Figure 1.11 Gold nanoparticle-based transphosphorylation catalysts "Reprinted with permission from; F. Manea, F. B. Houillon, L. Pasquato and P. Scrimin, *Angew. Chem. Int. Ed.*, 2004, **43**, 6165-6169, Copyright 2004, John Wiley and Sons" ⁵³

An early example of a nanoparticle that interacts with a low molecular weight substrate is Rotello's flavin receptor.^{56, 57} This AuNP contains two orthogonal binding sites on the surface, a diamidopyridine unit that can form hydrogen bonds with flavin, and a pyrene unit that can engage in π -stacking interactions (Figure 1.12). Strong binding was expected when both units are bound on the surface in such a fashion that they can bind simultaneously to the substrate. An increase of the affinity of the AuNPs was indeed detected when they were equilibrated with flavin. This result was assumed to be due to the dynamic adaptation of the surface distribution of the two ligands templated by the substrate to afford optimal binding arrangements.

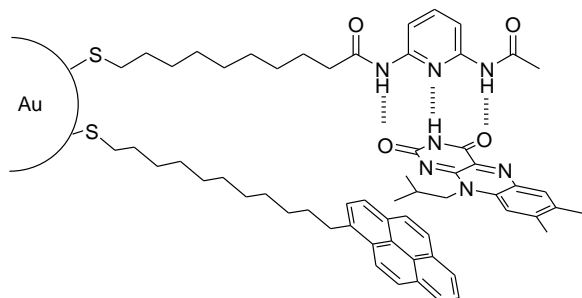


Figure 1.12 Schematic illustration of a flavin molecule binding to Rotello's AuNP, containing a diamidopyridine unit and a pyrene as binding sites

A AuNP-based receptor for flavin mononucleotide (FMN) was also described by Rotello. This receptor comprises a AuNP containing thiol ligands with quaternary ammonium head groups. Substrate binding is due to electrostatic interactions between the positively charged nanoparticle and the negatively charged substrate. Interestingly, a turn-off fluorescence sensor could be developed on the basis of this system (Figure 1.13).^{56, 58} It comprised the positively charged tetramethylammonium functionalized AuNPs and the FMN chromophore, whose fluorescence was quenched when bound to the nanoparticle. Quantitative binding analyses could be performed by following the dramatic decrease in the fluorescence intensity upon addition of the AuNP to the chromophore.

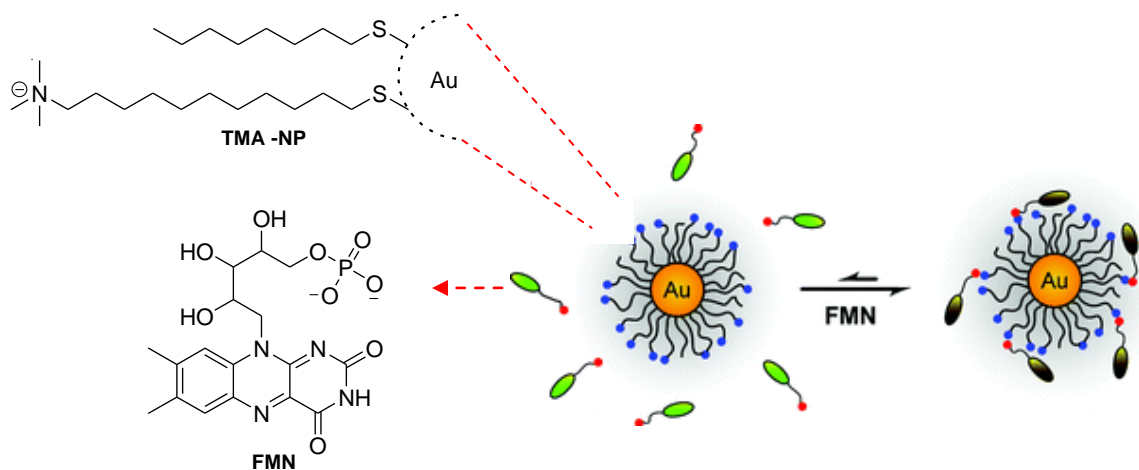


Figure 1.13 Rotello's flavoenzyme model system, "Reprinted with permission from; A. Bayir, B. J. Jordan, A. Verma, M. A. Pollier, G. Cooke and V. M. Rotello, *Chem. Commun.*, 2006, 4033-4035, Copyright 2006, Royal Society of Chemistry."

The AuNPs introduced by Prins' also demonstrate that incorporation of appropriate binding sites into nanoparticle monolayers induces affinity for small molecules (Figure 1.14).⁴⁵ These AuNPs are structurally related to Scrimin's receptors as they also contain zinc-triazacyclononane units. They were shown to possess high affinity for negatively charged substrates, in particular nucleotides. These systems turned out to be also highly attractive platforms for the development of responsive multivalent surfaces.

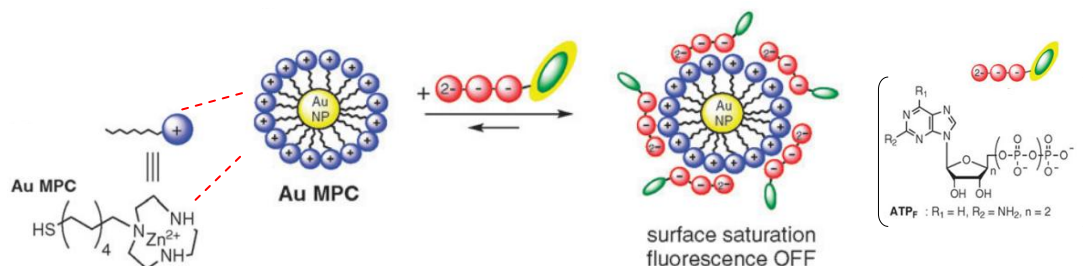


Figure 1.14 Self-assembly of fluorescent probes on the surface of AuNPs ⁴⁵

"Reprinted with permission from; G. Pieters, A. Cazzolaro, R. Bonomi and L. J. Prins, *Chem.*

Commun., 2012, **48**, 1916-1918, Copyright 2011, Royal Society of Chemistry"

Mancin et al. described AuNPs containing crown ethers for the binding of protonated primary amines in aqueous or methanol solutions (Figure 1.15).⁵⁹ These systems were able to selectively bind their analytes and, in the case of fluorescent substrate, also change their optical properties.

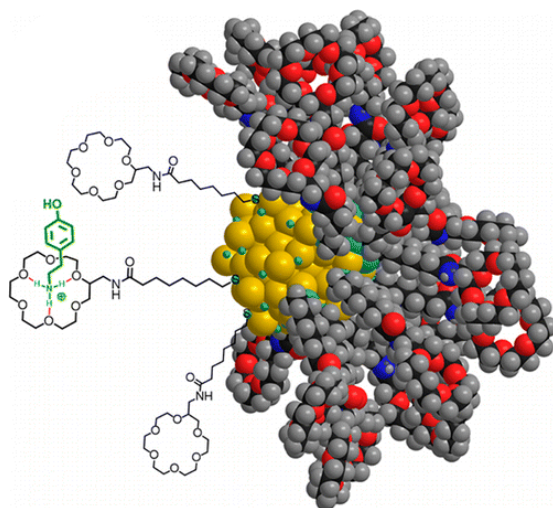


Figure 1.15. Mancin's crown ether-AuNPs that bind to primary amines in water, "Reprinted with permission from; M.-V. Salvia, G. Salassa, F. Rastrelli and F. Mancin, *J. Am. Chem. Soc.*, 2015, **137**, 11399-11406. Copyright 2015, American Chemical Society."

These selected examples thus show that attaching suitable binding sites to AuNPs can give rise to multifunctional receptors that can specifically interact with a given substrate even in competitive media.

1.2.3 Determination of Surface Structure of Gold Nanoparticles and their Interactions with Substrate Molecules

Despite progress in the development of characterization methods for nanoparticles, determining the number of ligands attached to a AuNP and, in particular, their distribution is still challenging. Characterization of AuNPs in solution by NMR spectroscopy is complicated by the broad signals in the spectra, so that limited information can often be obtained about the nature of the immobilized ligands and their amounts on the surface. An alternative method to investigate the composition of thiol-protected AuNP is to release the ligands first by using iodine.^{60, 61} This 'iodine decomposition' technique alleviates the problem of the broadness of the ligand signals in the NMR spectrum because once release from the surface, the ligands exhibit sharp signals in the spectra again. Their ratio can therefore be estimated from the integration of characteristic signals. Two different mechanisms were proposed in the literature for the role of iodine when added to a solution of thiol capped gold nanoparticles. The first mechanism was proposed by Chechik⁷² and involves the decomposition of the particles by oxidation of gold to form disulfides and a gold salt. Murray, on the other hand, suggested that iodine disturbs the stability of the nanoparticles and liberates the thiol ligands as disulfides.⁷⁸⁻⁸⁰

Various techniques have been used to quantitatively estimate the stability of AuNP complexes such as NMR, UV-Vis, and fluorescence spectroscopy and isothermal titration calorimetry. In general, titrations are performed during which one binding partner is gradually added to the other one and the change of a physical property associated with the binding event is followed. NMR spectroscopic binding studies typically rely on the change of the resonances of protons in the guest or the host during complex formation. They have been used, for instance, by Pochini et al. to study the recognition of quaternary ammonium cations by calix[4]arene functionalized AuNPs.^{62, 63}

UV- or fluorescence spectroscopy can be used if complex formation affects the position or the intensity of an absorption or emission band in the spectrum. Fluorescence spectroscopic binding studies are particularly attractive when studying complex formation of AuNPs because the fluorescence of a substrate is usually quenched when it binds to the nanoparticle.⁶⁴ This method was used by Prins et al., for example, to characterize the affinity of zinc-triazacyclo-

nonane-containing AuNPs towards fluorescent analogs of oligoanions.^{65, 66} Gradual addition of the fluorescent substrate to solutions of these AuNPs initially leads to quenching of the fluorescence. Only when the AuNPs are saturated, chromophore molecules start to appear in solution leading to an increase of fluorescence. The concentration of the substrate at which fluorescence becomes visible correlates with the stability of the complexes and the maximum amount of substrates that can be bound. Conversely, titrating the solution of a complex of an AuNP with a bound chromophore and adding a better substrate causes displacement of the chromophore and appearance of its emission band.

Isothermal titration calorimetry (ITC) allows direct measurement of the heat consumed or released during the binding event. For instance, the interactions between AuNPs and negatively charged proteins were investigated by Rotello et al. by using this technique to gain understanding of the thermodynamics and stoichiometry of these systems.⁶⁷

Recently, DOSY-NMR spectroscopy has become an attractive technique to analyze the intermolecular interactions in systems containing different binding partners, including ones in which one binding partner represents a AuNP.^{68, 69} This NMR technique allows measurements of diffusion coefficients based on the pulsed-field gradient spin-echo (PGSE) methodology and presents them as a 2D spectrum, where the chemical shifts are displayed in one dimension and the diffusion coefficients in the second one. The obtained diffusion coefficients can be related to the effective size and shape of a molecular species. In addition, DOSY-NMR spectroscopy also allows the estimation of association constants and the understanding of the intermolecular interactions in multi-component systems. Interactions of supramolecular nanoparticles composed of a hydrophobic dendrimer host molecule and hydrophilic guest molecules, for example, were investigated by using DOSY-NMR titrations.⁷⁰ The binding of phosphonic acid ligands to CdSe quantum dots has been also investigated by using this technique where quantitative replacement of oleic acid ligands on the quantum dots with incoming phosphonic acids could be monitored.⁷¹

2. Scope of the Project

The goal of this work was to synthesize artificial receptors based on gold nanoparticles for low molecular weight compounds. It has been shown that attaching a combination of different functional groups to the surface of nanoparticles allows them to cooperatively interact with a given substrate, thus improving affinity.⁷² In this work, this concept should be extended to the development of AuNP-based receptors for short peptides in water. Design of these receptors was inspired by a receptor described by Schneider, which was shown to bind di- and tripeptides in water by targeting their terminal ammonium and carboxylate groups as well as aromatic groups in the side chains (Figure 2.1).⁷³

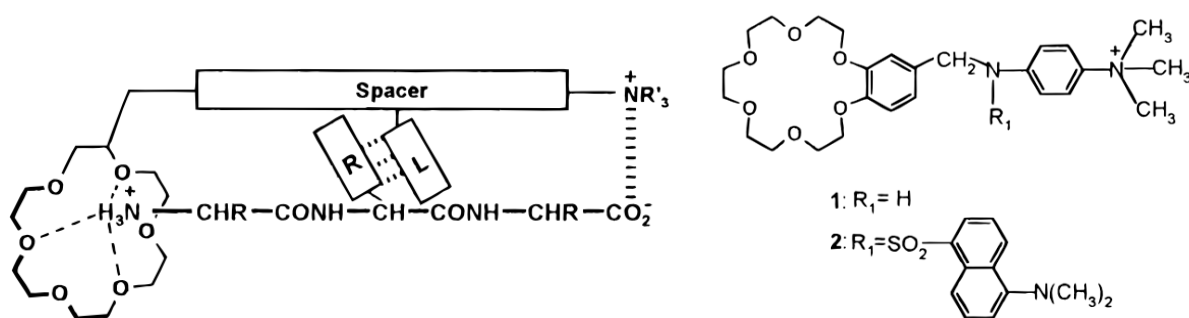


Figure 2.1 Schneider's synthetic receptor for peptide recognition in water,⁷³ "Reprinted with permission from; M. A. Hossain and H.-J. Schneider, *J. Am. Chem. Soc.*, 1998, **120**, 11208-11209.

Copyright 1998, American Chemical Society."

This receptor contains a crown ether that was expected to engage in interactions with the ammonium group of the substrate, a quaternary ammonium group that binds to the oppositely charged peptide carboxylate group, and an aromatic unit that can π -stack with aromatic peptide side chains. Affinities in water ranged between 30 and 2000 M^{-1} for dipeptides and tripeptides. Importantly, higher affinities were observed for tripeptides that contain a central aromatic amino acid, showing the contribution of aromatic interaction to the overall affinity. Another notable feature of the receptor is that the terminal binding sites possess negligible affinity for one another, so that no intra- or intermolecular self-recognition complicate the binding event.

The AuNPs designed on the basis of Schneider's receptor have the general structure shown in Figure 2.2. They contain the same structural components as the corresponding low molecular weight receptor. The linker components used to attach these binding sites to the gold nanoparticles derive from work of Scrimin.⁷⁴

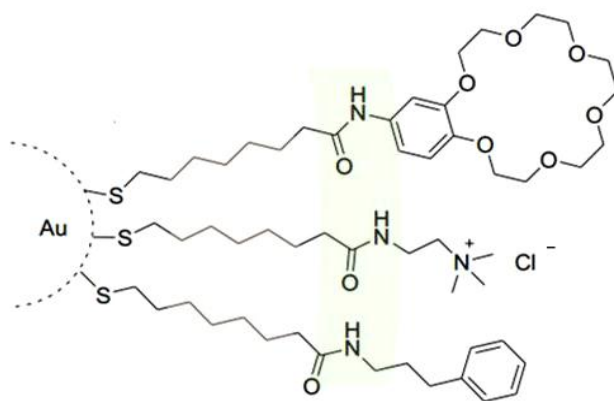


Figure 2.2 Schematic representation of the AuNP-based peptide receptors targeted in this thesis

Attachment of the ligands to the nanoparticles will be achieved through thiol groups. These thiol groups are located at the end of a hydrophobic chain that allows hydrophobic interactions around the gold core, thus providing a hydrophobic protective layer. The hydrophobic chains are attached via amide bonds to the peripheral polar functional groups that should mediate substrate recognition. The linking amide groups could potentially form hydrogen bonds with the neighboring amide groups on the AuNPs, thus contributing to their stability. The specific ligands required in this work for the decoration of the functionalized nanoparticles are shown in Figure 2.3.

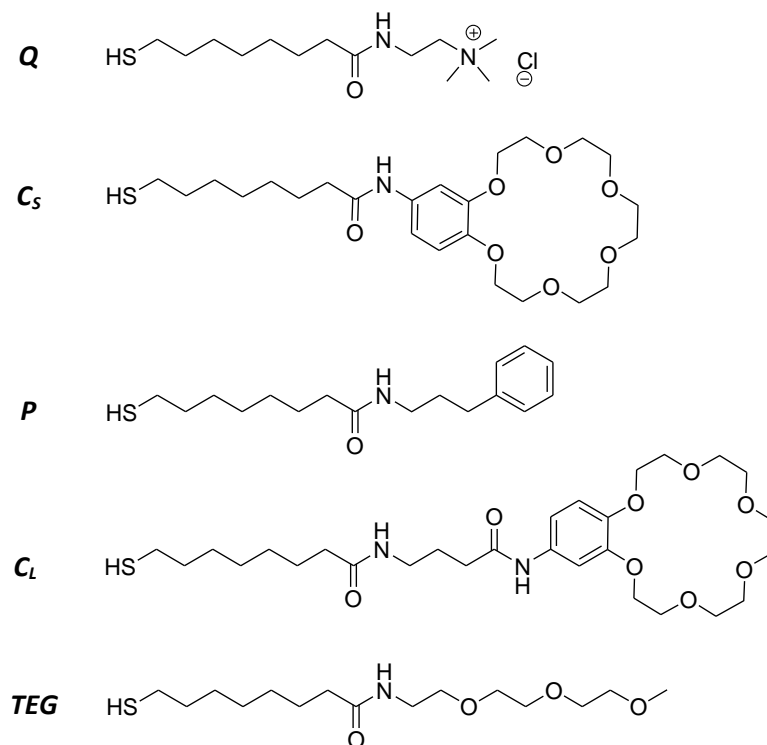


Figure 2.3 Chemical structures of the ligands required for nanoparticle syntheses

As in Schneider's receptor, a ligand with an ammonium group (**Q**) will be used to mediate binding to carboxylate groups in the peptide substrates. Ligands with crown ethers (**C_s** and **C_L**) should serve to bind to the substrate's ammonium group, and a ligand with an aromatic ring (**P**) should mediate aromatic interactions. Two ligands with crown ether will be considered, differing in the distance between the crown ether moiety and the amide group to explore the effect of the length of this ligand on the properties of the corresponding nanoparticles. Finally, ligand **TEG**, containing a triethyleneglycol unit, should also be included in the investigation because it could potentially allow diluting the other ligands on the gold surface with a polar but otherwise inert residue.

With respect to the size of the nanoparticles, a good control over the particle size with a narrow size distribution is essential for the applications of such systems as synthetic receptors.^{31, 32} Other factors are stability and accessibility of the functional groups on the nanoparticle surface. Because of the larger surface curvature of smaller nanoparticles, they were considered more

suitable for the desired application than larger ones.⁷⁵ These nanoparticles are typically accessible with relatively narrow size distribution and different surface bound ligands by using a range of synthetic methods.^{76, 77} The initial task of the thesis is to identify a suitable strategy, which would yield water soluble gold nanoparticles with small diameters (ca. 2 nm) containing a mixture of ligands deriving from the ones shown in Figure 2.3. Further aspects that need to be addressed are:

- i) the development of a strategy that allows preparation of functionalized AuNPs with a defined composition of the surface layer,
- ii) the characterization of these AuNPs in terms of size and structure,
- iii) the characterization of their binding properties.

The results will provide information whether the concept of attaching a combination of functional groups to the surface of AuNPs could represent a versatile and facile strategy for the synthesis of nano-sized multivalent receptors, whose binding properties can be varied in a wide range by adapting the type and number of recognition elements to the targeted substrate.

3. Results and Discussions

3.1 Ligand Syntheses

All ligands were synthesized from a common building block, namely 8-(acetylthio) octanoic acid **1**. This compound was prepared by treating 8-bromooctanoic acid with potassium thioacetate (Figure 3.1). The thioacetate group serves as a protecting group that needs to be cleaved prior to attaching the ligands to the gold nanoparticles.⁷⁸

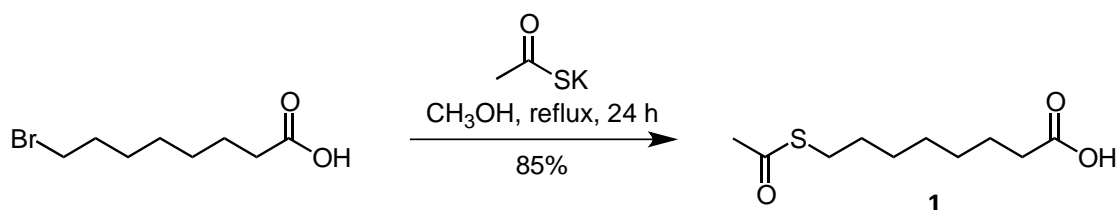


Figure 3.1 Synthesis of compound **1**

For the synthesis of the ligand **TEG_{Ac}**, containing a triethylene glycol group, triethylene glycol monomethyl ether was reacted with 4-toluenesulfonyl chloride.⁷⁴ The resulting tosylate **2** was then converted into the corresponding azide by using sodium azide. The azide group was finally reduced with triphenylphosphine to produce the amine **4** (Figure 3.2).

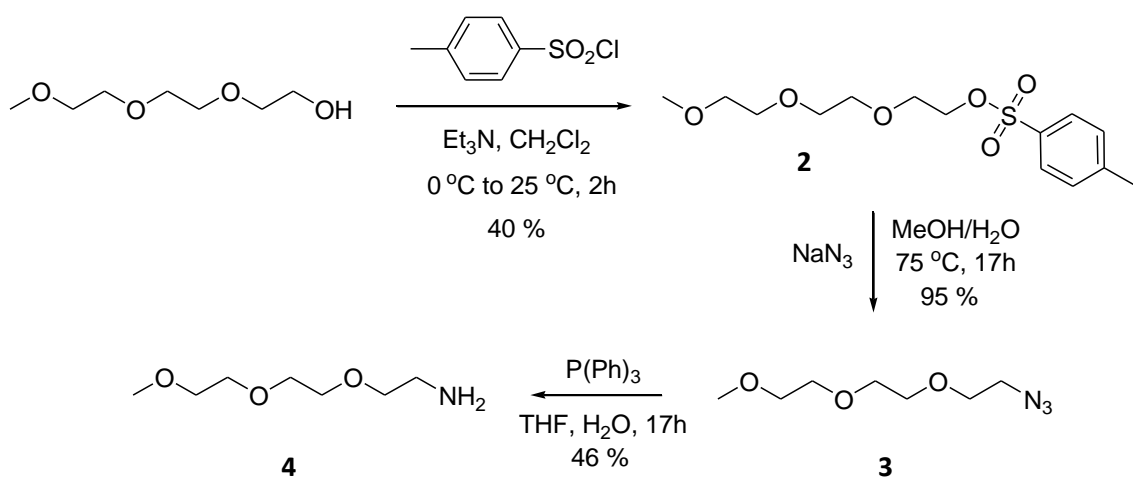


Figure 3.2 Synthesis of the compound **4**

Coupling of **1** and **4** was achieved by, first, transforming **1** into the acid chloride with thionylchloride and then reacting **4** and **5** in the presence of DIEA to afford **TEG_{Ac}** (Figure 3.3).

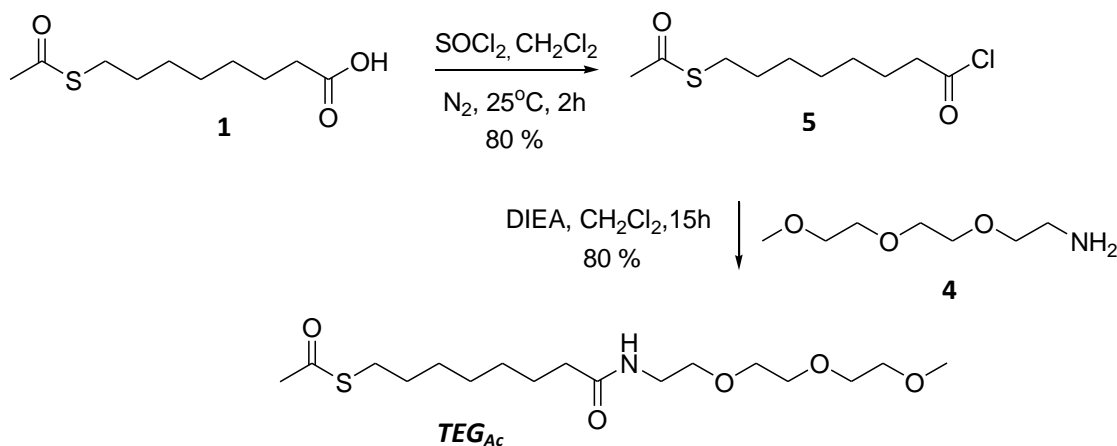


Figure 3.3 Synthesis of **TEG_{Ac}**

Ligand **Q_{Ac}** was prepared by coupling commercially available 2-amino-*N,N,N*-trimethylethanaminium chloride with **1** under the influence of *N,N'*-dicyclohexylcarbodiimide (DCC) (Figure 3.4).

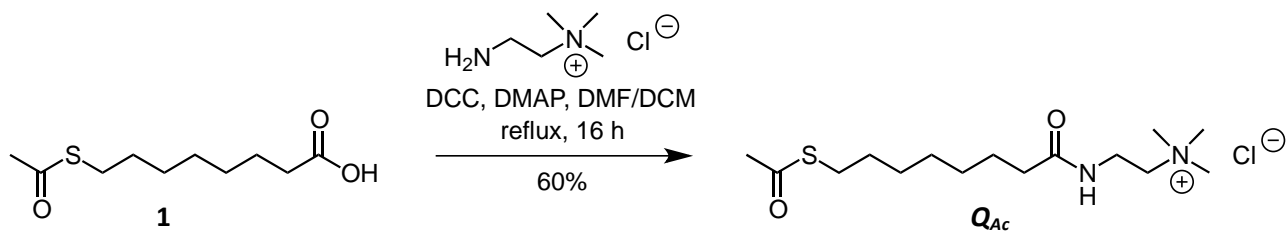
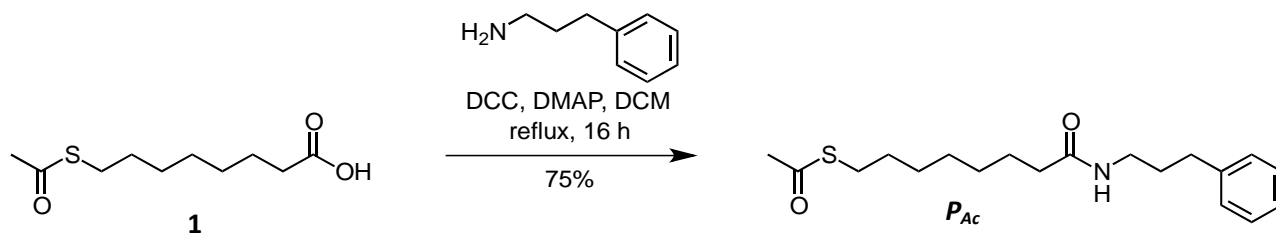
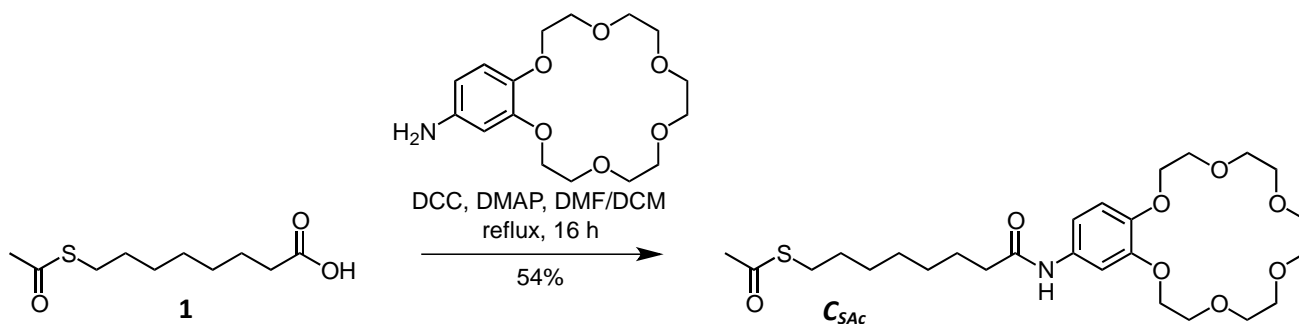


Figure 3.4 Synthesis of protected ligand **Q_{Ac}**

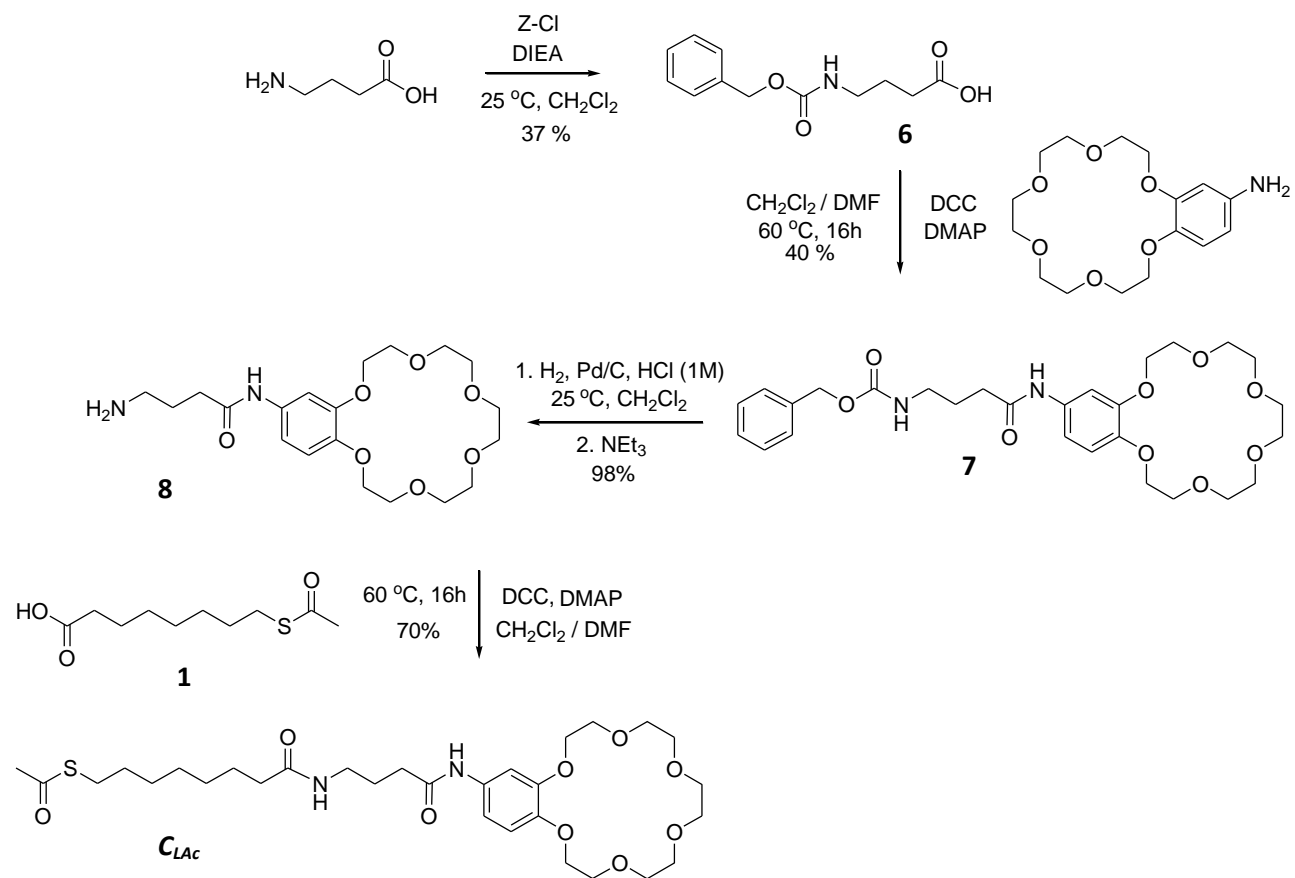
Ligand **P_{Ac}** resulted from the DCC mediated coupling of 3-phenyl-1-propylamine to **1** (Figure 3.5). The yield of the coupling step was 75 % in this case.

Figure 3.5 Synthesis of protected ligand P_{Ac}

The synthesis of the ligand C_{SAc} , bearing a crown ether moiety, was also performed by using the DCC coupling strategy. As starting materials, the commercially available 4'-aminobenzo-18-crown-6 was used and the carboxylic acid **1** (Figure 3.6).

Figure 3.6 Synthesis of protected ligand C_{SAc}

For the synthesis of C_{LAc} , 4-aminobutanoic acid was reacted with benzyl chloroformate to yield the corresponding Z-protected derivative **6**. This compound was coupled with 4'-aminobenzo-18-crown-6 by using DCC as coupling agent. Deprotection of the Z-group in the resulting product **7** was achieved by palladium catalyzed hydrogenation. Afterwards, the resulting amine **8** was coupled to **1** by using DCC to afford the protected C_{LAc} ligand with a yield of 70 % (Figure 3.7). All ligands were fully characterized and obtained in analytically pure form.

Figure 3.7 Synthesis of the ligand C_{LAc}

3.2 Syntheses of the Mixed Monolayer Protected Gold Nanoparticles

Prior to the nanoparticle syntheses, a deprotection procedure was established to release the thiol groups in the ligands. There are two alternative methods that can be used for the removal of the acetyl protecting group, namely acidic and basic conditions. Both methods were considered. For the deprotection under basic conditions, a solution of ligand **TEG_{Ac}** in methanol was reacted with 150 equivalent of DIEA at room temperature. For the deprotection in the presence of acid, a methanolic solution of **TEG_{Ac}** was reacted with a solution of HCl in 1,4-dioxane (6 N, 60 eq.) (Figure 3.8).

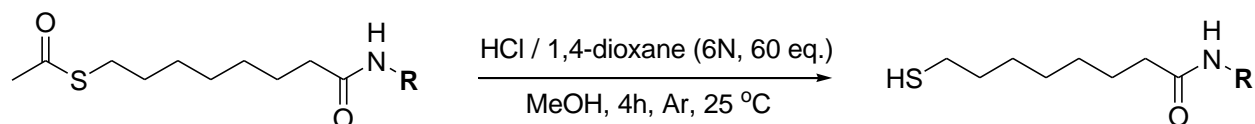


Figure 3.8 Deprotection of the acetyl protected ligands under acidic conditions

Both reactions were performed in closed vials under inert conditions. Their course was followed by taking samples from the reaction vessels at regular time intervals, evaporating the solvent, dissolving the residue in CDCl_3 , and recording a $^1\text{H-NMR}$ spectrum to follow the progressive disappearance of the acetyl CH_3 signal. These investigations showed that under the basic conditions deprotection was not completed even after 5 d. On the other hand, complete deprotection was observed under the acidic conditions already after 4 h. Therefore, acidic conditions were used for all deprotection reactions (Figure 3.9).

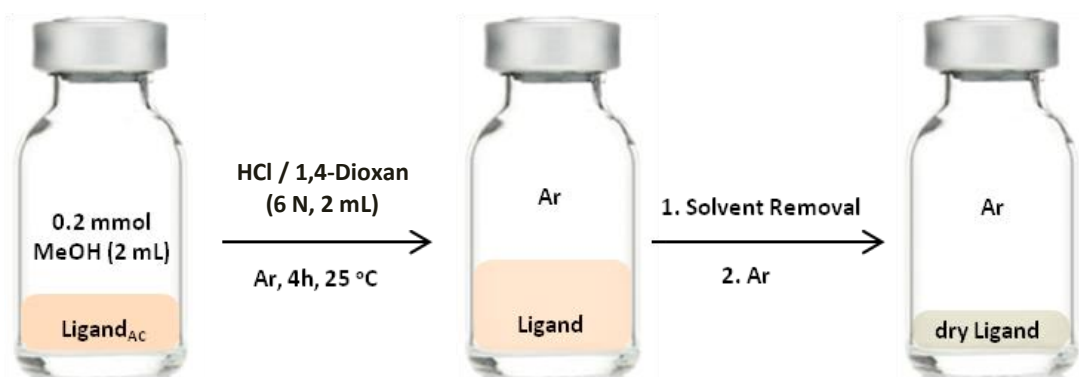


Figure 3.9 Schematic representation of the deprotection procedure

The relatively fast rate of deprotection under these conditions is advantageous because the risk of unwanted oxidative disulfide formation can thus be minimized. The comparison of the ^1H -NMR spectra of C_{SAC} and C_{S} are shown in Figure 3.10 as an example.

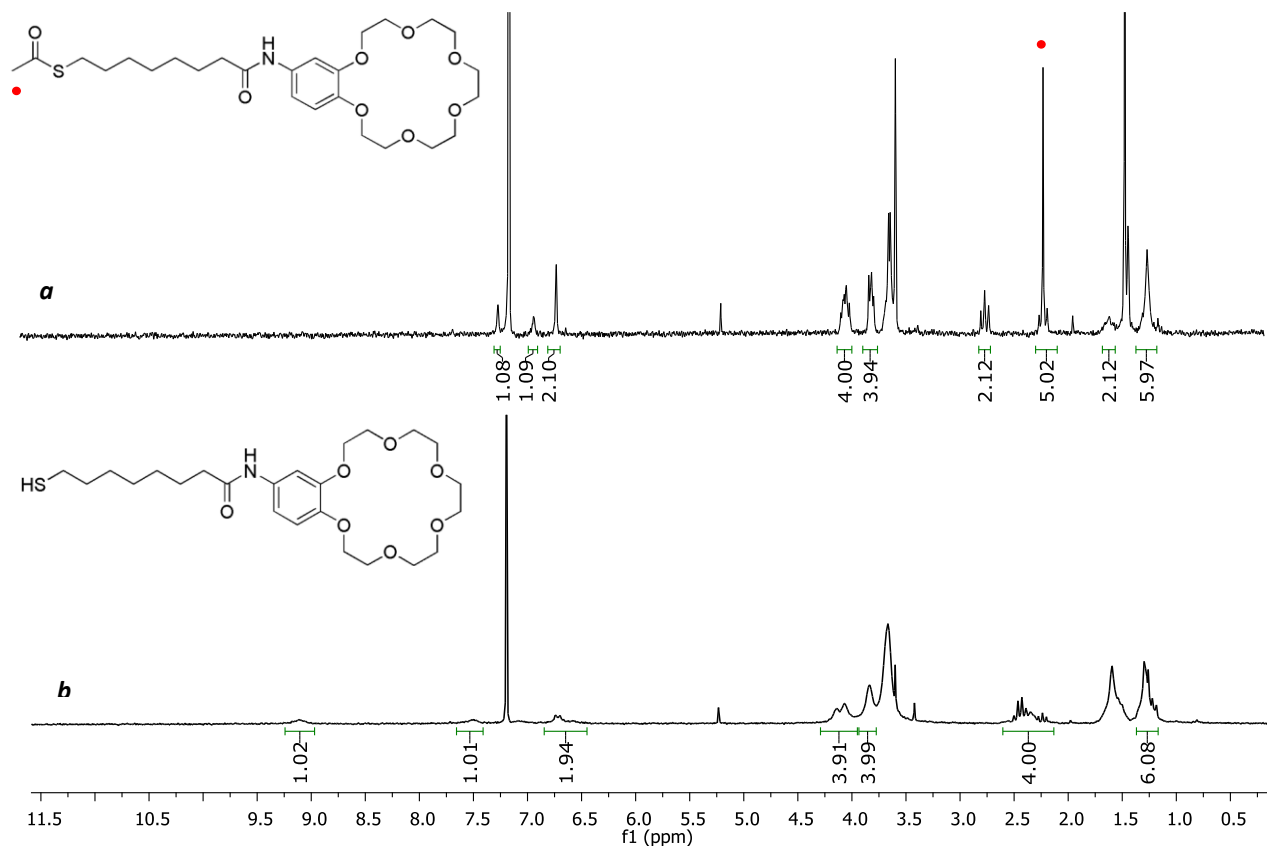


Figure 3.10 ^1H -NMR spectra of C_{S} (a) and C_{SAC} (b). The signal of the acetyl methyl group is marked with a red dot.

The free thiols obtained after removal of the solvent were immediately dissolved in degassed methanol under an argon atmosphere to avoid disulfide formation prior to the attachment to the AuNPs.

The approach used for the synthesis of the mixed monolayer protected nanoparticles followed a strategy originally introduced by Scrimin.⁷⁴ This method involves the initial synthesis of

nanoparticle **NP A**, containing weakly bound dioctylamines as protective ligands. The exchange of these amines with the functionalized deprotected thiols can then be performed in a second step.³⁷ This method has the advantage of that it allows a better control over the ratio of the surface bound ligands than exchanging ligands of a thiol protected nanoparticle with other thiols. In the latter case, the ratio of the ligand on the resulting nanoparticles depends on the propensity of the incoming ligands to replace the already present ones. Synthesizing mixed monolayer protected nanoparticles with a desired ligand ratio therefore requires finely tuned reaction conditions with the relative concentration ratios of the incoming ligands in the reaction mixture not necessarily reflecting their ratio in the product. When starting from **NP A**, nanoparticles can be obtained whose ligand ratio on the surface is controlled by the ligand ratio in the exchange solution, rendering this approach more convenient for the preparation of mixed monolayer protected nanoparticles (Figure 3.11).³⁷

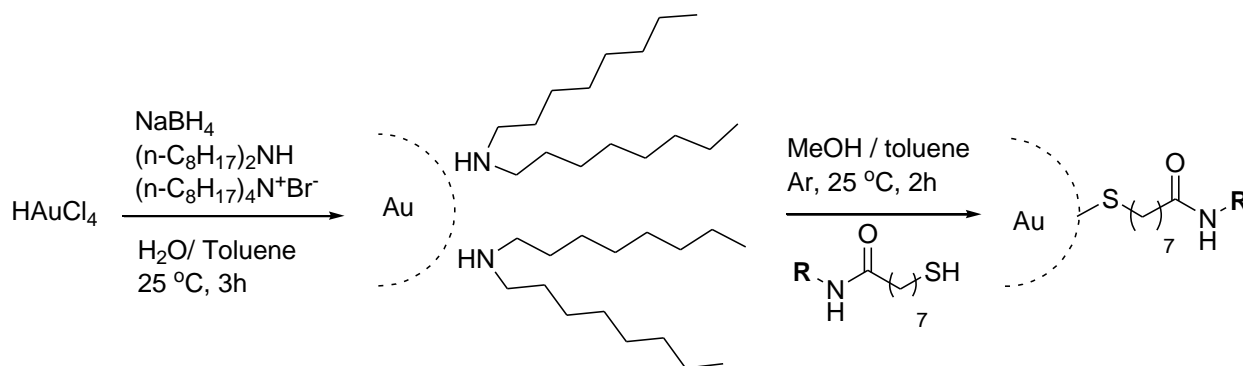


Figure 3.11 Synthesis of AuNPs via ligand exchange reaction

For the preparation of the nanoparticles, a freshly prepared solution of **NP A** in toluene was used from which a series of nanoparticles was synthesized. To this end, a certain amount of a ligand, or the same overall amount of a mixture of ligands (for AuNPs with one or two types of ligands: $n(\text{lig}_{\text{tot}})=0.04\text{ mmol}$, for those with three types of ligands $n(\text{lig}_{\text{tot}})=0.045\text{ mmol}$) was added to the **NP A** solution (40 mL). After stirring the reaction mixture for 2 h, the water soluble particles formed were observed to precipitate. Addition of water transferred them into the aqueous phase. The products were isolated by discarding the toluene phase and evaporating

the water. In order to check the reproducibility of the results at least three independently prepared batches of each AuNP were used for the characterization and binding studies.

Initially, **NP TEG** was synthesized containing only one ligand type. These nanoparticles were purified by repeatedly performing size-exclusion chromatography on a Sephadex LH-20 column. The $^1\text{H-NMR}$ spectrum of the product obtained is shown in Figure 3.12a. It shows a series of broad peaks at the chemical shifts of the protons of the organic ligands. The observed line broadening is due to the short relaxation times of the ligand protons once they are bound to the nanoparticles.⁷⁹ The broadness of peaks therefore proved the successful nanoparticle synthesis. In addition, a number of sharp peaks are visible in the spectrum that indicate the presence of impurities, which could not be separated chromatographically.

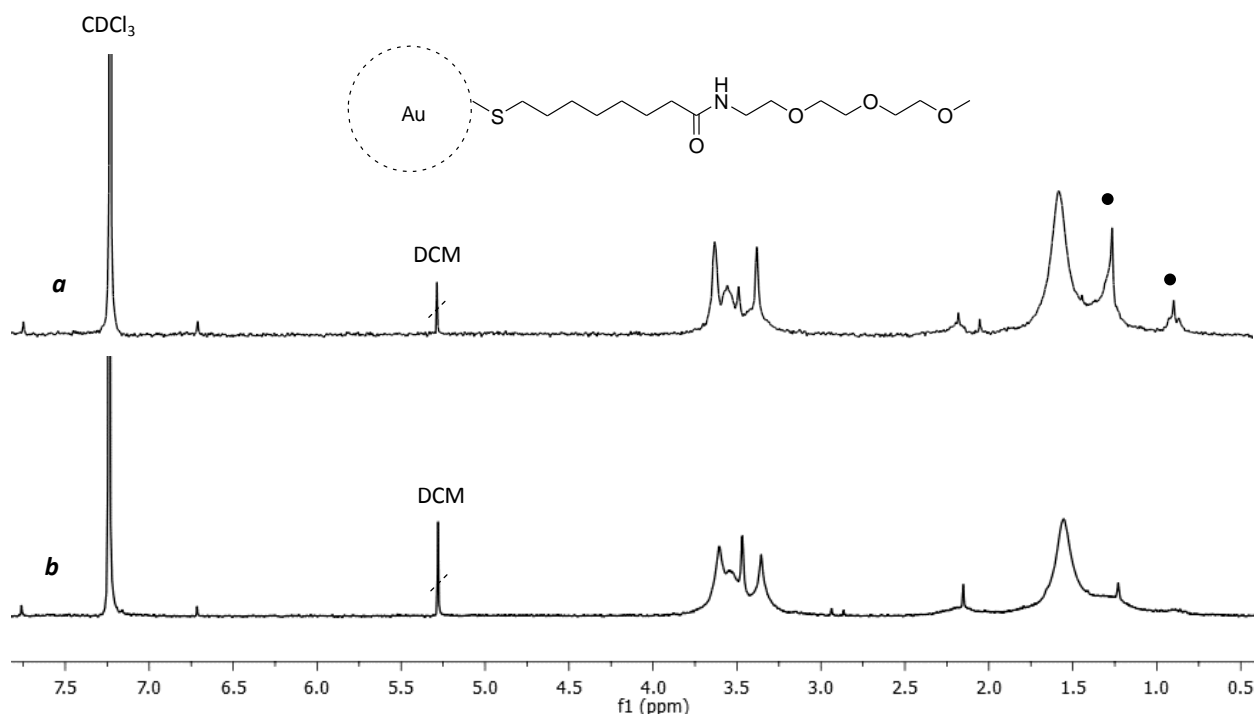


Figure 3.12 $^1\text{H-NMR}$ spectra of **NP TEG** purified via (a) size-exclusion chromatography and (b) membrane filtration. Impurities in spectrum (a) are marked with dots.

Because of the insufficient purity of the AuNPs obtained after size-exclusion chromatography another purification method was tested, which involved repeated washing of the nanoparticles

by using molecular weight cutoff membranes. This method proved to be more practical, leading to pure particles as shown by the $^1\text{H-NMR}$ spectrum in Figure 3.12b. Therefore, this method was consistently used for the purification of the AuNPs prepared in this thesis.

The structure of the AuNPs prepared in this work are shown in Figure 3.13. All AuNPs contain ligand **Q** to ensure water solubility. **NP Q** only contains **Q** while AuNPs **NP QP**, **NP QC_S**, **NP QC_L** additionally contain, respectively, ligands **Q**, **C_S** and **C_L**. The two nanoparticles **NP QPC_S** and **NP QPC_L** contain all three respective ligands. As all nanoparticles should contain a substantial amount of binding sites on their surface, a 1:1 ligand ratio was chosen for nanoparticles containing two ligand types. In the case of **NP QPC_S** and **NP QPC_L** care had to be taken that these nanoparticles remained water soluble. Therefore, it was decided that the content of **Q** of these nanoparticles should be 50% while the other two ligands should be present on the nanoparticle surface in equal amounts.

Based on the assumption that the ratio of surface bound ligands on the nanoparticles would reflect the ratio of the ligands used in the exchange reactions, AuNP **NP A** was treated with equimolar mixtures of the respective ligands for the preparation of **NP QP**, **NP QC_S**, and **NP QC_L**. Indeed, iodine composition of the prepared nanoparticles and determination of the surface bound ligands by $^1\text{H-NMR}$ spectroscopy (see chapter 3.3.6) confirmed the desired 1:1 ratio of the two ligands in the products. Synthesis of the AuNPs containing three ligand types required a more careful optimization of the reaction conditions, however. When treating **NP A** with a 2:1:1 ratio of ligands **Q**, **P** and **C_S**, respectively, the AuNP obtained containing the three ligands in a ratio of 15:2:3, showing that ligand **Q** was preferentially adsorbed. The amount of **Q** was therefore reduced in the exchange reaction and all three ligands were used in equimolar amounts. When using 0.015 mmol of each ligand, the desired 2:1:1 ratio of ligands **Q**, **P** and **C_S** on the nanoparticles could be achieved. The same conditions could be also used to synthesize **NP QPC_L**. **NP TEG** was not included in this set of nanoparticles since **TEG** ligands would not provide binding sites for the substrates. Table 3.1 summarizes the conditions used for the preparation of all nanoparticles.

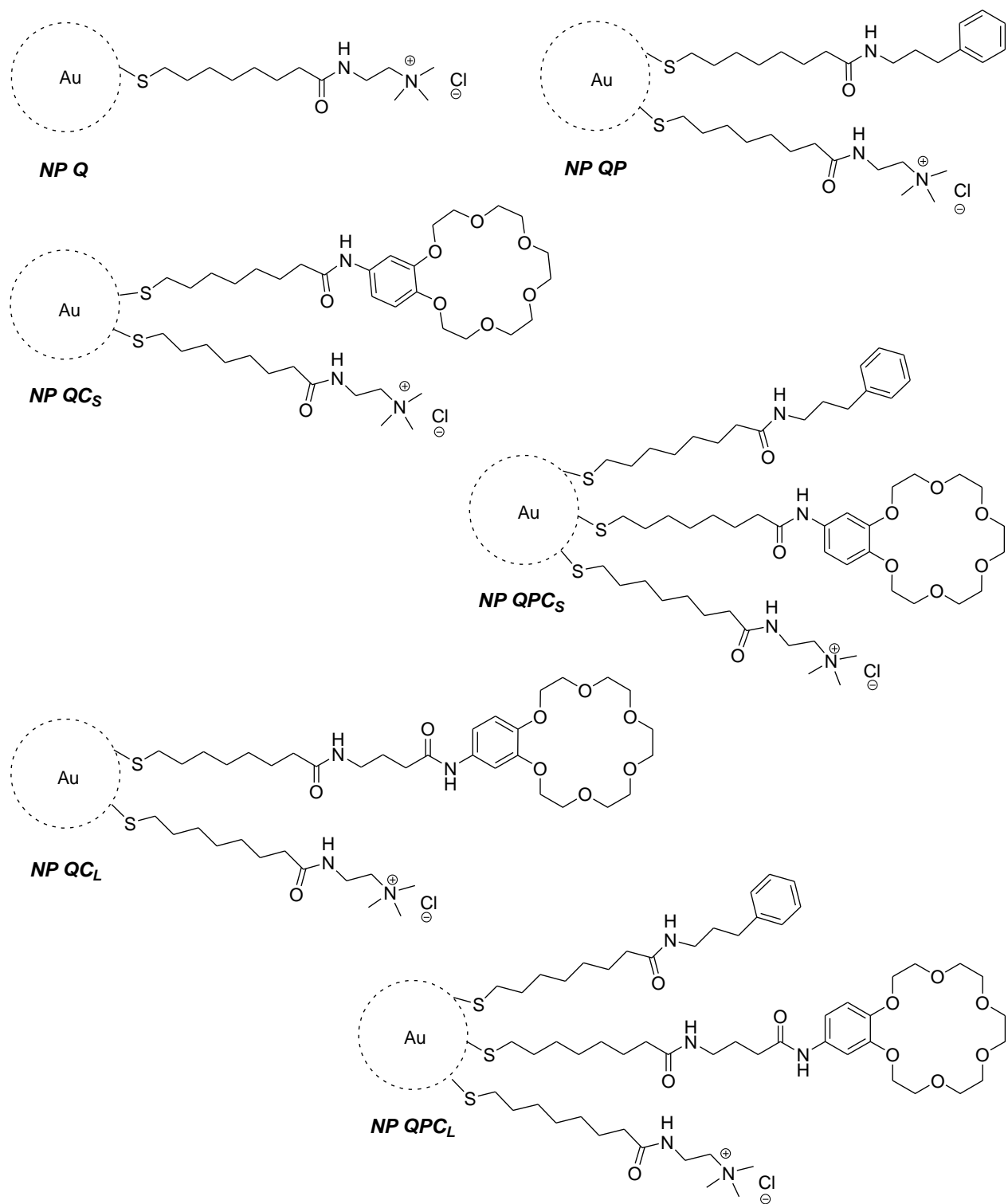


Figure 3.13 Schematic representation of the prepared nanoparticles

Table 3.1 Amounts of ligands used for the syntheses of all nanoparticles for **NP A**. The amounts refer to the amount of **NP A** present in 40 mL of the toluene stock solution obtained in the synthesis of this AuNP.

| Nanoparticles | NP A solution / mL | Q / mmol | C_S / mmol | P / mmol | C_L / mmol | Yield (mg) |
|---------------------------|---------------------------|-----------------|-----------------------------|-----------------|-----------------------------|------------|
| NP Q | 40 | 0.04 | - | - | - | 17 |
| NP QC_S | 40 | 0.02 | 0.02 | - | - | 20 |
| NP QP | 40 | 0.02 | - | 0.02 | - | 15 |
| NP QPC_S | 40 | 0.015 | 0.015 | 0.015 | - | 19 |
| NP QC_L | 40 | 0.02 | - | - | 0.02 | 23 |
| NP QPC_L | 40 | 0.015 | - | 0.015 | 0.015 | 21 |

Figure 3.14 shows the protocol used for the syntheses of these AuNPs in a schematic fashion by using the example of **NP QPC_S**.

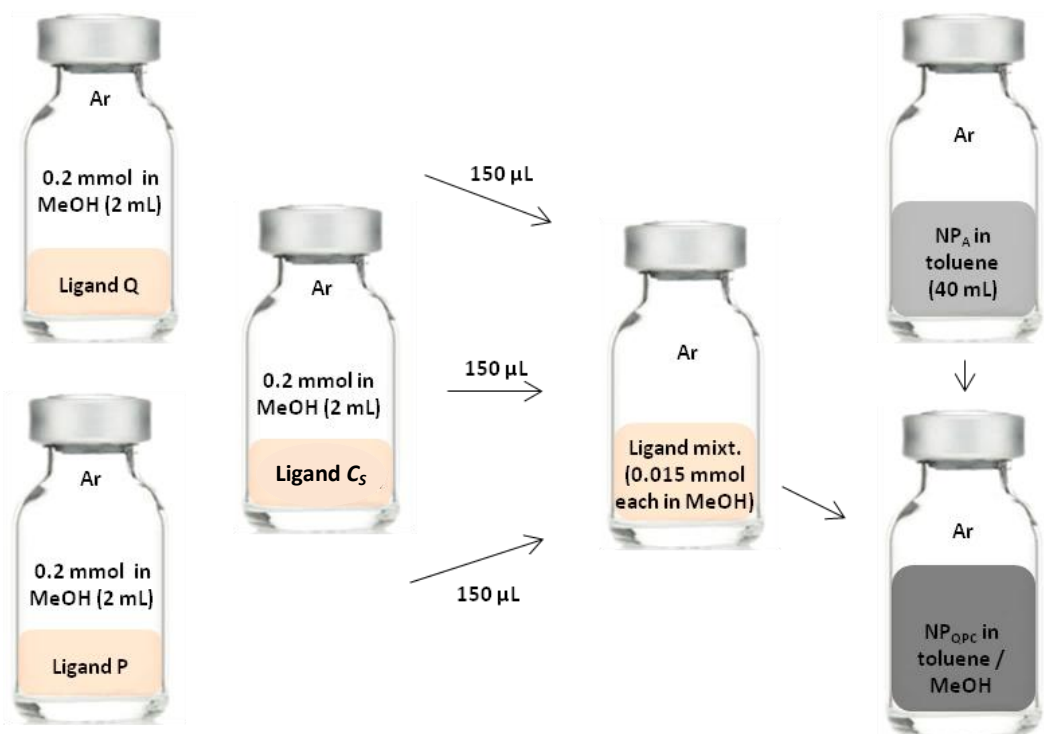


Figure 3.14 Schematic representation of the synthesis of **NP QPC_S**

Isolation of the nanoparticles involved transfer into water and purification by using membrane filtration.

3.3 Nanoparticle Characterization

The prepared nanoparticles were characterized by NMR and UV-Vis spectroscopy, transmission electron microscopy (TEM) and dynamic light scattering (DLS). The surface compositions of the nanoparticles were determined by ^1H -NMR spectroscopy after iodine decomposition.

3.3.1 ^1H -NMR Spectroscopy

^1H -NMR spectra of the nanoparticles were recorded in D_2O at $25\text{ }^\circ\text{C}$. The obtained spectra showed broad peaks due to shorter relaxation times of the ligand protons with respect to the relaxation times in the unbound state, confirming that the ligands are firmly attached to the nanoparticles.

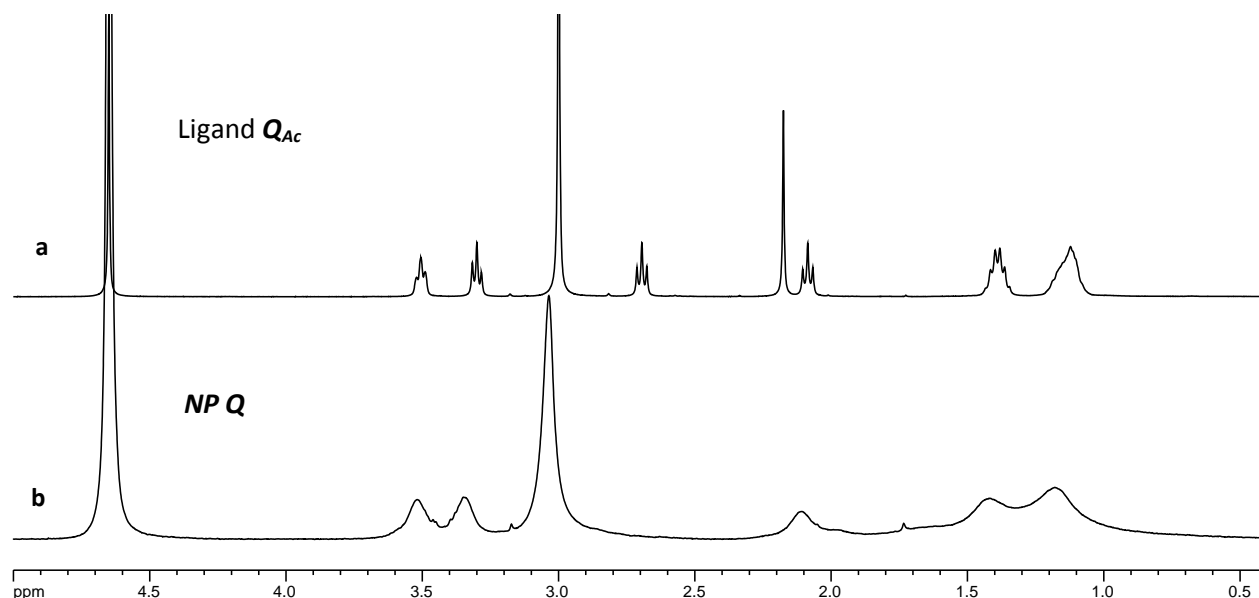


Figure 3.15 ^1H -NMR spectra of (a) ligand Q_{Ac} and of (b) NP Q in D_2O at $25\text{ }^\circ\text{C}$

Figure 3.15 shows the comparison of the $^1\text{H-NMR}$ spectra of Q_{Ac} in D_2O (a) and of NP Q (b). The resonances of the nanoparticle match those of the free ligand with the exception of the acetyl CH_3 signal that is absent in the nanoparticle spectrum. The absence of sharp signals in the nanoparticle spectrum furthermore confirms that no unbound ligands are present. Also the mixed monolayer protected nanoparticles exhibited excellent purity as judged from their $^1\text{H-NMR}$ spectra. Figure 3.16 shows the spectrum of NP QPC_L as an example.

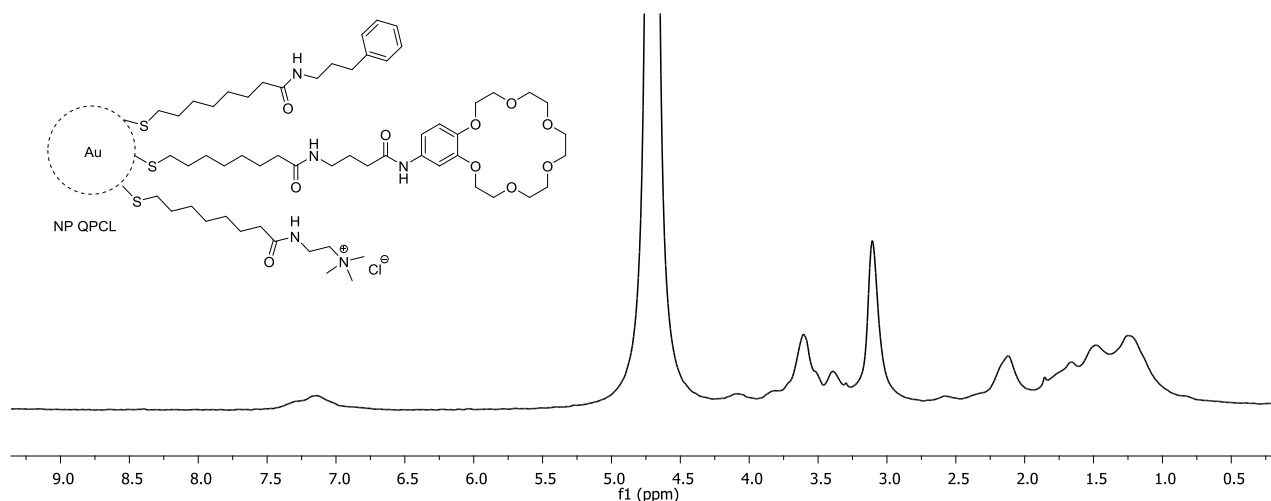


Figure 3.16 The $^1\text{H-NMR}$ spectrum of the NP QPC_L in D_2O

3.3.2 UV-Vis Spectroscopy

Figure 3.17 shows the UV-Vis spectrum of NP Q in the range of 200-800 nm recorded in D_2O . Only a weak surface plasmon resonance band was observed around 515 nm indicating that these nanoparticles have diameters of ca. 2 nm.²⁵ Bands that would account for the presence of larger nanoparticles are absent. Similar results were obtained for other nanoparticles.

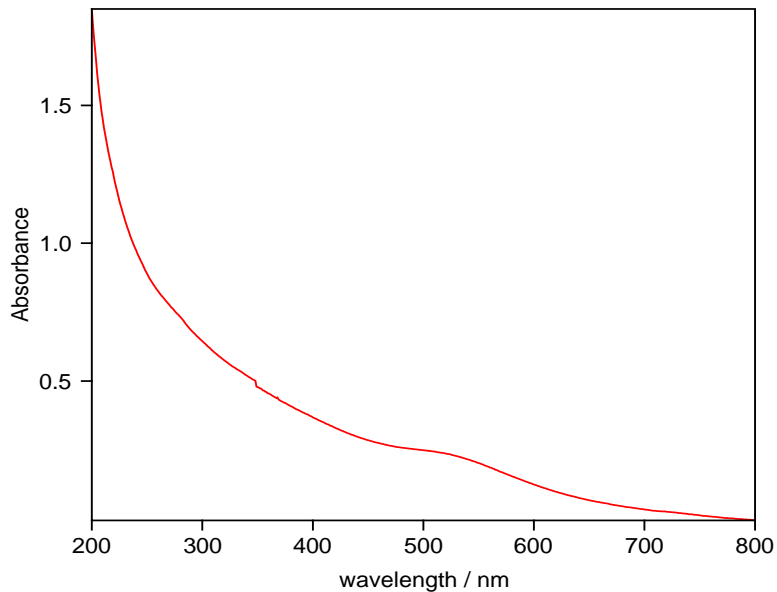


Figure 3.17 UV spectrum of **NP Q** in water

3.3.3 Transmission Electron Microscopy

Figure 3.18-23 show the TEM images of the prepared nanoparticles together with histograms describing the size distribution of the particles observed in these pictures. According to these measurements, the prepared nanoparticles had gold cores with diameters ranging from 1.9 to 2.6 nm. Table 3.2 summarizes the results.

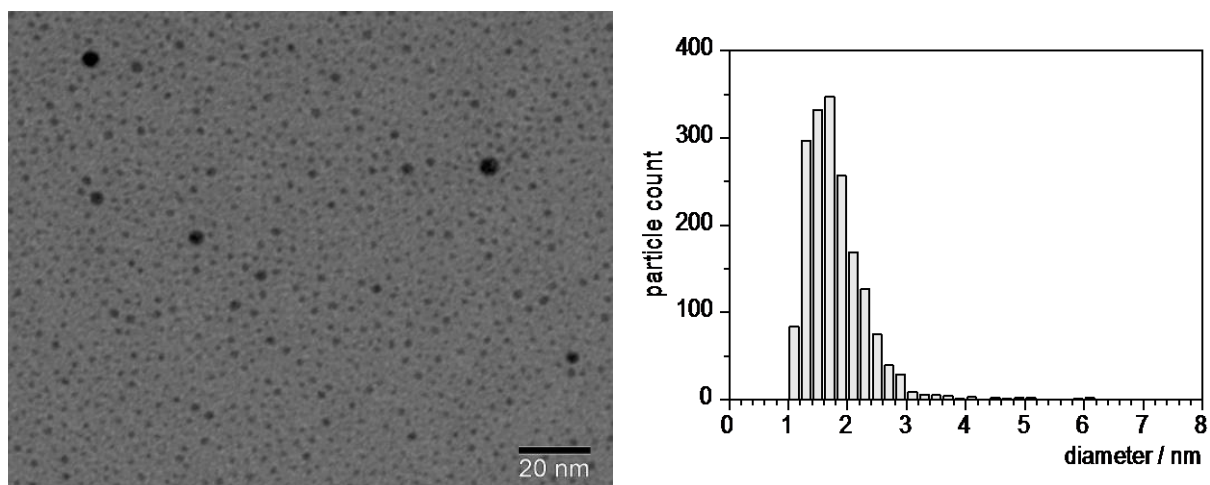


Figure 3.18 TEM image and histogram of **NP Q**

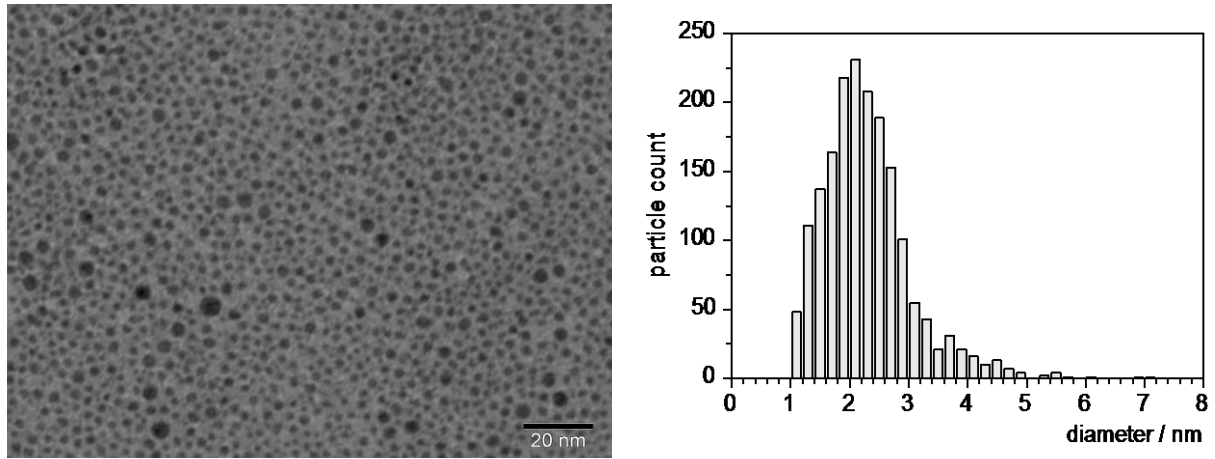


Figure 3.19 TEM image and histogram of *NP QCs*

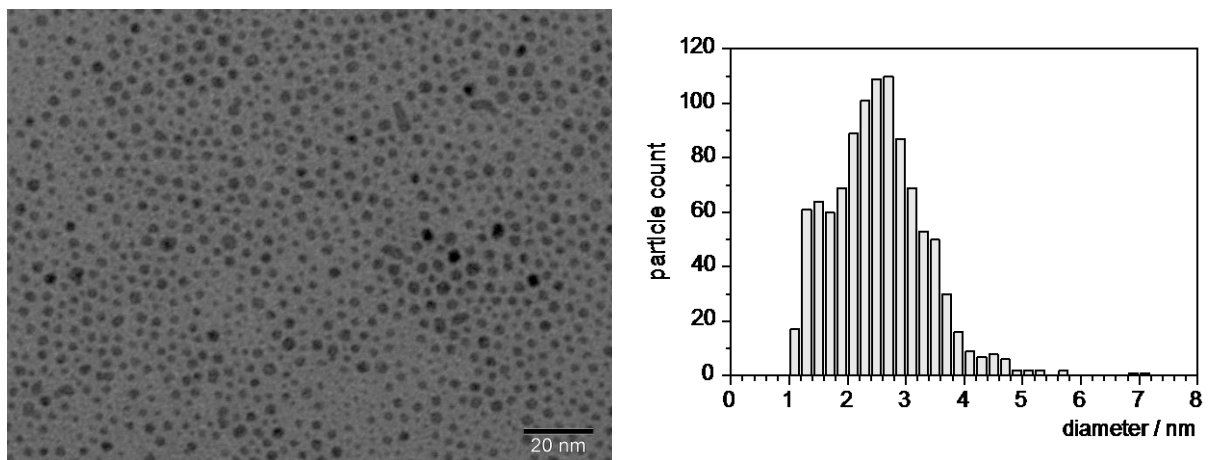


Figure 3.20 TEM image and histogram of *NP QP*

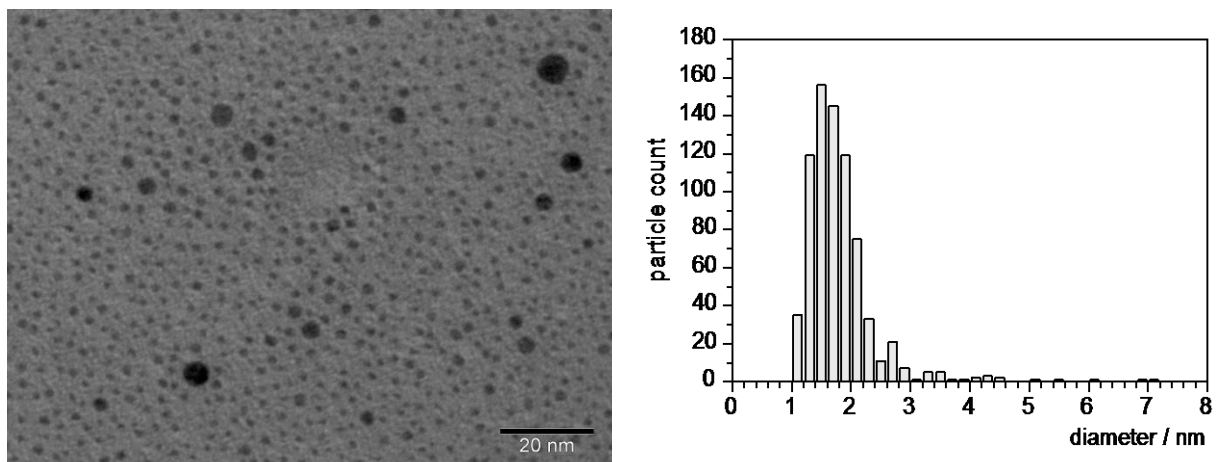


Figure 3.21 TEM image and histogram of *NP QCs*

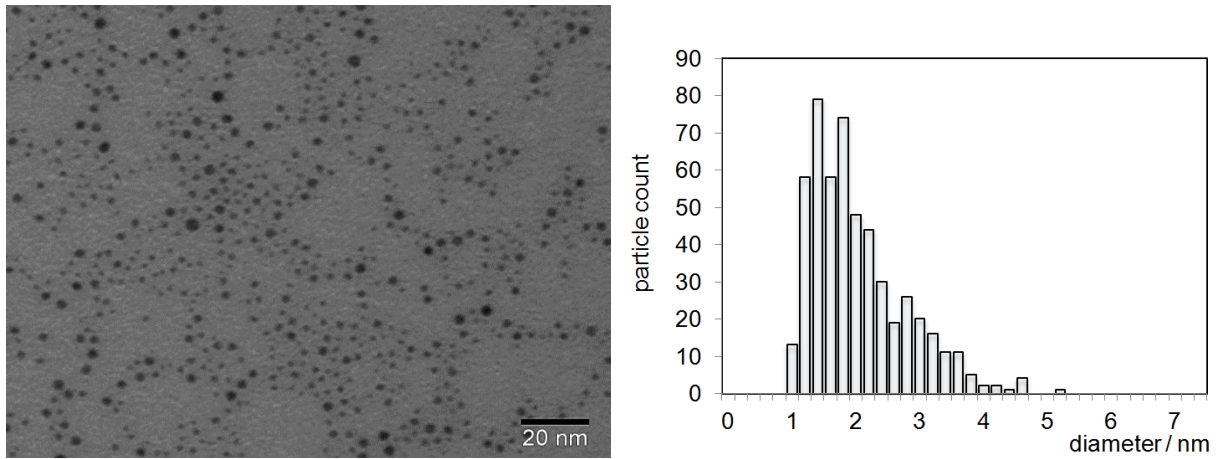


Figure 3.22 TEM image and histogram of ***NP QC_L***

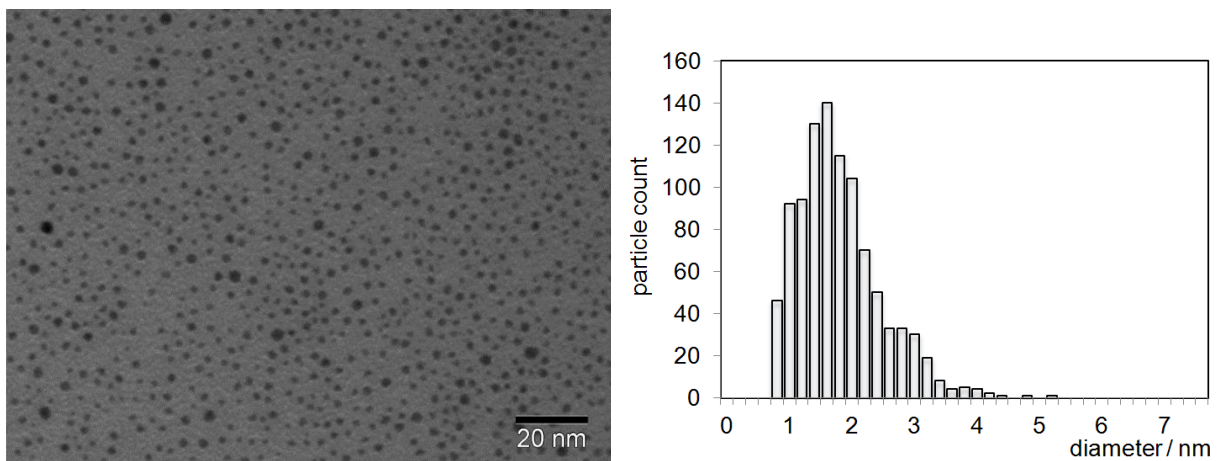


Figure 3.23 TEM image and histogram of ***NP QPC_L***

Table 3.2 Average diameters of the nanoparticles according to the TEM measurements

| | d_{TEM} / nm |
|---------------------------------|----------------|
| <i>NPQ</i> | 1.9 ± 0.6 |
| <i>NPQP</i> | 2.6 ± 0.8 |
| <i>NPQCs</i> | 2.5 ± 0.7 |
| <i>NPQPCs</i> | 1.9 ± 0.5 |
| <i>NPQC_L</i> | 2.0 ± 0.4 |
| <i>NPQPC_L</i> | 2.0 ± 0.5 |

3.3.4 Dynamic Light Scattering

Another method that was used to obtain information about the size of the nanoparticles is Dynamic Light Scattering. This method measures the speed with which particles and molecules that are in constant random thermal motion (Brownian motion) diffuse in solution and relates it to their size. The method initially provides diffusion coefficients of the particles that are converted to hydrodynamic diameters by using the Stokes-Einstein equation¹³ (Equation 3.1), where k is the Boltzmann's constant, T is the temperature (300 K), η is the viscosity of the solvent (D_2O), D is the diffusion coefficient of the nanoparticles, and d_h is the hydrodynamic diameter. The results of the DLS measurements are shown in Figure 3.24.

$$d_h = \frac{kT}{3\pi\eta D} \quad \text{Equation 3.1}$$

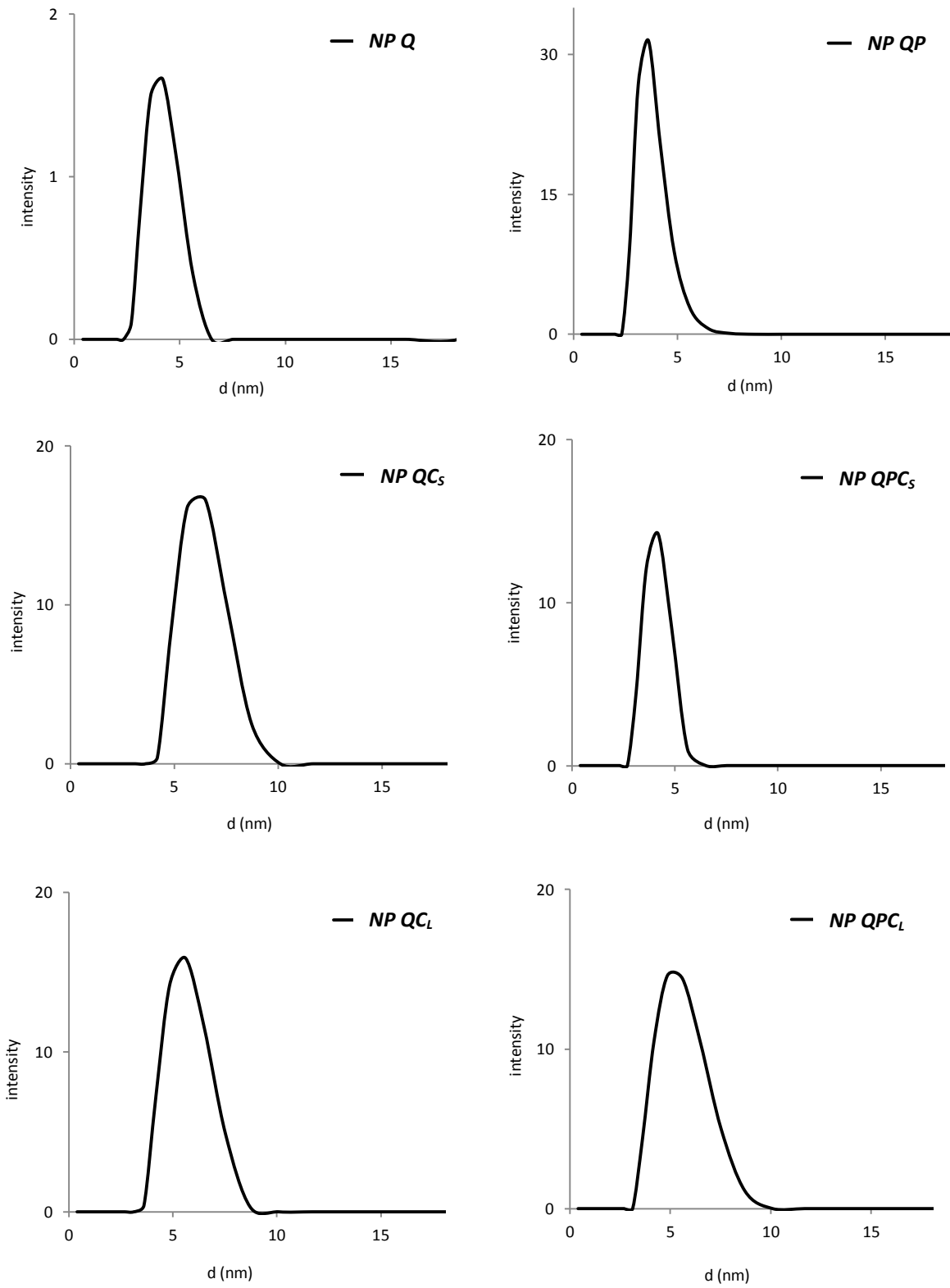


Figure 3.24 Results of the DLS measurements

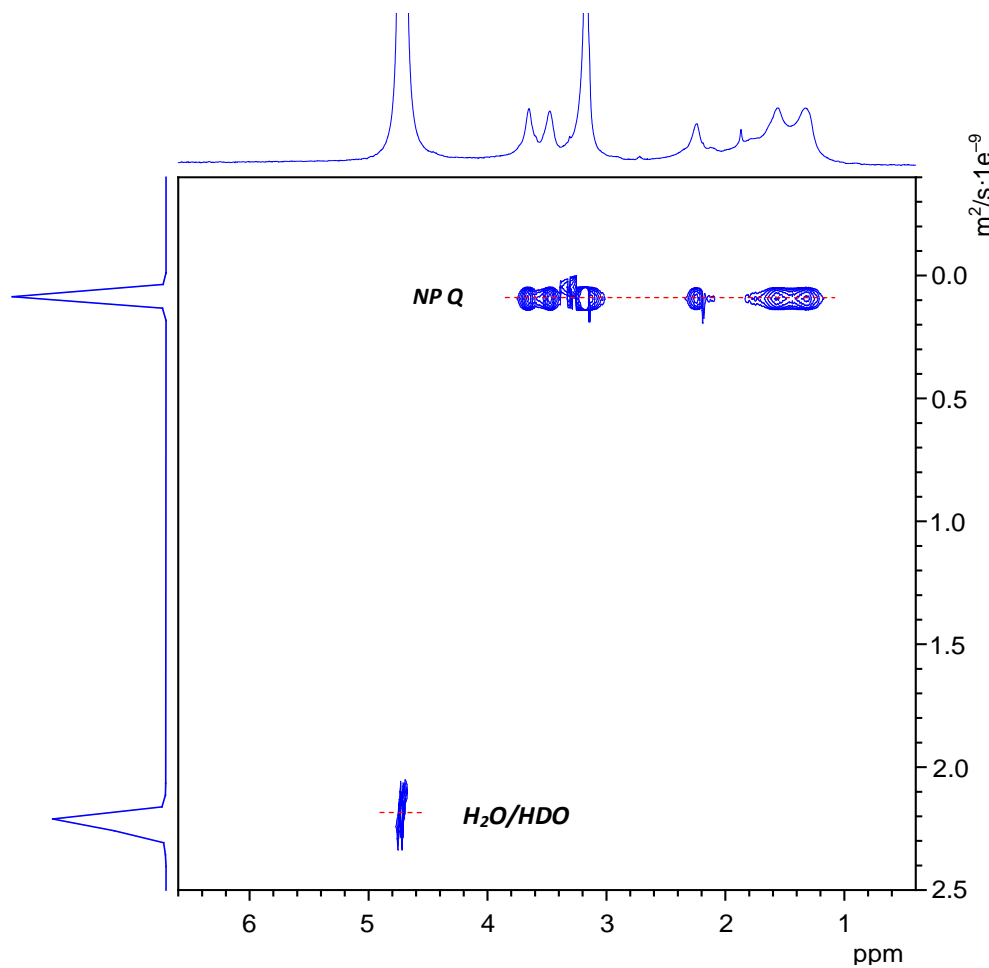
Table 3.3 shows that the hydrodynamic diameters of the nanoparticles were in the range of 4.1 to 6.2 nm according to the DLS measurements.

Table 3.3 Hydrodynamic diameters of nanoparticles from DLS measurements

| | d_{DLS} / nm |
|---------------------------------|----------------|
| <i>NPQ</i> | 4.1 ± 0.1 |
| <i>NPQP</i> | 6.0 ± 0.1 |
| <i>NPQC_s</i> | 6.2 ± 0.1 |
| <i>NPQC_s</i> | 4.1 ± 0.2 |
| <i>NPQC_L</i> | 5.6 ± 0.1 |
| <i>NPQPC_L</i> | 5.4 ± 0.1 |

3.3.5 DOSY NMR Spectroscopy

DOSY-NMR spectroscopy was used as a tool complementary to DLS to determine the diffusion coefficients of the prepared nanoparticles. In a DOSY-NMR spectrum, chemical shifts of species in solution are plotted against their diffusion coefficients. The chemical shifts are obtained by Fast Fourier transformation (FFT) of the time domain data. The diffusion coefficients are obtained by an inverse Laplace transformation (ILT) of the signal decay data.⁸⁰

3.25 2D DOSY NMR spectrum of **NP Q**

The DOSY-NMR spectra of the nanoparticles were recorded at 300 K and in D₂O. The diffusion coefficients of the individual species in the solution were referenced to the diffusion coefficient of water, which amounts to $2.18 \pm 0.03 \times 10^{-9} \text{m}^2 \text{s}^{-1}$ at 300 K according to the measurements. The diffusion coefficients of the nanoparticles were then used to estimate hydrodynamic diameters by using the Stokes-Einstein equation. The results are shown in Table 3.4.

Table 3.4 Diffusion coefficients and diameters of nanoparticles estimated by DOSY-NMR

| | D / m ² s ⁻¹ | d _{DOSY} /nm |
|---------------------------|------------------------------------|-----------------------|
| NP Q | 8.1 x 10 ⁻¹¹ | 5.0 ± 0.1 |
| NP QP | 7.4 x 10 ⁻¹¹ | 5.5 ± 0.1 |
| NP QC_S | 7.2 x 10 ⁻¹¹ | 5.6 ± 0.1 |
| NP QC_S | 8.0 x 10 ⁻¹¹ | 5.0 ± 0.1 |
| NP QL | 7.3 x 10 ⁻¹¹ | 5.6 ± 0.1 |
| NP QPC_L | 7.5 x 10 ⁻¹¹ | 5.4 ± 0.1 |

3.3.6 Iodine Decomposition

The binding properties of the prepared nanoparticles were expected to depend sensitively on the ratio of the different functional groups bound to their surface. Unfortunately, it was not possible to estimate this ratio directly from the ¹H-NMR spectra of the different nanoparticles because of the pronounced line broadening. The nanoparticles were therefore decomposed by addition of iodine. The ratios of different ligands on the nanoparticles were then determined by integrating characteristic signals of the released ligands in the ¹H-NMR spectra of the resulting solutions. An internal standard (2,4,6-trimethoxy-1,3,5-triazine) was used to follow the decomposition process and confirm that it went to completion. In addition, the integral of the signal of this standard could be used to calculate the absolute amounts of the ligands on each nanoparticle. For the determination of the ligand ratios, at least two signals of each ligand were used in order to increase reliability of the results. The ¹H-NMR spectrum of **NP QPC_S**, after iodine decomposition is shown in Figure 3.26 as an example.

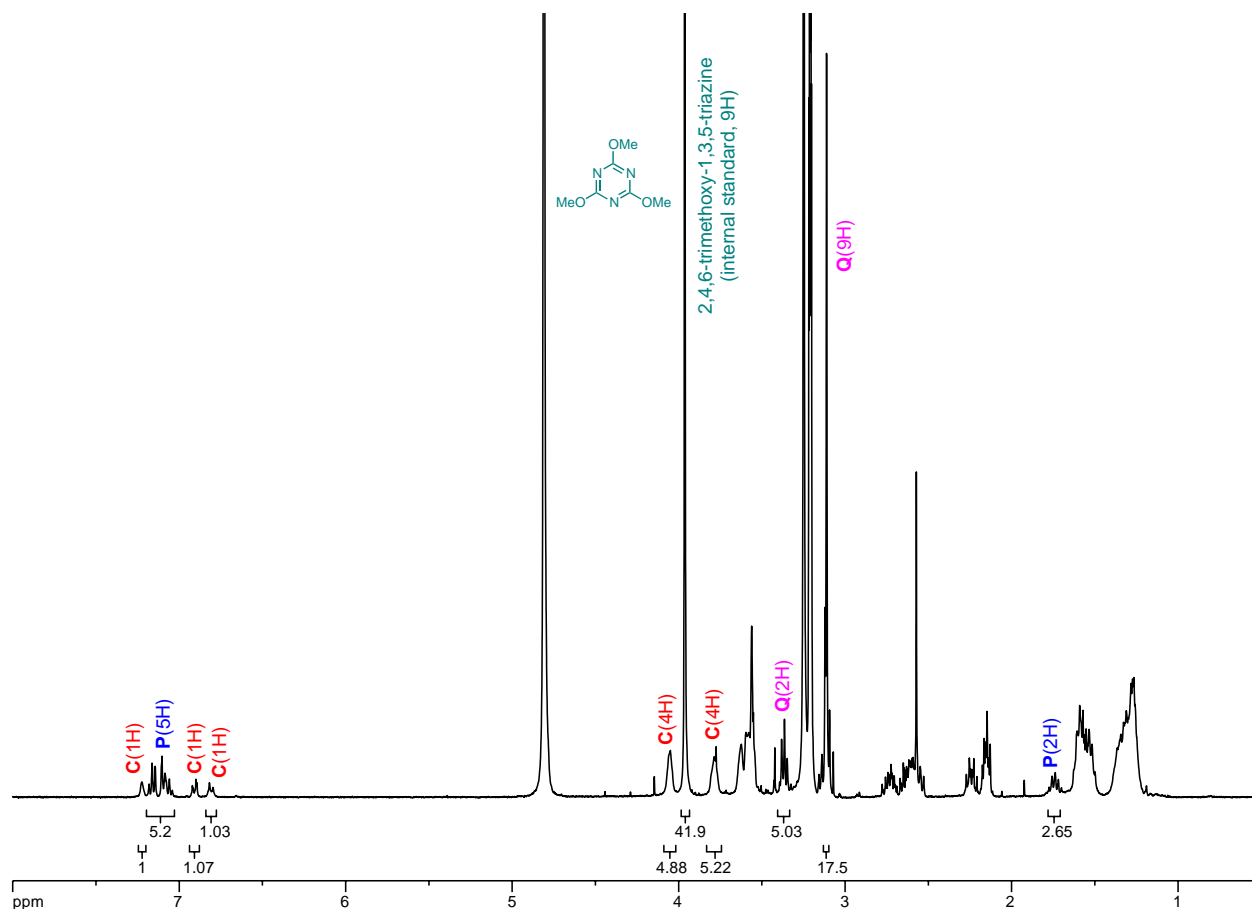


Figure 3.26 $^1\text{H-NMR}$ of NP QPC_5 after iodine decomposition

The peaks used for the assessment of surface composition and the peak belonging to the internal standard at 3.95 ppm are marked in this spectrum with different colors. By relating the integrals of the ligand signals to the one of the internal standard, and considering the known amount of the internal standard, the total amount of ligands per mg of nanoparticle could be calculated. Table 3.5 shows the results of a typical measurements by using the example of NP QPC_5 . For this measurement 2.2 mg of the nanoparticle was used and the solution contained 1.87×10^{-6} mol of the internal standard. Integration of ligand protons gave the integrals for the internal standard and for each ligand (lines 3 to 6 of Table 3.5). From these integrals, the amounts of the three ligands in solution and their total molar amount were calculated. The molar amounts were used to estimate the masses of the ligands showing that of the 2.2 mg of sample, 0.64 mg represented the organic components while 1.56 mg or 7.9×10^{-6} mol were

gold. Together with the total molar amount of adsorbed ligands this leads to a ratio of gold atoms to number of ligands of 4.27.

Table 3.5 Gold/ligand ratio calculation for *NP QPC_s*

| <i>NP QPC_s</i> | | | |
|---------------------------------------|-----------------------|---------|-------------------------|
| amount of nanoparticles | 2.20 | mg | |
| molar amount of the internal standard | 1.87×10^{-6} | mol | |
| ∫ internal standard (9H) | 3.99 | (per H) | |
| ∫ Q | 1.88 | (per H) | |
| ∫ P | 1.01 | (per H) | |
| ∫ Cs | 1.06 | (per H) | Relative Ligand Content |
| Molar amount Q | 8.83×10^{-7} | mol | 48 % |
| Molar amount P | 4.72×10^{-7} | mol | 25 % |
| Molar amount Cs | 4.97×10^{-7} | mol | 27 % |
| total molar amount of ligands | 1.85×10^{-6} | mol | |
| amount Q | 0.26 | mg | |
| amount P | 0.14 | mg | |
| amount Cs | 0.24 | mg | |
| amount Au | 1.56 | mg | |
| # Au/# Lig | 4.27 | | |

The same procedure was applied to evaluate the composition of all prepared nanoparticles. Table 3.6 summarizes the relative amounts of ligands present on the prepared nanoparticles obtained from these experiments. These experiments were performed at least three times to test the reproducibility, and the errors for the ligand ratios were estimated as $\pm 5\%$.

Table 3.6 Surface layer composition of the prepared nanoparticles resulting from the iodine decomposition experiments (estimated errors $\pm 5\%$)

| Nanoparticles | Q | QP | QC _s | QPC _s | QC _L | QPC _L |
|---------------------------|-----|----|-----------------|------------------|-----------------|------------------|
| Ligand Q (%) | 100 | 47 | 53 | 48 | 50 | 41 |
| Ligand P (%) | - | 53 | - | 25 | - | 30 |
| Ligand C _s (%) | - | - | 47 | 27 | - | - |
| Ligand C _L (%) | - | - | - | - | 50 | 29 |

3.3.7 Discussion

The NMR spectroscopic analyses of the prepared AuNPs showed only broad signals in the spectra, indicating that all nanoparticles were pure and did not contain residual unbound ligands or other impurities.

The UV-Vis spectra provided initial information about the sizes of the nanoparticles. The absence of a clear SPR band in these spectra showed that the diameters of the nanoparticles were around 2 nm.²⁵ This result was confirmed by transmission electron microscopy.

The corresponding images and histograms showed that the core diameters of all synthesized nanoparticles were in the expected range of ca. 2 nm with small differences. The diameters observed for the different nanoparticles were reproducible for different batches. Notably, for **NP QP** and **NP QCs** larger diameters, respectively 2.6 and 2.5 nm, were observed while all other nanoparticles have diameters between 1.9-2.0 nm. At the moment it is unclear why certain nanoparticles turned out to be larger than the others although they were prepared from the same batch of **NP A**. It seems as if exchange reactions and potentially also the nature of the ligands affect the size of the nanoparticles in exchange reactions in some extent.

The DLS results provided information about the hydrodynamic diameters of the nanoparticles including the organic monolayer. The obtained diameters are therefore consistently larger than

the diameters obtained by TEM, which only reflect the sizes of the gold cores. Relating the diameters obtained from DLS and TEM allows calculations of the thickness of the monolayers L_{shell} according to $L_{shell} = (d_{DLS} - d_{TEM}) / 2$.

These calculations were based on the assumption of having globular shaped particles. They yielded thicknesses of 1.1 nm for the nanoparticles **NP Q** and **NP QPCs** and of 1.7-1.8 nm for the other nanoparticles (Table 3.7).

Table 3.7 Hydrodynamic diameters of nanoparticles from DLS measurements, average diameters from TEM, and the calculated thickness of the ligand shell

| | d_{DLS} / nm | d_{TEM} / nm | L_{shell} / nm |
|---------------------------|----------------|----------------|------------------|
| NP Q | 4.1 ± 0.1 | 1.9 ± 0.6 | 1.1 ± 0.7 |
| NP QP | 6.0 ± 0.1 | 2.6 ± 0.8 | 1.7 ± 0.9 |
| NP QC_S | 6.2 ± 0.1 | 2.5 ± 0.7 | 1.8 ± 0.8 |
| NP QC_S | 4.1 ± 0.2 | 1.9 ± 0.5 | 1.1 ± 0.6 |
| NP QC_L | 5.6 ± 0.1 | 2.0 ± 0.4 | 1.8 ± 0.5 |
| NP QPC_L | 5.4 ± 0.1 | 2.0 ± 0.5 | 1.7 ± 0.6 |

The calculated values for the monolayer thicknesses (L_{shell}) were compared with the lengths of the ligands, estimated from the calculated ligand structures with the alkyl chains in their thermodynamically preferred extended conformations, by using Chem3D (Figure 3.27). The results show that the determined L_{shell} is mostly smaller than the predicted ligand lengths even when considering the relatively large errors of L_{shell} , indicating that the ligands most likely prefer folded conformations when bound to the nanoparticle surface.

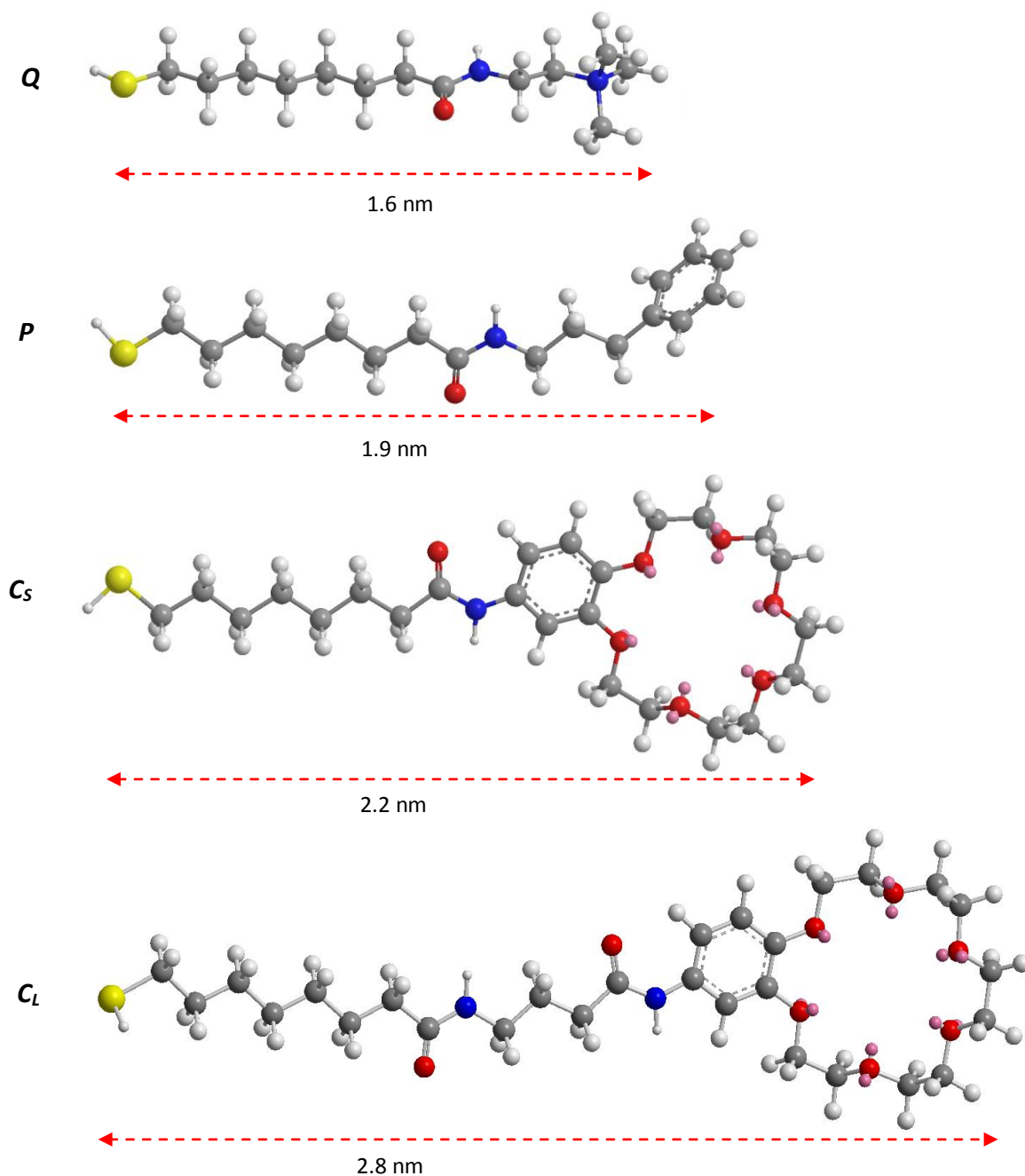


Figure 3.27 Extended conformations of the ligands and their corresponding lengths. The images were generated by using Chem3D Ultra 8.0 (Cambridge Soft).

The hydrodynamic diameters of the nanoparticles determined by DLS and DOSY-NMR spectroscopy are compared in Table 3.8. This table shows that the results are in good agreement. The nanoparticles that had slightly larger core diameters (**NP QP** and **NP QCs**) also displayed slightly larger hydrodynamic diameters, and the nanoparticles with longer ligands (**NP QC_L** and **NP QPC_L**) also possessed larger hydrodynamic diameters.

Table 3.8 Comparison of the hydrodynamic diameters of the nanoparticles estimated by DLS and DOSY-NMR spectroscopy

| | d_{DLS} / nm | d_{DOSY} / nm |
|---------------------------|----------------|-----------------|
| NP Q | 4.1 ± 0.1 | 5.0 ± 0.1 |
| NP QP | 6.0 ± 0.1 | 5.5 ± 0.1 |
| NP QCs | 6.2 ± 0.1 | 5.6 ± 0.1 |
| NP QPCs | 4.1 ± 0.2 | 5.0 ± 0.1 |
| NP QC_L | 5.6 ± 0.1 | 5.6 ± 0.1 |
| NP QPC_L | 5.4 ± 0.1 | 5.4 ± 0.1 |

Iodine decomposition provided detailed information about the composition of the prepared nanoparticles, also confirming the presence of the corresponding ligands on the surface. All mixed monolayer protected nanoparticles contained ca. 50 % of ligand **Q**, ensuring water solubility. The other portion comprised the second ligand in case only two ligands were bound to the surface. In the case of **NP QPC_S** and **NP QPC_L**, the ligand **P** and **C_S** or **C_L** were present in almost equal amounts.

The use of the internal standard also allowed determining of the ratio of ligands and gold atoms on the nanoparticles. This ratio depends on the packing density of the ligands on the nanoparticle surface and on particle size. Leff et al.⁸¹ introduced a model that allows calculation of the number of gold atoms in a nanoparticle of given size, the number of surface atoms, and

the number of ligands by using the equations 3.2-3.4. This model, developed to estimate the composition of gold crystals decorated with dodecanethiol molecules, is based on the assumption of closely packed ligands with a specific distance between them. The number of gold atoms was calculated by using equation 3.2 where n is number of gold atoms and v_g is the volume of one gold atom which amounts to ca. $\sim 17 \text{ \AA}^3$. For the calculations performed in this work, the radius of the gold core $d_{TEM}/2$ was calculated from the diameters obtained in the TEM measurements.

$$n = 4\pi (d_{TEM}/2)^3 / (3v_g) \quad \text{Equation 3.2}$$

The number of surface gold atoms (n_{out}) was calculated by using equation 3.3 where the radius of the nanoparticles is reduced by the thickness of one layer of gold atoms, which is estimated to amount to 2.38 \AA .

$$n_{out} = (4\pi/3v_g) [(d_{TEM}/2)^3 - (d_{TEM}/2 - 2.38)^3] \quad \text{Equation 3.3}$$

Finally, the number of thiol ligands was calculated using equation 3.4. Here it is assumed that each thiol on the surface of a gold nanoparticle occupies an area of 21.4 \AA^2 .

$$n_{thiol} = 4\pi (d_{TEM}/2)^2 / (21.4) \quad \text{Equation 3.4}$$

Table 3.9 shows the application of the Leff model to **NP QPC_s**. This nanoparticle has a diameter measured by TEM of 1.9 nm. According to equations 3.2-3.4, it should therefore contain 211 gold atoms of which 122 are located on the surface. The number of ligands on the surface was thus calculated to amount to 53.

The iodine decomposition experiment of this nanoparticle yielded a ratio #gold atoms/ #ligands of 4.27. If the nanoparticle contains 211 gold atoms it should therefore feature 49 ligands on the surface, a value closely matching the one predicted theoretically.

Table 3.9 Calculated and experimental values for surface coverage for **NP QPC₅**

| NP QPC₅ | | |
|-------------------------------|-------|--------------------------------------|
| NP diameter | 1.90 | nm |
| # Au atoms in nanoparticle | 211 | } Calculated values (Leff et al.) |
| # surface Au atoms | 122 | |
| # ligands on surface | 53 | |
| coverage (# Lig/# surface Au) | 43.3% | |
| # Au/# Lig | 4.27 | } Experimental values |
| # ligands on surface | 49 | |
| coverage (# Lig/# surface Au) | 40.4% | |

The same calculations were performed for all prepared nanoparticles and the results are summarized in Table 3.10. This table shows that the calculated numbers of ligands on the surface of the individual nanoparticles and the predicted ones based on the Leff model are in good agreement for every nanoparticle. The table also contains the experimental surface coverage of the nanoparticles calculated from equation 3.5.

$$(\# \text{ ligands on surface} / \# \text{ gold surface atoms}) \times 100 \quad \text{Equation 3.5}$$

The surface coverages thus calculated are consistently lower than the value predicted by Murray for dodecanethiol functionalized gold nanoparticles with a diameter of 2 nm, which should amount to 52%.⁸²

Table 3.10 The number of surface ligands and gold atoms, and the surface coverages of the prepared nanoparticles

| Nanoparticles | Q | QP | QC _s | QPC _s | QC _L | QPC _L |
|-----------------------------|------|------|-----------------|------------------|-----------------|------------------|
| d_{TEM} (nm) | 1.90 | 2.60 | 2.50 | 1.90 | 1.96 | 1.98 |
| # gold atoms | 211 | 541 | 481 | 211 | 232 | 239 |
| # total ligand | 48 | 113 | 97 | 49 | 56 | 55 |
| coverage (theoretical) (%) | 43.3 | 40.3 | 40.6 | 43.3 | 43.0 | 42.9 |
| coverage (experimental) (%) | 39.3 | 45.8 | 43.0 | 40.4 | 43.0 | 40.9 |

To summarize, the exchange reaction used to prepare the mixed monolayer protected nanoparticles afforded the desired products in high purity. These particles had core diameters of 1.9-2.6 nm, while the thickness of the monolayers were 1.1-1.8 nm. Comparison with the calculated maximum lengths of the ligands indicated that they likely adopt folded conformations on the nanoparticle surfaces. Moreover, the iodine experiments provided information about the number of ligands on the nanoparticle surfaces, which were in good agreement with theoretically predicted numbers.

An aspect that could not be clarified is the observation that the isolated mixed monolayer protected nanoparticles turned out to have different diameters, even if they were prepared from the same batch of precursor nanoparticle **NP A**. Whether nanoparticle size or nanoparticle aggregation is affected during the exchange reaction or is possibly influenced by the ligands present in the reaction mixture should be the subject of further investigations.

3.4 Binding Studies

3.4.1 ^1H -NMR Spectroscopy

Estimation of the strength with which nanoparticles form supramolecular complexes is challenging because the binding model, i.e. the number of low molecular weight target molecules that bind to each nanoparticle, is often not well defined. Various analytical techniques have been used in order to quantitatively estimate the strengths of these interactions, for example isothermal titration calorimetry or NMR, UV-Vis, and fluorescence spectroscopy. In all cases, the change of a measurable physical property caused by the binding event is used to obtain qualitative or quantitative information about the interacting binding partners.

NMR spectroscopy is one of the most useful techniques for the evaluation of binding equilibria in systems, in which molecular recognition takes place between host and guest molecules. Under the conditions where fast exchange occurs on the NMR time scale, one signal is observed for the complex at the population-averaged chemical shift of the corresponding free binding partner and its complex.⁸³ By changing the ratio of the binding partners, a binding isotherm can be obtained that allows quantification of binding strength provided that complex stoichiometry is known.

To evaluate whether NMR spectroscopy is a suitable method to quantify the binding of peptides to the functionalized nanoparticles, ^1H -NMR titration experiments were performed. In these titrations, increasing amounts of **NP Q** were added to a solution of GlyGly (0.05 mM) in D_2O . The chemical shifts of peaks of the peptide were followed in order to assess the effect of the presence of the nanoparticles.

The obtained NMR spectra showed small but clearly visible downfield shifts of peptide signals with increasing nanoparticle concentration, which indicate that interactions could indeed occur (Figure 3.28).

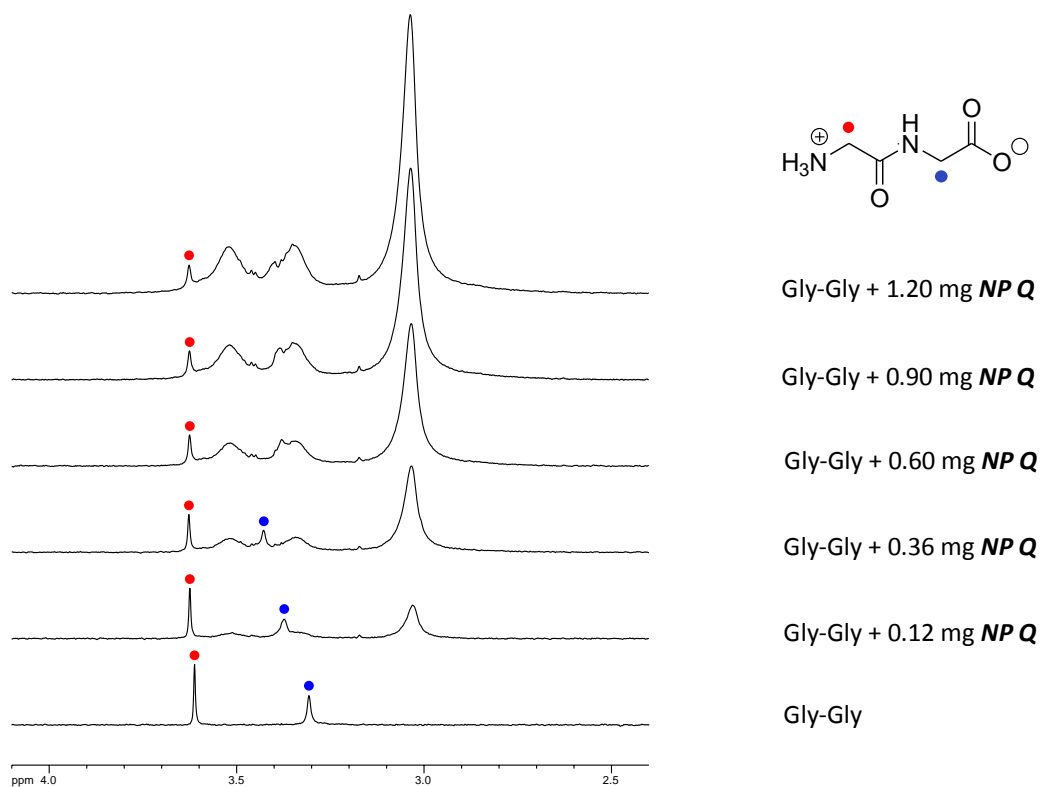


Figure 3.28 ^1H NMR titration of **NP Q** with GlyGly (0.05 mM) in D_2O

Of the two peptide signals, the one which is more shielded at 3.3 ppm was observed to experience the larger shift in the presence of the nanoparticle. This signal was assigned to the protons in the CH_2 group of the C-terminal glycine residue of the dipeptide according to the literature.⁸⁴ Pronounced overlaps of the peptide signals and those of the nanoparticle made it difficult to follow the course of the signal shifts during the whole titration.

The interaction of **NP QPC₅** with the dipeptide Gly-Phe was investigated analogously. Also in this case, overlaps of peptide and nanoparticle signals were observed and the multiplicity of the peptide signals further complicated following their shifts.

3.4.2 DOSY-NMR Spectroscopy

DOSY-NMR spectroscopy is increasingly used to analyze intermolecular interactions in multicomponent systems and to estimate association constants.^{69, 85} The applicability of DOSY NMR spectroscopy to follow binding equilibria derives from the fact that host and guest molecules in their respective free states have their own diffusion coefficients, depending on their size and molecular weight. When these molecules engage in binding equilibria that are fast exchange on the NMR time scale, the observed diffusion coefficient (D_{obs}) is a weighted average of the diffusion constants of the free (D_{free}) and the bound (D_{bound}) states.⁸⁰ Thus, if D_{free} and D_{bound} are known, the fraction of the complex and its association constant can be calculated. Specifically, the fraction χ of the complex in an equilibrium can be calculated from Equation 3.6.

$$\chi = (D_{free} - D_{obs}) / (D_{free} - D_{bound}) \quad \text{Equation 3.6}$$

When it is difficult to determine D_{bound} , i.e. the diffusion constant of the complex, certain assumptions can be made. If, for example, one binding partner has a significantly higher molecular weight than the other one, complex formation will likely not affect the diffusion constant of this species to a large extent and this constant can therefore be assumed to equal D_{bound} . This should be the case for peptide binding to the investigated nanoparticles, where D_{free} is the diffusion constant of the peptide, D_{bound} that of the nanoparticle and D_{obs} the apparent diffusion constant of the peptides in mixtures of nanoparticles and peptides. Equation 3.2 thus allows calculation of the fraction of peptides bound to the nanoparticles.

To test the applicability of DOSY-NMR spectroscopy for the evaluation of dipeptide binding to the nanoparticles, solutions were prepared containing mixtures of a dipeptide and a nanoparticle and DOSY-NMR spectra were recorded. As dipeptides, Gly-Gly and Gly-Phe were chosen. To ensure comparability of the measurements, the same dipeptide concentrations were used and the nanoparticles were used in amounts that lead to comparable overall concentrations of the surface bound ligands. These amounts were calculated based on the estimated compositions of the nanoparticles. The diffusion coefficients of free dipeptides D_{free}

were determined in independent experiments. Figure 3.29 shows the DOSY-NMR spectrum of a mixture of **NP Q** and Gly-Phe in D₂O as an example.

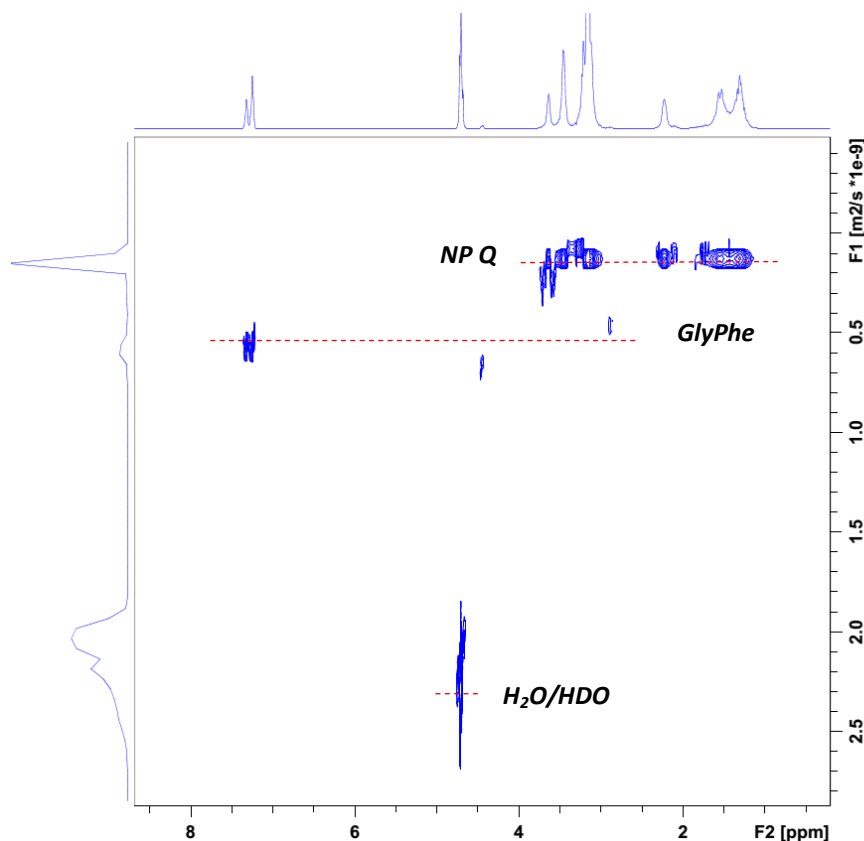


Figure 3.29 2D DOSY NMR spectrum of a mixture of **NP Q** ($c(\text{lig}_{\text{tot}}) = 1.9$ mM) and Gly-Phe (0.96 mM) in D₂O

This 2D spectrum shows the ¹H-NMR spectrum of the mixture of **NP Q** and Gly-Phe on one axis and the diffusion coefficients on the other. The different diffusion coefficients of the nanoparticle, of the peptide, and also of the residual H₂O molecules in the solution are clearly visible. The diffusion coefficients were typically determined by nonlinear fitting of the intensity against the gradient strength curve obtained from the DOSY-NMR measurements by using a routine implemented in the TopSpin software. In some spectra, overlapping signals of nanoparticles and dipeptides were observed, and the diffusion coefficients D_{obs} were in these cases determined by resolving the decay of the overlapping peaks by biexponential fitting, using the independently determined nanoparticle diffusion coefficients as known values.⁸⁶ The

diffusion coefficient of HDO exhibited excellent reproducibility throughout all measurements. The obtained diffusion coefficients were used to calculate the fractions of bound peptide χ by using equation 3.6. The results of all measurements are summarized in Table 3.11.

Table 3.11 Results of the DOSY-NMR measurements performed in D₂O at 300 K with a dipeptide concentration of 0.072 nM

| | total ligand concentration / mM | D_{free} / $\times 10^{-9} \text{ m}^2 \text{ s}^{-1}$ | D_{bound} / $\times 10^{-10} \text{ m}^2 \text{ s}^{-1}$ | D_{obs} / $\times 10^{-9} \text{ m}^2 \text{ s}^{-1}$ | χ / % |
|--------------------------|------------------------------------|--|--|---|---------------|
| NP Q + Gly-Phe | 1.88 | 5.82 | 0.81 | 3.93 | 38 |
| NP QCs + Gly-Phe | 1.81 | 5.82 | 0.72 | 4.24 | 31 |
| NP QP + Gly-Phe | 1.90 | 5.82 | 0.74 | 4.75 | 21 |
| NP QCL + Gly-Phe | 2.11 | 5.82 | 0.70 | 4.15 | 33 |
| NP QPCs + Gly-Phe | 1.99 | 5.82 | 0.80 | 1.91 | 78 |
| NP QPCL + Gly-Phe | 1.92 | 5.82 | 0.75 | 1.68 | 81 |
| NP Q + Gly-Gly | 1.88 | 7.49 | 0.81 | 5.36 | 32 |
| NP QCs + Gly-Gly | 1.80 | 7.49 | 0.72 | 5.94 | 23 |
| NP QP + Gly-Gly | 1.90 | 7.49 | 0.74 | 6.22 | 19 |
| NP QCL + Gly-Gly | 2.11 | 7.49 | 0.70 | 4.62 | 42 |
| NP QPCs + Gly-Gly | 1.99 | 7.49 | 0.80 | 4.25 | 48 |
| NP QPCL + Gly-Gly | 1.92 | 7.49 | 0.75 | 3.73 | 56 |

Table 3.11 clearly shows that DOSY-NMR spectroscopy provided quantitative information about the extent to which the dipeptides interacted with the nanoparticles. Titrations were therefore subsequently performed by measuring the DOSY-NMR spectra of solutions that contained a constant nanoparticle concentration and increasing amounts of a dipeptide. Because these measurements were rather time consuming, they were only performed with dipeptide Gly-Phe and the nanoparticles **NP Q**, **NP QP**, **NP QCs** and **NP QPCs**.

In all titrations, a continuous increase of the diffusion coefficient of the peptide was observed with increasing peptide concentrations, indicating the expected decrease of χ in the same

direction. The fraction of bound peptide calculated from the observed diffusion coefficients, plotted against peptide concentration yielded the graphs shown in Figure 3.30.

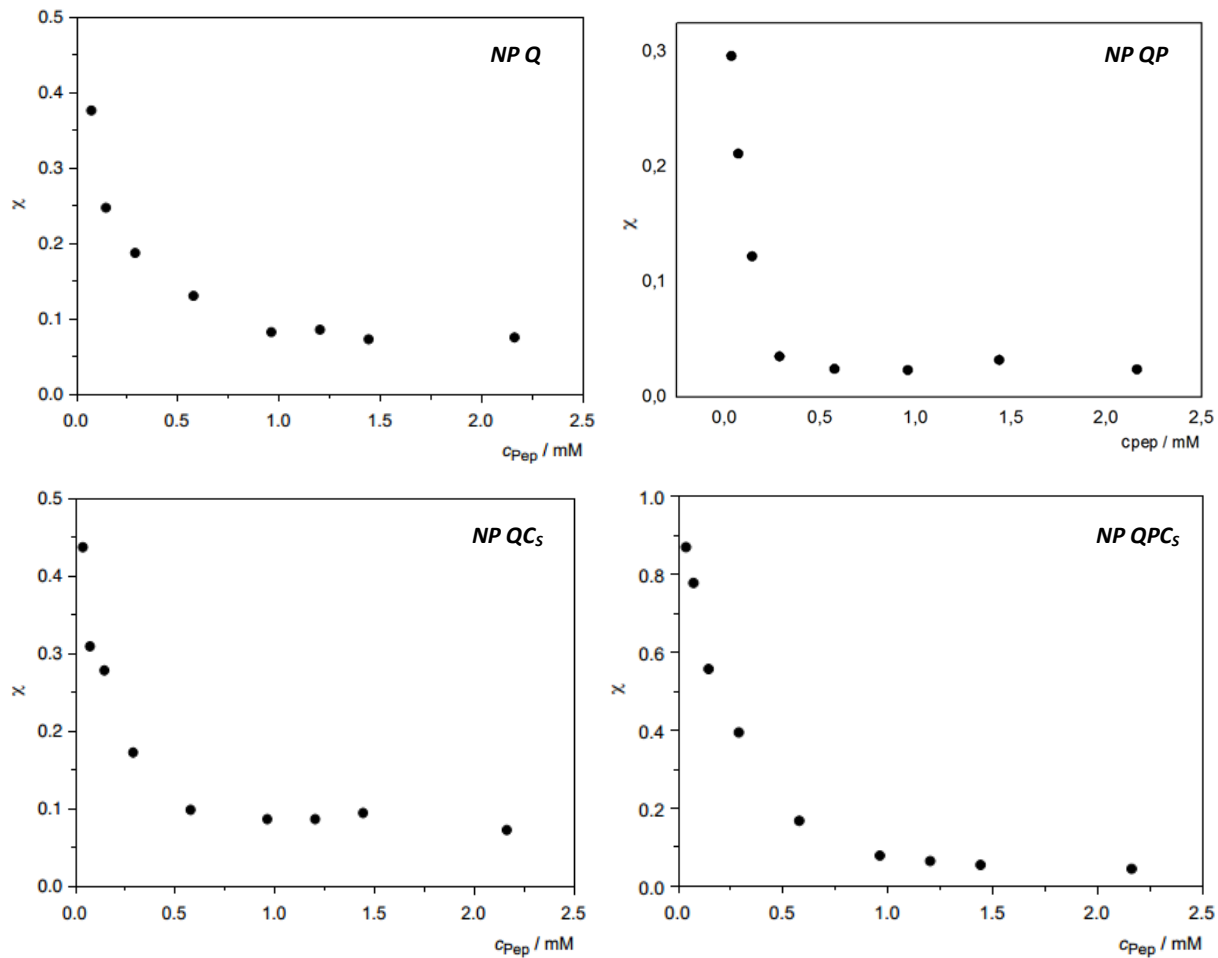


Figure 3.30 Changes of the fractions of bound Gly-Phe in the presence of nanoparticles **NP Q**, **NP QP**, **NP QC₅** and **NP QPC₅** with increasing peptide concentration

3.4.3 Fluorescence Spectroscopy

Fluorescence spectroscopy was used as an independent means to characterize the binding properties of the prepared nanoparticles and to verify the results obtained by DOSY-NMR spectroscopy.

Fluorescence spectroscopy is used in a number of analytical applications such as medicinal diagnostic or cellular and molecular imaging.⁸⁷ The fluorescence spectra of the amino acids tryptophan (Trp) and tyrosine (Tyr) contain, for instance, important information about the environment of these amino acids in proteins.⁸⁸ One advantage of fluorescence spectroscopy is its high sensitivity. The use of this method requires, however, that a suitable fluorescence chromophore is present in the investigated systems or that it can be easily introduced.⁸⁹⁻⁹⁴

The interaction between supramolecular binding partners of which one or both contains a fluorescence chromophore can lead to an increase ('turn-on') or a decrease ('turn-off', quenching) of the emission.⁹⁵ In the case of gold nanoparticles, binding of fluorescent chromophores to the particles typically results in the quenching of their emission. This quenching is attributed to the effects of the plasmon field of the nanoparticles on the transition of the excited state of the chromophore to the ground state. The level of quenching depends on the field strength in addition to the size of the gold nanoparticle. This effect has been used in a number of molecular sensing applications.⁹⁶⁻¹⁰¹

One example of the use of fluorescence spectroscopy for the characterization of the binding of a low molecular weight compound to monolayer protected AuNPs has been described by Rotello.⁵⁶ It involves the binding of anionic flavin mononucleotides to trimethylammonium functionalized AuNPs, which resulted in a dramatic decrease of fluorescence that also allowed obtaining quantitative information about the strength of binding. To transfer this concept to the investigation of the nanoparticles studied in this work, peptide Gly-Trp (Figure 3.31) was used as a substrate.

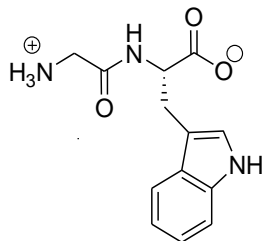


Figure 3.31 Chemical structure of dipeptide Gly-Trp

In order to determine the optimum excitation wavelength of dipeptide Gly-Trp in aqueous media, emission spectra of a solution of Gly-Trp (1.5×10^{-6} M) in water were recorded at different excitation wavelengths. Figure 3.32 shows the series of spectra obtained in the range of 200-500 nm when the excitation wavelength was varied between 250-320 nm.

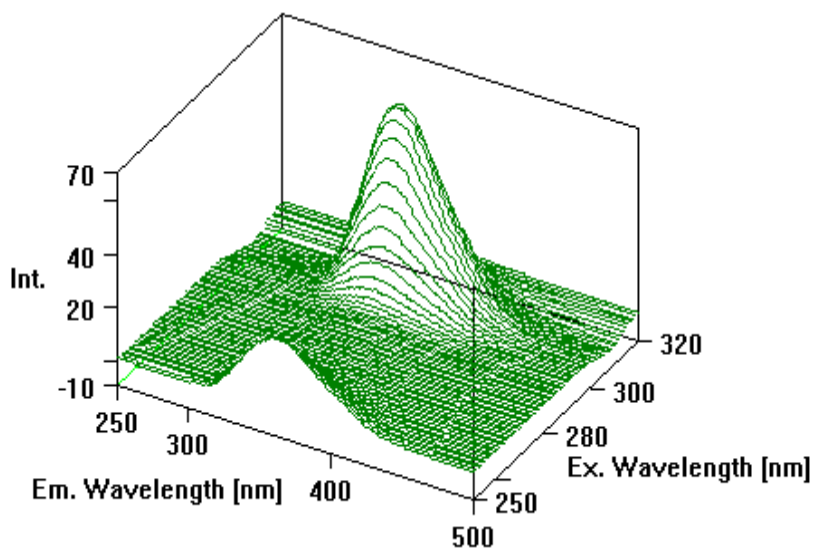


Figure 3.32 Stack plot of the emission spectra obtained when exciting a solution of a Gly-Trp (1.5×10^{-6} M) in water with wavelengths ranging between 250 and 320 nm

The excitation wavelength leading to the most pronounced emission was found to be 295 nm. The corresponding fluorescence spectrum obtained by exciting Gly-Trp at 295 nm is shown in Figure 3.33. It shows that the maximum of the emission band is located at 360 nm.

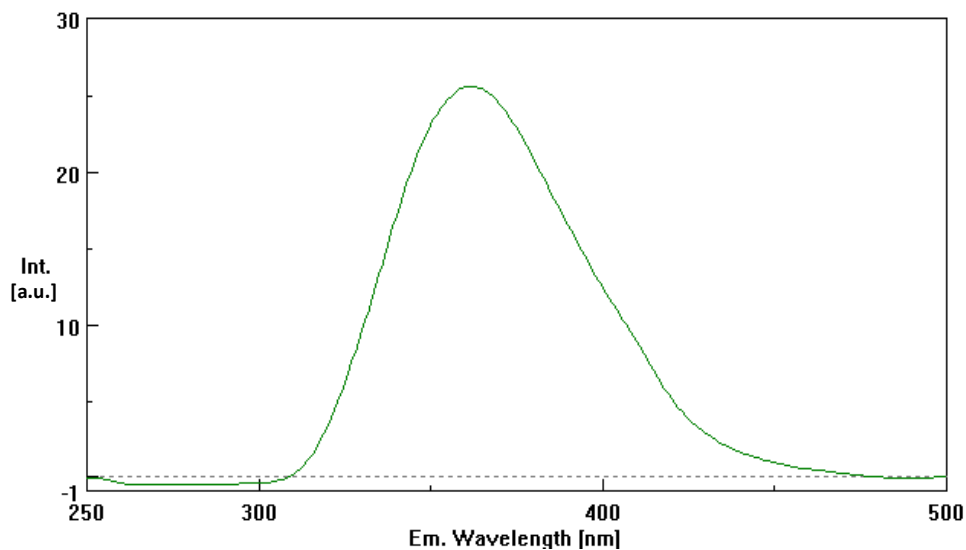


Figure 3.33 Fluorescence spectrum of a solution of Gly-Trp (1.5×10^{-6} M) in water (excitation wavelength 295 nm)

Figure 3.34 shows that the intensity of the emission band of Gly-Trp slowly decreases when the solution is continuously irradiated at 295 nm, demonstrating that photo-bleaching occurs to some extent under these conditions. After 30 minutes, ca. 12% decrease in fluorescent intensity of the sample was observed.

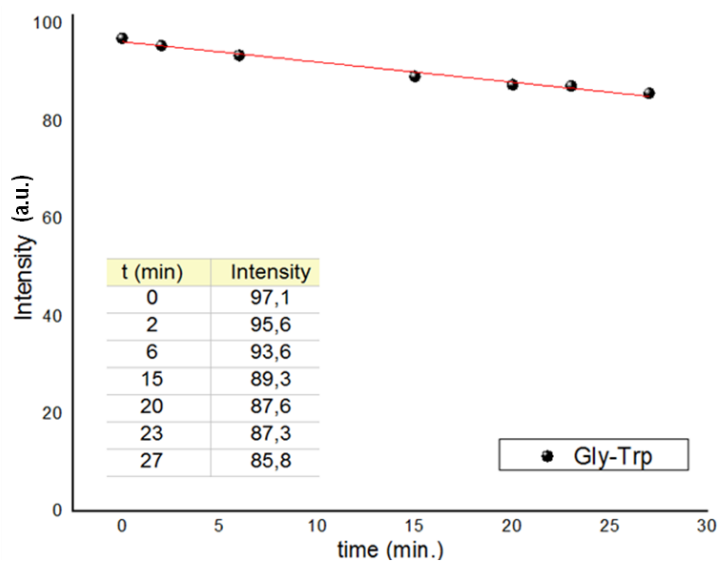


Figure 3.34 Photo-bleaching of Gly-Trp (0.33 mM) irradiated at 295 nm for 30 min in water

Because the binding studies require precise measurement of the fluorescence intensity of Gly-Trp, this photo-bleaching should be avoided. Fluorescence intensity was therefore determined in the binding studies by following the intensity at the fixed wavelength of 360 nm for only 60 s. Figure 3.35 shows the result of such a measurement when using a solution of Gly-Trp (1.5×10^{-6} M) in water.

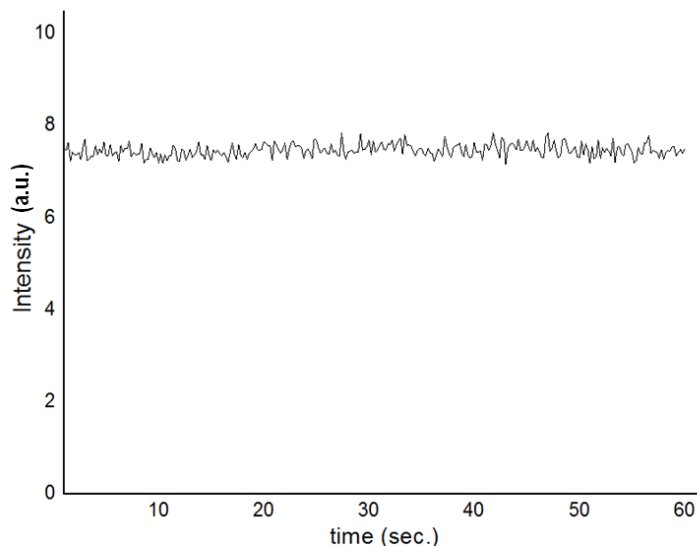


Figure 3.35 Intensity of the emission at 360 nm of a solution of Gly-Trp (1.5×10^{-6} M) in water (excitation wavelength 295 nm) when irradiated for 60 s.

To identify the best concentration regime for the binding studies in which peptide concentration and fluorescence intensity ideally correlate in a linear fashion, the emission intensities of solutions of Gly-Phe at 360 nm were measured when varying the peptide concentration between 0.015 and 0.67 mM. Figure 3.36 shows the results.

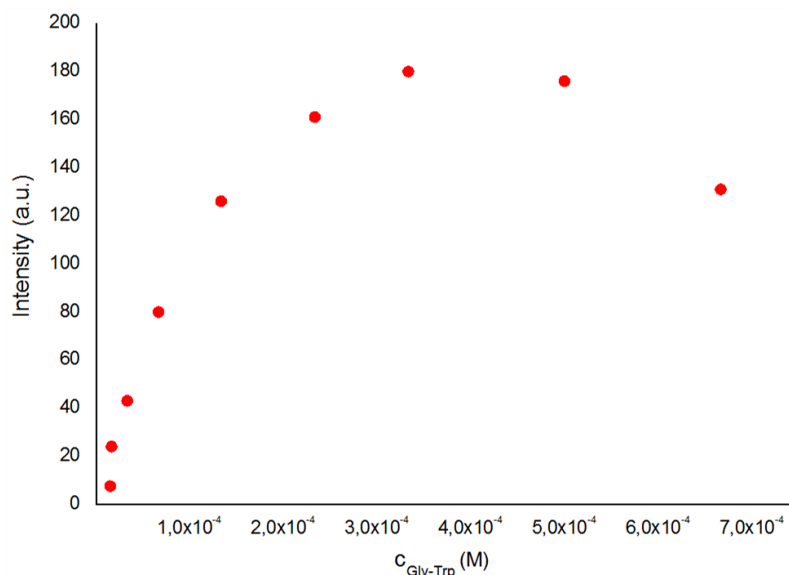


Figure 3.36 Dependence of the emission intensity of Gly-Trp at 360 nm in water on the peptide concentration (excitation wavelength 295 nm)

Figure 3.36 shows that fluorescence intensity increases when increasing the concentration of Gly-Trp, although not linearly when the dipeptide concentration exceeds 0.4 nM. Above this concentration, self-quenching sets in so that intensity decreases at higher peptide concentrations. These results suggested that the binding studies should best be performed at concentrations below 0.4 nM, depending on the desired concentrations of AuNPs in the titration experiments.

For the binding studies, increasing amounts of a solution of nanoparticle was added to Gly-Trp (1.5×10^{-6} M) in water and the fluorescence intensity was recorded at 360 nm. Figure 3.37 shows the results of such a titration for **NP Q** as an example. The nanoparticle stock solutions for these measurements were prepared by dissolving amounts of the nanoparticles in water that yield a total ligand concentration of 1.9 ± 0.2 mM in every case.

The figure clearly shows the expected decrease of fluorescence intensity with increasing nanoparticle concentration, which could be due to the binding of the peptide to the nanoparticle and the associated fluorescence quenching. It has to be considered, however, that the optical transmission of the solution strongly decreases when adding nanoparticles, which

also causes a loss of emission intensity. In addition, also scattering effects could reduce the overall emission intensity of the solution. To evaluate the extents to which these effects influence the measurement, an independent titration was performed by using an aqueous NaCl solution (0.2 M) as solvent instead of water. The presence of the salt is expected to suppress binding of the peptide to the nanoparticle thus eliminating the specific binding effects on the fluorescence intensity. The change of fluorescent intensity when increasing the nanoparticle concentration in the salt solution is also plotted in Figure 3.37

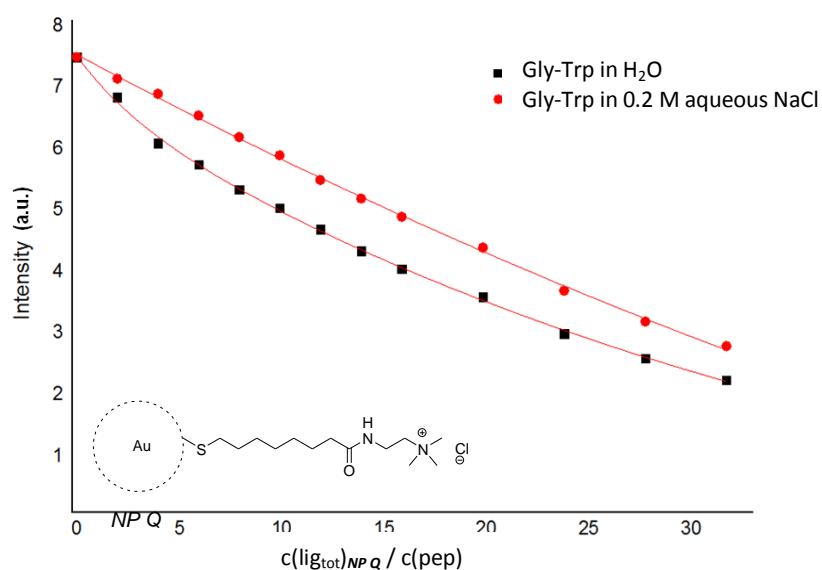


Figure 3.37 Decrease of fluorescence intensity when adding increasing amounts of **NP Q** to solutions of Gly-Trp (1.5×10^{-6} M) in water (black squares), and in 0.2 M aqueous NaCl (red circles)

As expected, increasing the nanoparticle concentration in the solution causes a substantial reduction of fluorescence intensity which almost linearly correlates with nanoparticle concentration. However, the reduction is stronger in the absence of salts, i.e. under conditions where interactions between the peptide and the nanoparticle are believed to occur. The difference between the curves shown in Figure 3.38 therefore provide evidence for the interaction of Gly-Trp with **NP Q**.

The titrations were subsequently repeated under the same conditions in the presence of the other nanoparticles. The results, shown in Figure 3.38, look qualitatively similar, with the curves that include the effects of specific binding of the dipeptide to the different nanoparticles lying below the ones associated with quenching by other means than binding. Differences are also noted between the individual titrations mainly involving the extents to which the binding curves differ from the reference ones. For **NP QP**, **NP QC_S** and **NP QC_L** the respective pairs of curves have similar distances as those observed for **NP Q**.¹⁰² The nanoparticles containing all three ligands, namely **NP QPC_S** and **NP QPC_L**, cause a notably stronger decrease of the fluorescent emission of Gly-Trp than the other nanoparticles.

3. Results and Discussion

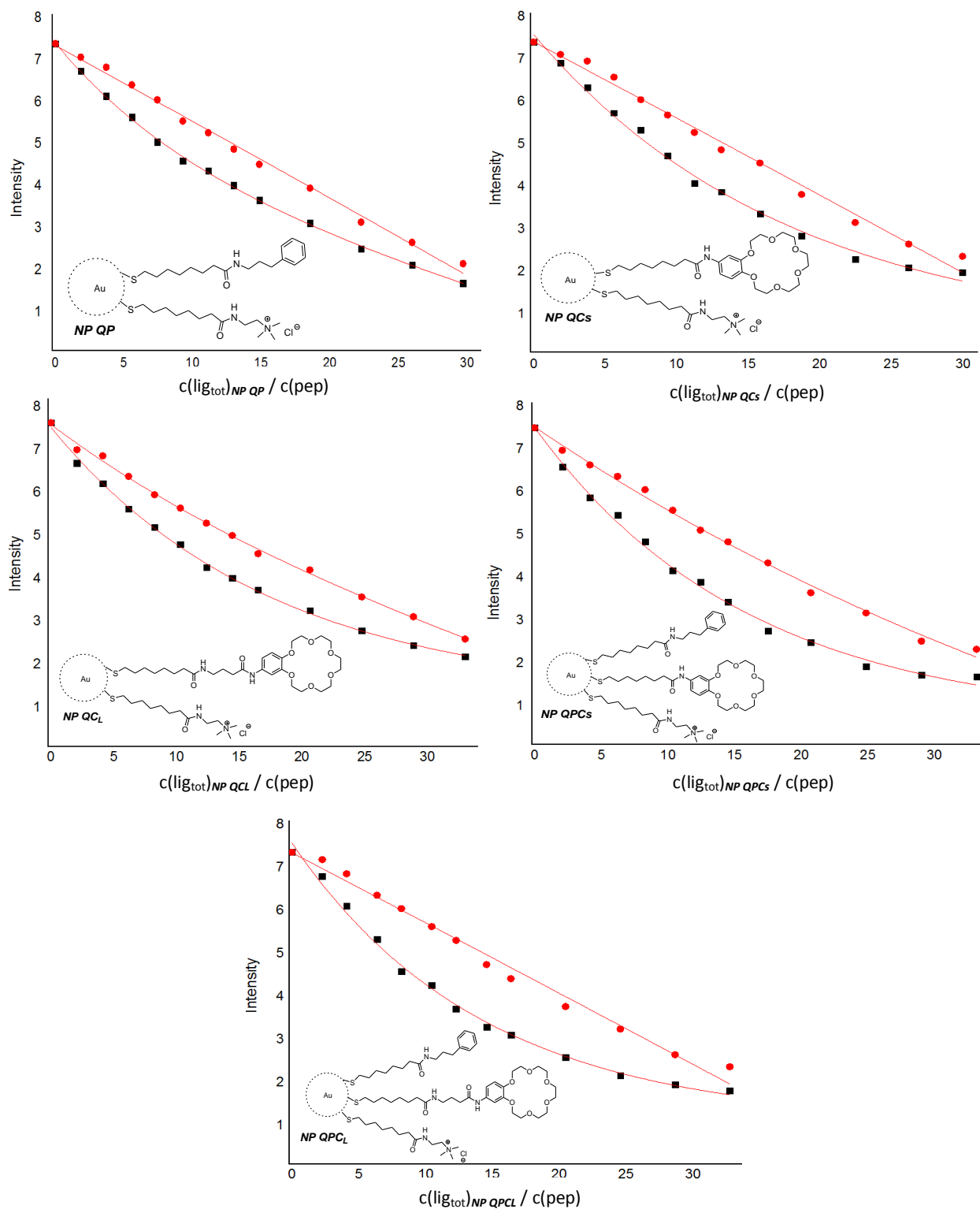


Figure 3.38 Decrease of fluorescence intensities when adding increasing amounts of **NP QP**, **NP QCs**, **NP QPCs**, **NP QCL** and **NP QPCL** to Gly-Trp (1.5×10^{-6} M) in water (black squares), and in 0.2 M aqueous NaCl (red circles).

3.4.4 Discussion

The shifts of the Gly-Gly signals in the $^1\text{H-NMR}$ spectra, observed upon addition of **NP Q** indicate that interactions between the dipeptide and the nanoparticles occur, likely involving electrostatic interactions between the carboxylate groups of the dipeptide and the positively charged nanoparticle.

Indeed, the dipeptide signal that was found to be more strongly affected by the presence of the nanoparticle was assigned to belong to the C-terminal glycine residue. It has to be considered, however, that the chemical shifts of the methylene protons of Gly-Gly are strongly affected by the pH.⁸⁴ The pH of the solution can even cause the two CH_2 signals of Gly-Gly to change their sequence in the NMR spectrum so that the assignment made in this work is not yet fully confirmed. In addition, the observed movement of the CH_2 signal may alternatively be due to slight pH changes induced by the presence of the nanoparticle. Further systematic studies are therefore required to obtain information about the causes for the observed changes in the $^1\text{H-NMR}$ spectrum and the mode with which the dipeptide actually binds to the nanoparticles. Independently, $^1\text{H-NMR}$ spectroscopy is not suitable to obtain quantitative information about the strength of binding because of the pronounced overlap of nanoparticle and peptide signals.

In this context, DOSY-NMR spectroscopy turned out to be much more useful. DOSY-NMR spectroscopy indeed confirmed that the peptides bind to the nanoparticles. The diffusion coefficient of the dipeptides decrease in the presence of nanoparticles showing they are partly adsorbed. Table 3.11 shows that **NP Q**, containing only quaternary ammonium ligands, binds 30-40% of the peptide molecules present in solution under the conditions of the measurement. Incorporating crown ether or phenyl moieties in addition to quaternary ammonium groups into the AuNP surface layers did not improve the amount of the bound peptide significantly. On the contrary, nanoparticles **NP QPC_S** and **NP QPC_L**, that have three different binding sites (**Q**, **P** and **C_{S/L}**) exhibited substantially higher affinities to both peptides than the other AuNPs, possibly because the aromatic units are required to “dilute” the binding sites on the AuNP surface thus, providing arrangements that allow the quaternary ammonium ions and crown ether moieties to cooperatively engage in binding interactions. This effect is substantially more pronounced for Gly-Phe, indicating that aromatic interactions are likely to contribute to complex stability.

Moreover, no pronounced effect of the structure of the different crown ether ligands was observed. However, there was a distinct difference in the affinities of nanoparticles **NP QC_S** and **NP QC_L** to Gly-Gly, which is less pronounced in the case of Gly-Phe. This effect may be due to a slight advantage induced by ligand **C_L** on peptide binding, which is, however lost, once the ligand **P** is present or the substrate structurally differs from Gly-Gly.

The results compiled in Table 3.1 provide qualitative information about the effects of surface composition on dipeptide affinity of the prepared nanoparticles. To obtain more quantitative information, titrations were performed, the results of which are shown in Figure 3.30. Deriving binding constants from these curves is complicated by the fact that the stoichiometry underlying complex formation is unknown. A more appropriate method to quantitatively describe these binding isotherms is therefore the model developed by Langmuir that describes adsorption of small molecules to solid surfaces, forming ultimately a monolayer. Langmuir isotherms have been used to quantify the binding of nanoparticles with multiple binding sites to their respective substrates.¹⁰³⁻¹⁰⁵ For example, the Langmuir treatment was used to characterize the binding of Bovine serum albumin via electrostatic interactions to negatively charged citrate protected gold nanoparticles,^{106, 107} the adsorption of functionalized gold nanoparticles onto hydroxy-apatite to assess the applicability of these nanoparticles for targeted delivery to bone mineral,¹⁰⁸ or the adsorption of thiolated DNA molecules on gold nanoparticles.¹⁰⁷ Describing adsorption equilibria by using the Langmuir isotherm has the advantage that it is not required to know the exact mode with which molecules are adsorbed on surfaces or how many functional groups on the surface are needed on average to bind a single guest molecule. As quantitative parameters of the Langmuir description, an equilibrium constant is obtained that allows comparison of the properties of different surfaces in a quantitative fashion. In addition, the isotherm affords information about the maximum number of molecules that can be adsorbed on the surface. The isotherms obtained by fitting the graphs depicted in Figure 3.30 to the Langmuir equation 3.7 are shown in Figure 3.39.

$$\chi = C_{\max} \cdot K / (1 + K \cdot C_{\text{pep}}) \quad \text{Equation 3.7}$$

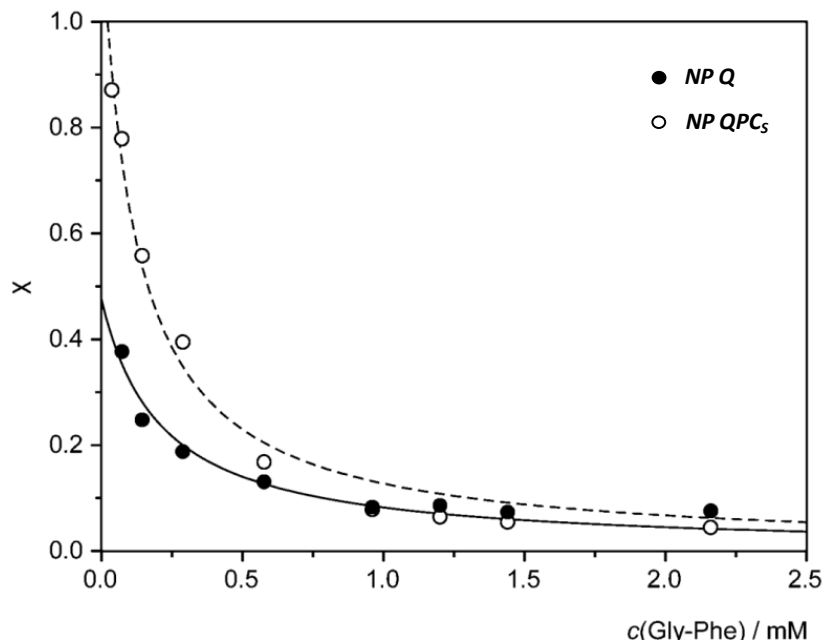


Figure 3.39 Langmuir isotherms for Gly-Phe binding to **NP Q** and **NP QPC₅** calculated from the data summarized in Table 3.12

Figure 3.39 shows the Langmuir isotherms for Gly-Phe binding to **NP Q** and **NP QPC₅**. The underlying non-linear regressions yielded the corresponding equilibrium constants K and the maximum fractions of bound peptide c_{\max} . Relating c_{\max} to the amounts of ligands on the nanoparticles provided information about the average number of ligands required to bind one peptide molecule. The results are summarized in Table 3.12. The fitting of the curve obtained for **NP QP** was unsuccessful, presumably due to a larger scattering of the data. Therefore, an association constant could not be calculated. Unfortunately, this titration could not be repeated during this Ph.D. thesis because all DOSY-NMR measurements were performed in Wageningen.

Table 3.12 Nonlinear regression results for **NP Q**, **NP QC₅** and **NP QPC₅**

| | $K \times 10^{-3} \text{ M}^{-1}$ | $c_{\text{max}} / \text{mM}$ | $c(\text{lig}_{\text{tot}}) / c_{\text{max}}$ |
|---------------------------|-----------------------------------|------------------------------|---|
| NP Q | 4.8 ± 1.2 | 0.10 | 18.9 |
| NP QC₅ | 5.4 ± 1.4 | 0.09 | 20.1 |
| NP QPC₅ | 8.3 ± 1.5 | 0.14 | 13.9 |

The association constants calculated by using the Langmuir treatment confirmed the trends observed in the data in Table 3.11: a small difference was observed in the affinities of **NP Q** and **NP QC₅** for Gly-Phe, which may be an effect of the crown ether ligand in **NP QC₅**. **NP QPC₅** possesses the highest affinity for Gly-Phe confirming the other results and again indicating the importance of the three orthogonal binding sites for peptide recognition.

The calculated ratios $c(\text{lig}_{\text{tot}}) / c_{\text{max}}$ obtained from the Langmuir treatment show that for **NP Q** and **NP QC₅** the ligand/peptide ratio amounts to ca. 20. Thus, a significant number of ligands on these nanoparticles are presumably not involved in direct interactions with the peptide. In the case of **NP QPC₅** the ligand/peptide ratio decreases to 14. This nanoparticle therefore contains more binding sites than **NP Q** and **NP QC₅**. Also in this case the number of ligands per peptide is, however, significantly higher than expected if one assumes that every ligand is involved in a productive recognition event. A possible explanation could be that many ligand arrangements exist on the nanoparticle surfaces that cannot contribute to peptide binding. The number of productive recognition sites is probably controlled by statistics during nanoparticle synthesis and future studies also need to address strategies how to improve the number of binding sites on the nanoparticles.

Fluorescence spectroscopy required changing the substrate to one with a fluorescence chromophore, namely Gly-Trp. Gly-Trp and Gly-Phe are, however, structurally related and their binding to the nanoparticles can therefore be expected to be similar. Addition of nanoparticles to an aqueous Gly-Trp solution caused the expected quenching of fluorescence. This quenching is stronger than that observed in analogous measurements, in which the binding of Gly-Trp to

the nanoparticles was suppressed by addition of NaCl. Thus, also fluorescence spectroscopy provided evidence for peptide binding to the nanoparticles.

Figure 3.40 shows the comparison of fluorescent titration curves obtained in the measurements with nanoparticles **NP Q** and **NP QPC₅**. The more pronounced decrease of fluorescent intensity observed in the presence of **NP QPC₅** indicated that the nanoparticle containing the three functional groups has a higher peptide affinity, a result consistent with the one of the DOSY-NMR measurements. Unfortunately, no suitable mathematical model could be derived during this Ph.D. thesis to extract quantitative information from these binding isotherms.

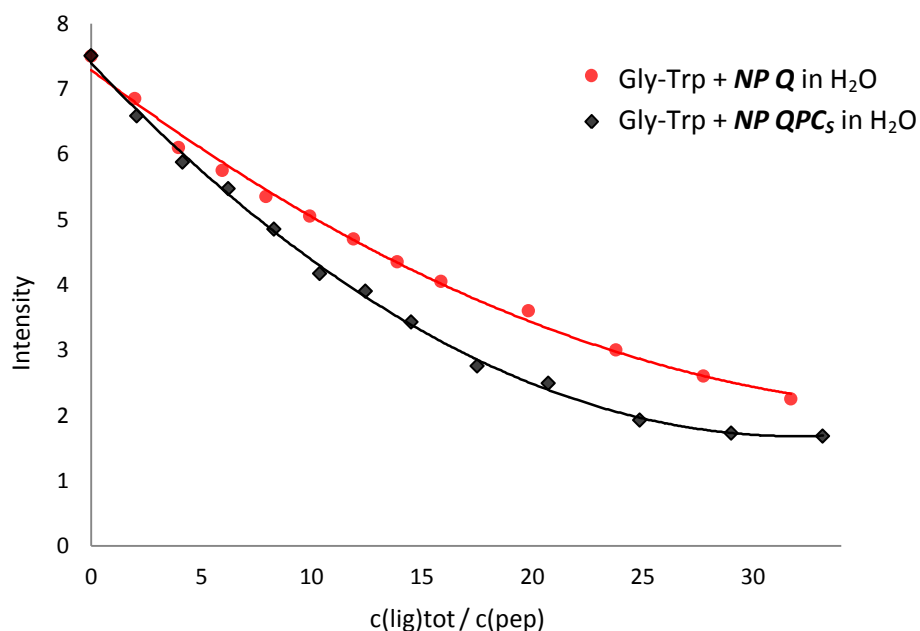


Figure 3.40 Comparison of fluorescent titration curves of **NP Q** and **NP QPC₅**

DOSY-NMR spectroscopy and fluorescence spectroscopy thus revealed similar trends of peptide affinity: nanoparticles containing a combination of three orthogonal functional groups (**NP QPC₅** and **NP QPC₄**) are more efficient in binding to dipeptides than mono or difunctionalized analogues. This result is mainly attributed to the dilution of the specific binding sites on the nanoparticle surface by the hydrophobic residue in ligand **P**. Arrangements are thus induced on the nanoparticle surface, which allow the quaternary ammonium group in **Q** and the crown

ethers in ligands C_S or C_L to better interact with the peptides in a cooperative fashion than if the ligand P is absent. Since this effect is more pronounced for binding of Gly-Phe, aromatic interactions are likely to also contribute to complex stability.

In spite of the observed affinities of $NP QPC_S$ and $NP QPC_L$ for dipeptides, the extent to which the fluorescence of Gly-Trp is quenched in the presence of these nanoparticles turned out to be relatively modest. By contrast, the binding of flavin mononucleotide to a positively charged ammonium groups has been shown to result in a dramatic decrease of fluorescence, which could even be used to quantify binding strength.⁵⁶ This pronounced difference may be due to the fluorescence properties of flavin mononucleotide combined with the higher charge of this substrate that renders its affinity to an oppositely charged nanoparticle higher. As a consequence, nanoparticles with even larger affinity for peptides are required to render fluorescence spectroscopy a useful method for the evaluation of binding properties.

4. Summary and Outlook

This Ph.D. dissertation addressed the development of new artificial receptors for low molecular weight compounds, in this case for peptides, on the basis of mixed monolayer protected gold nanoparticles. Specifically, these nanoparticles combined different functional groups on their surface that could engage in interactions with the chosen substrates provided that these binding sites are spatially appropriately arranged. The attractiveness of this approach lies in the ease of preparation of these nanoparticles once a library of functional thiols containing appropriate binding sites for a given substrate is available and its enormous flexibility.

To test this concept, gold nanoparticles were prepared containing four different types of functional ligands (**Q**, **P**, **C_S** and **C_L**). These ligands were chosen such that they contain functional groups that can interact with terminal amino and carboxylate groups of short unprotected peptides and with aromatic side chains in water. The ligands were synthesized in their protected forms as thioacetates. Syntheses of nanoparticles were performed by a ligand exchange reaction strategy, using the deprotected thiol forms of the ligands and dioctylamine protected gold nanoparticles as precursors. Using this technique, six different nanoparticles were prepared with a good control over the ratio of the surface bound ligands (**NP Q**, **NP QP**, **NP QC_S**, **NP QPC_S**, **NP QC_L** and **NP QPC_L**). Figure 4.1 shows **NP QPC_S** and its potential interactions with dipeptide Gly-Phe as an example.

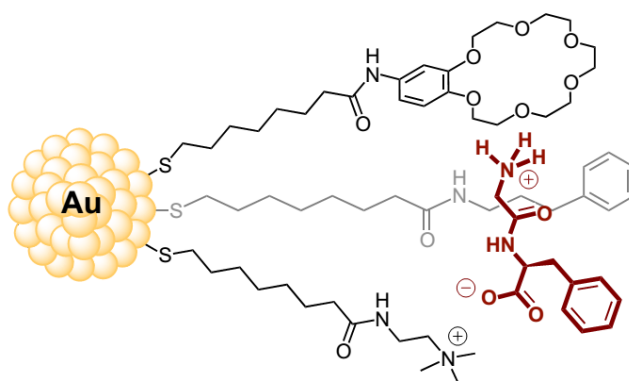


Figure 4.1 Schematic representation of **NP QPC_S** and its potential interactions with Gly-Phe, "Reprinted with permission from; S. Yapar, M. Oikonomou, A. H. Velders and S. Kubik, *Chem. Commun.*, 2015, **51**, 14247-14250, Copyright 2015, The Royal Society of Chemistry"

Surface composition was characterized by using an iodine decomposition strategy followed by $^1\text{H-NMR}$ spectroscopic determination of the ligand ratios. All nanoparticles containing more than one ligand type contained ca. 50% of the positively charged ligand **Q** that ensures water solubility and was expected to serve as a binding site for the carboxylate group of the peptides. Nanoparticles with two different ligands, namely **NP QP**, **NP QC_S**, **NP QC_L** contained both ligands with a ca. 1:1 ratio. Nanoparticle **NP QP** contained a phenyl group in addition to the quaternary ammonium group of **Q** that should mediate interactions with aromatic residues in the substrates. Nanoparticles with ligands **C_S** or **C_L** contained crown ethers. These ligands differ in the lengths of the chain between the thiol and the [18]crown-6 units, the latter of which was expected to bind to the amino group of the peptides. Finally, nanoparticles with three ligand types, namely **NP QPC_S** and **NP QPC_L** contained 50% **Q** and a ca. 1:1 ratio of the other two ligands.

By using an internal standard in the iodine decomposition experiments it was possible to also obtain detailed information about the number of gold atoms in the individual nanoparticles and the number of ligands.

Further characterization of these nanoparticles was performed by using $^1\text{H-NMR}$, DOSY-NMR and UV-Vis spectroscopy, in addition to TEM and DLS measurements. These measurements mainly provided information about the sizes of the prepared nanoparticles. Specifically, the diameters of the cold cores were estimated by TEM measurements to range between 1.9-2.6 nm. DOSY-NMR spectroscopy and DLS measurements provided information about the sizes of the nanoparticles including their protective monolayers. Both methods gave relatively consistent results, showing that the overall diameters of the nanoparticles ranged between 5.0-5.6 nm.

The affinities of the prepared nanoparticles for dipeptides were evaluated in water. Binding studies were performed by using $^1\text{H-NMR}$, DOSY-NMR, and fluorescence spectroscopy. As substrates, the dipeptides Gly-Gly, Gly-Phe, and Gly-Trp were used. $^1\text{H-NMR}$ spectroscopy indicated qualitatively that even the simplest nanoparticle, containing only ligand **Q**, interacts with the dipeptides in water. DOSY-NMR spectroscopy confirmed this result and also provided more qualitative information about peptide affinity. These measurements showed that

combining ligand **Q** with another ligand containing either an aromatic (**P**) or a crown ether moiety (**C_S**, **C_L**) does not lead to a substantial improvement of affinity. This result is in contrast to work by Schneider who has shown that combining a quaternary ammonium group and a crown ether on a rigid scaffold gives rise to a low molecular weight receptor for peptides in water. Combining the same functional groups on the surface of a gold nanoparticle is obviously not sufficient to ensure their cooperative action in substrate binding.

When combining the positively charged ligand **Q** with a crown ether (**C_S**) and an aromatic residue (**P**) in nanoparticle **NP QPC_S**, a nanoparticle with a substantially higher peptide affinity was obtained than when using only two ligand types. Affinity of **NP QPC_S** for Gly-Phe is slightly higher than for Gly-Gly, indicating that aromatic interactions contribute to affinity. The positive effect of **P** on binding strength was attributed to an ability of **P** to induce arrangements on the nanoparticle surface that allow the ligands **Q** and **C_S** to better engage in interactions with the substrate.

Quantitative information about affinity was obtained from DOSY-NMR titrations followed by treating the obtained results on the basis of Langmuir isotherms. These titrations furthermore showed that only a small fraction of the ligands in the nanoparticle surface engage in interactions with the substrate.

The fluorescence measurements qualitatively confirmed these results by showing that fluorescence of dipeptide Gly-Trp is more strongly quenched in the presence of **NP QPC_S** than in the presence of nanoparticles containing only two ligand types. These measurements were complicated by strong effects of the nanoparticles on the emission of Gly-Trp that are not related to binding so that no quantitative information about affinity could be derived.

Overall this work introduces a promising concept for the preparation of new nano-sized receptors. The strategy is highly modular and easily allows adapting the receptor selectivity to a given substrate by varying the type, number, and ratio of binding sites on the nanoparticle surface. An additional advantage could be that the optical properties of gold nanoparticles could also allow the development of optical probes on the basis of this strategy. Disadvantages are the still relatively limited methods to structurally characterize mixed monolayer protected nanoparticles and their surface composition. Also obtaining information about binding

properties, in particular quantitative information about affinity, is not straightforward. This work shows that DOSY-NMR spectroscopy is a powerful analytical technique, but it is still not widely available and very time consuming.

The most significant drawback of nanoparticle-based receptors is that their binding properties not only depend on the ratio of the ratio of the ligands present on their surface but, even more importantly, on the spatial arrangement, which is not yet possible to control. In this respect, dynamic chemistry that uses template effects to access the thermodynamically most stable product, which could potentially be the complex between a given substrate and a nanoparticle containing exchangeable ligands, represents a promising approach. First examples of using dynamic chemistry for the development of nanoparticle-based functional systems¹⁰⁹⁻¹¹⁴ have been described. Future work will have to show whether this approach can also be used to optimize the binding properties of the nanoparticle-based receptors developed in this work.

5. Experimental Part

5.1 Materials

The solvents and starting materials for the syntheses of the ligands and the nanoparticles are commercially available and were used without further purification unless otherwise noted. They were obtained from the following sources: Acros Organics, VWR, Sigma Aldrich, Fluka, TCI-Tokyo Chemical Industry, and Alfa Aesar.

5.2 Analytical Methods

NMR Spectroscopy

^1H -NMR and ^{13}C -NMR spectroscopy were recorded using a Bruker AVANCE III HD 400 NMR spectrometer. The chemical shifts δ are denoted in ppm. They were assigned by using the residual signals of the solvent as reference.

^1H : $\delta(\text{CDCl}_3) = 7.26$, $\delta(\text{methanol-}d_4) = 3.31$, $\delta(\text{DMSO-}d_6) = 2.50$

^{13}C : $\delta(\text{CDCl}_3) = 77.2$, $\delta(\text{DMSO-}d_6) = 39.5$, $\delta(\text{methanol-}d_4) = 49.0$

The multiplicities of the signals in the ^1H -NMR were abbreviated as:

s = singlet, d = doublet, t = triplet, q = quartet, m = multiplet and bs = broad singlet.

The coupling constants J are given in Hertz (Hz).

Diffusion Ordered NMR Spectroscopy (DOSY-NMR)

DOSY NMR measurements were performed on a 500 MHz Bruker Avance III NMR spectrometer, equipped with a 5 mm TXI probe head at 300 K. The pulse sequence was a stimulated echo bipolar gradient pulse (stebpgp1s), with the DOSY spectra acquired for each sample having 32 increments (exponential array) and 32 scans. The gradient pulse length (δ) amounted to 6.0 ms, and the big delta (Δ) 150.0 ms.

Elemental Analysis

Elemental analyses were determined by using an Elementar Vario Microcube elemental analyzer.

Melting Points

A Müller SPM-X 300 apparatus was used to determine the melting points of the prepared compounds.

MALDI-TOF-Mass Spectrometry

The mass spectra of the compounds were recorded by using a Bruker Ultraflex TOF/TOF spectrometer. Sample preparation was carried out by mixing solutions of the respective compound with 2,5-dihydroxybenzoic acid as the matrix on a support plate.

Infrared Spectroscopy

The infrared spectra of the ligands and intermediates were recorded by using a Spectrum BX Perkin-Elmer FT-IR System.

UV-Vis Spectroscopy

Characterization by UV-Vis spectroscopy was done by using a Varian Cary 100 Conc UV-Vis Spectrophotometer. The spectra were recorded in the range 200-800 nm. For the UV-Vis analysis, a sample of nanoparticle (1 mg) was dissolved in HPLC grade water (0.35 mL) and 100 μ L of this solution was taken and diluted to 3 mL in a quartz UV cuvette by adding water.

Transmission Electron Microscopy

TEM images were recorded by using a JEOL JEM1011 microscope with an acceleration voltage of 80 kV. The measurements were performed by dissolving the nanoparticles in water. A drop of the solution was placed on a copper grid and dried before recording the TEM images. These images were then processed with the *ImageJ* software to determine the average core diameters and produce the histograms .

Dynamic Light Scattering Experiments

To measure the sizes of the nanoparticles, DLS experiments were performed by using a Zetasizer Nano S90 (Malvern) Spectrometer (with 90 degree scattering optics) at 25 °C using water as solvent. To measure the diffusion speed, the particles were illuminated with a laser. The scattering intensity at a specific angle (90°) and the intensity changes were analyzed to give the size and the size distribution. For these experiments, nanoparticles (0.5 mg) were dissolved in HPLC grade water (0.25 mL) and placed in micro cuvettes. The measurements were performed by keeping the temperature constant at 25 °C.

Fluorescence Spectroscopy

A JASCO FP-6200 spectrofluorometer with a Xe lamp as a source of radiation was used for the fluorescence measurements.

Column Chromatography

Acros Organics silica gel 60 A (0.06-0.20 mm) was used for the purification of the compounds and Macherey-Nagel silica gel 60 (0.04-0.06 mm) was used for flash column chromatography.

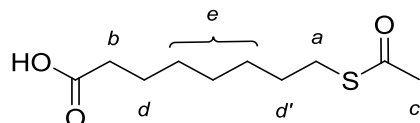
Thin Layer Chromatography

Merck silica gel 60 F254 on aluminum support was used as TLC plates.

Syringes and Pipettes

Hamilton gas-tight micro syringes and BRAND Transferpette®S micropipettes were used for accurate volumetric handling of the solutions during the reactions and titrations.

5.3 Ligand Syntheses

5.3.1 Synthesis of Compound 1 ¹¹⁵

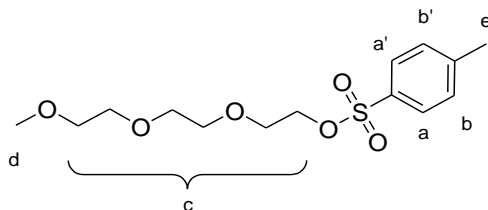
To a solution of 8-bromooctanoic acid (3 g, 13.4 mmol) in methanol (100 mL), potassium thioacetate (3 g, 26 mmol) was added and the mixture was refluxed for 24 h. After cooling, the solvent was evaporated and the crude product was dissolved in water (50 mL). The solution was extracted with dichloromethane (3 x 50 mL), the organic layer was collected, dried over Na₂SO₄ and the solvent was evaporated. The obtained material was purified by column chromatography (SiO₂, dichloromethane/hexane, 1:1) to afford the product as a beige solid.

Yield: 2.5 g, 85%

¹H NMR (400 MHz, 25 °C, CDCl₃) δ: 2.86 (t, 2H, ³J = 7.3 Hz, H_d), 2.35 (t, 2H, ³J = 7.6 Hz, H_b), 2.33 (s, 3H, H_c), 1.65-1.55 (m, 4H, H_{d,d'}), 1.38-1.34 (m, 6H, H_e) ppm

¹³C NMR (100.6 MHz, 25 °C, CDCl₃) δ: 196.9, 180.2, 34.6, 31.1, 30.1, 29.8, 29.6, 29.4, 29.3, 25.3 ppm

IR wavenumber/cm⁻¹: 3474 (m), 2931 (m), 2858 (w), 1723 (w), 1660 (s), 1487 (w), 1438 (m), 1408 (m), 1386 (s), 1255 (m), 1090 (s), 1063 (w), 658 (s)

5.3.2 Synthesis of Compound 2 ¹¹⁵

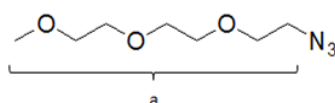
A solution of tosyl chloride (14.0 g, 0.73 mol) and triethylene glycol monomethyl ether (10 mL,

0.64 mol) in dry dichloromethane (300 mL) was stirred under nitrogen at 25 °C for 24 hours. Then, the reaction mixture was concentrated to 50 mL by evaporation and extracted with water (50 mL). The organic layer was collected, dried over anhydrous Na₂SO₄, and the solvent was evaporated. The product was obtained as a colorless oil.

Yield: 8 g, 40 %.

¹H-NMR [400 MHz, 25 °C, MeOD] δ: 7.75 (d, 2H, H_{a,a'}); 7.21 (d, 2H, H_{b,b'}); 3.76-3.54 (m, 12H, H_c); 3.35 (s, 3H, H_d); 2.36 (s, 3H, H_e) ppm.

5.3.3 Synthesis of Compound 3¹¹⁵

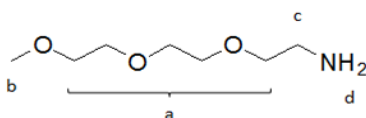


Under a nitrogen atmosphere, compound **2** (3 g, 9.42 mmol) and NaN₃ (7.33 g, 113 mmol) were dissolved in a mixture of 2:1 water-methanol (30 mL). The reaction mixture was heated to 75 °C and stirred at this temperature for 17 hours. It was then concentrated, diluted with water (50 mL), and extracted with dichloromethane (3 x 30 mL). The organic layer was collected, dried over anhydrous Na₂SO₄, and the solvent was evaporated. The product was obtained as a colorless oil.

Yield: 1.7 g, 95 %

¹H-NMR [400 MHz, 25 °C, CDCl₃] δ: 3.66-3.36 (m, 15H, H_a) ppm.

5.3.4 Synthesis of Compound 4¹¹⁵



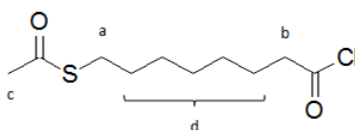
Triphenylphosphine (3.15 g, 12 mmol) was added to a solution of **3** (2.0 g, 10.7 mmol) in dry

THF (27 mL). The mixture was stirred under nitrogen at 25 °C for 15 h. Then, water (7.7 mL) was added and stirring was continued for additional 2 hours. The solvent was evaporated, the residue was dissolved in toluene (70 mL) and water (100 mL) was added. The mixture was stirred until phosphine oxide was dissolved. The aqueous portion was extracted with toluene (2 x 30 mL). The combined aqueous layers were evaporated to dryness. The residue was dissolved in dichloromethane and dried over anhydrous Na₂SO₄. The product was obtained after evaporation of the solvent as a yellow oil.

Yield: 900 mg, 46 %

¹H-NMR [400 MHz, 25 °C, CDCl₃] δ: 3.74-3.51 (m, 10H, H_a); 3.37 (s, 3H, H_b); 2.89 (t, 2H, J= 5.2 Hz, H_c); 2.60 (s, 2H, H_d)

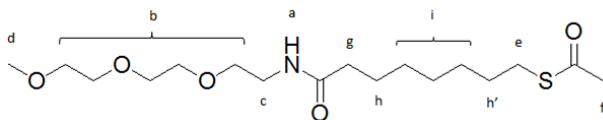
5.3.5 Synthesis of Compound 5 ¹¹⁵



Thionyl chloride (196 μL, 2.7 mmol) was added to a solution of compound **1** (520 mg, 2.4 mmol) in dry dichloromethane (10.5 mL). The reaction mixture was stirred at 25 °C for 3 h and the solvent was removed by evaporation. The residue was dissolved in toluene (4 mL) and the solvent was removed. The product was isolated chromatographically (SiO₂, 1:1 (v/v) dichloromethane/ethyl acetate).

Yield: 461 mg, 80 %

¹H-NMR [400 MHz, 25 °C, CDCl₃] δ: 2.84 (t, 2H, J=7.3 Hz, H_a); 2.32 (t, 2H, J=7.5 Hz, H_b); 2.30 (s, 3H, H_c); 1.64-1.30 (m, 10H, H_d) ppm.

5.3.6 Synthesis of Protected Ligand TEG_{Ac}^{115} 

To a solution of **5** (630 mg, 2.55 mmol) in dry dichloromethane (10 mL), a solution of **4** (390 mg, 2.40 mmol) in dichloromethane (10 mL) was added followed by diisopropylethylamine (1.05 mL, 5.10 mmol). The reaction mixture was stirred at 25 °C for 18 h under an argon atmosphere. Then, the mixture was extracted with 1 M HCl (2x 15 mL), the organic layer was collected and the solvent was removed. The product was isolated chromatographically (SiO₂, 1:1 (v/v) hexane/ethyl acetate) as a colorless oil.

Yield: 700 mg, 80 %.

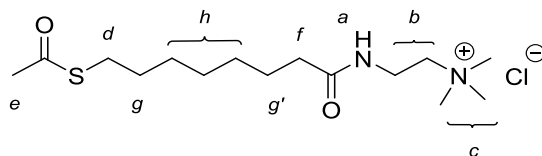
¹H-NMR [400 MHz, 25 °C, CDCl₃] δ: 6.09 (bs, 1H, H_a); 3.67-3.53 (m, 10H, H_b); 3.48-3.43 (m, 2H, H_c); 3.38 (s, 3H, H_d); 2.85 (t, 2H, *J*=7.2 Hz, H_e); 2.32 (s, 3H, H_f); 2.17 (t, 2H, *J*=7.5, H_g); 1.65-1.52 (m, 4H, H_{h,h'}); 1.32-1.29 (m, 6H, H_i) ppm.

¹³C-NMR [100.6 MHz, 25 °C, D₂O] δ: 196.5, 173.6, 72.3, 70.9, 70.8, 70.6, 70.4, 59.5, 39.5, 37.0, 31.1, 29.9, 29.6, 29.3, 29.0, 26.0.

MALDI-TOF MS *m/z* %: 364.2 (95) [M+H]⁺, 386.3 (100) [M+Na]⁺, 402.3 (75) [M+K]⁺.

Elemental Analysis (C₁₇H₃₃NO₅S): calcd (%) **C** 56.17, **H** 9.15, **N** 3.85, **S** 8.82

found (%) **C** 55.90, **H** 8.89, **N** 3.71, **S** 8.72

5.3.7 Synthesis of Protected Ligand Q_{Ac}^{116} 

To a solution of **1** (600 mg, 2.7 mmol) in dichloromethane (50 mL) and dimethylformamide (5 mL), *N,N'*-dicyclohexylcarbodiimide (800 mg, 3.9 mmol) and 4-dimethyl-aminopyridine (50 mg, 0.4 mmol) were added, followed by 2-amino-*N,N,N*-trimethyl ethanaminium chloride (500 mg, 3.6 mmol). The reaction mixture was refluxed for 16 hours under a nitrogen atmosphere. Afterwards, the solvent was evaporated, cold acetone (2 mL) was added to the residue, and the solution was filtered to remove residual dicyclohexyl urea. The filtrate was evaporated and the addition of acetone, filtration, and evaporation was repeated three times. The crude product was thus obtained as a light yellow sticky oil. To obtain it as an analytically pure product, further purification was performed by flash column chromatography (SiO₂, methanol). Fractions containing the product were collected and evaporated to dryness. The residue was dissolved by addition of dichloromethane (2 mL), and the resulting suspension was filtered to remove silica gel. The filtrate was evaporated to afford the product as a colorless sticky oil.

Yield: 650 mg, 60%

¹H NMR (400 MHz, 25 °C, CDCl₃) δ: 8.69 (s, 1H, H_a), 3.74 (m, 4H, H_b), 3.38 (s, 9H, H_c), 2.77 (t, 2H, ³J = 7.5 Hz, H_d), 2.25 (s, 3H, H_e), 2.22 (t, 2H, ³J = 7.7 Hz, H_f), 1.60-1.42 (2xm, 4H, H_{g,g'}), 1.18-1.29 (m, 6H, H_h) ppm

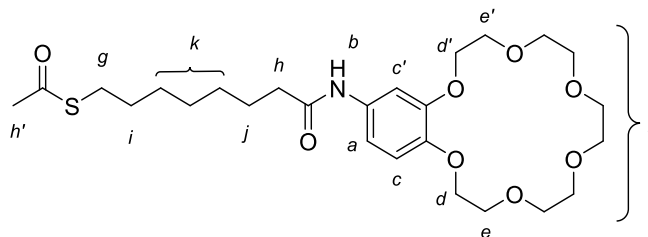
¹³C NMR (100.6 MHz, 25 °C, CDCl₃) δ: 196.2, 174.8, 65.8, 54.2, 36.2, 34.4, 30.7, 29.4, 29.1, 29.1, 28.8, 28.6, 25.3 ppm

IR wavenumber/cm⁻¹: 3364 (m) 3252 (m), 3026 (w), 2928 (s), 2855 (m), 1687 (s), 1654 (s), 1541, 1480, 1353, 1133, 955

MALDI-TOF MS *m/z* (%): 303.1 (100) [M-Cl]⁺

Elemental Analysis (C₁₅H₃₁ClN₂O₂S·0.5H₂O): calcd (%) **C** 51.78, **H** 9.27, **N** 8.05, **S** 9.22

found (%) **C** 51.64, **H** 9.00, **N** 7.91, **S** 9.13

5.3.8 Synthesis of Protected Ligand C_{SAC} 

To a solution of **1** (160 mg, 0.7 mmol) in dichloromethane (30 mL) and dimethylformamide (3 mL), *N,N'*-dicyclohexylcarbodiimide (185 mg, 0.9 mmol) and 4-dimethylaminopyridine (12 mg, 0.1 mmol) were added, followed by 4'-aminobenzo-18-crown-6 (200 mg, 0.6 mmol). The resulting reaction mixture was refluxed for 16 h under a nitrogen atmosphere. Afterwards, the solvent was evaporated and the product was purified chromatographically (SiO₂, ethyl acetate) to afford a white powder.

Yield: 170 mg, 54 %

Mp: 113-115 °C

¹H NMR (400 MHz, 25 °C, CDCl₃) δ: 7.29 (s, 1H, H_a), 6.97 (s, 1H, H_b), 6.75 (s, 2H, H_{c,c'}), 4.04-4.10 (2xm, 4H, H_{d,d'}), 3.81-3.85 (m, 4H, H_{e,e'}), 3.60-3.70 (m, 12H, H_f), 2.78 (t, 2H, ³J = 7.3 Hz, H_g), 2.21-2.26 (m, 5H, H_{h,h'}), 1.70-1.61 (m, 2H, H_i), 1.55-1.44 (m, 2H, H_j), 1.25-1.35 (m, 6H, H_k) ppm

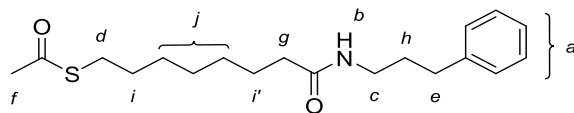
¹³C NMR (100.6 MHz, 25 °C, CDCl₃) δ: 196.2, 171.1, 149.2, 145.4, 132.2, 114.8, 112.1, 106.9, 70.8, 70.8, 70.7, 70.6, 69.7, 69.6, 69.5, 68.9, 37.5, 30.7, 29.4, 29.0, 28.7, 28.5, 25.4 ppm

IR wavenumber/cm⁻¹: 3285 (m), 3075 (w), 2929 (m), 2854 (m), 1681 (s), 1650 (s), 1601 (w), 1544 (m), 1513 (m), 1410, 1247, 1126 (s), 1086, 1055, 947, 845, 721

MALDI-TOF MS *m/z* (%): 527.4 (63) [M+H]⁺, 550.5 (100) [M+Na]⁺, 566.5 (68) [M+K]⁺

Elemental Analysis (C₂₆H₄₁NO₈S): calcd (%) **C** 59.18, **H** 7.83, **N** 2.66, **S** 6.08

found (%) **C** 59.16, **H** 8.06, **N** 2.62, **S** 5.67

5.3.9 Synthesis of Protected Ligand P_{Ac} 

To a solution of **1** (500 mg, 2.3 mmol) in dichloromethane (30 mL), *N,N'*-dicyclohexylcarbodiimide (700 mg, 3.4 mmol) and 4-dimethylaminopyridine (70 mg, 0.6 mmol) were added, followed by 3-phenylpropan-1-amine (0.27 mL, 1.9 mmol). The resulting reaction mixture was refluxed for 16 h under a nitrogen atmosphere. Afterwards, the solvent was evaporated and the product was purified chromatographically (SiO₂, acetone/hexane, 1:1). The yellow solid collected after evaporation of the product fractions was dissolved in dichloromethane and the product was precipitated by pouring the solution into cold ether. The beige product was collected by filtration, washed with ether, and dried.

Yield: 480 mg, 75 %

Mp: 205-207 °C

¹H NMR (400 MHz, 25 °C, CDCl₃) δ: 7.33-7.04 (m, 5H, H_a), 5.32 (s, 1H, H_b), 3.22 (q, 2H, ³J = 6.6 Hz, H_c), 2.78 (t, 2H, ³J = 7.2 Hz, H_d), 2.59 (t, 2H, ³J = 7.6 Hz, H_e), 2.25 (s, 3H, H_f), 2.04 (t, 2H, ³J = 7.5 Hz, H_g), 1.77 (q, 2H, ³J = 7.3 Hz, H_h), 1.43-1.54 (m, 4H, H_{i,i'}), 1.19-1.24 (m, 6H, H_j) ppm

¹³C NMR (100.6 MHz, 25 °C, CDCl₃) δ: 196.1, 173.1, 141.4, 128.4, 128.3, 126.0, 39.2, 36.6, 33.3, 31.2, 30.6, 29.4, 29.0, 28.7, 28.5, 25.6 ppm

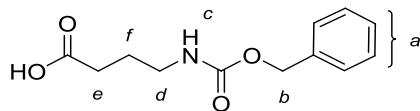
IR wavenumber/cm⁻¹: 3325 (m), 3063 (w), 3029 (w), 2926 (m), 2851 (m), 1682 (m), 1640 (s), 1544 (s), 1452 (w), 1244 (m), 1115 (m), 1088 (m), 744, 698, 634

MALDI-TOF MS *m/z* (%): 336.3 (100) [M+H]⁺, 358.3 (56) [M+Na]⁺, 374.3 (10) [M+K]⁺

Elemental Analysis (C₁₉H₂₉NO₂S): calcd (%) **C** 68.02, **H** 8.71, **N** 4.18, **S** 9.56

found (%) **C** 68.10, **H** 8.94, **N** 4.39, **S** 9.86

5.3.10 Synthesis of Compound 6



To a solution of γ -aminobutyric acid (5 g, 48.5 mmol) and *N,N*-diisopropylethylamine (10 mL) in dry dichloromethane (150 mL), benzyl chloroformate (10,4 mL, 97 mmol) was added at 0 °C. The reaction mixture was stirred at 25 °C for 16 hours. Then, the solvent and amine were removed by evaporation and the product was isolated chromatographically (SiO₂, 2:1 (v/v) hexane/ethyl acetate) to afford the product as a light-yellow solid.

Yield: 4.2 g, 37 %

Mp : 61-62 °C

¹H-NMR [400 MHz, 25 °C, CDCl₃] δ : 7.42-7.30 (m, 5H, H_a), 5.12 (s, 2H, H_b), 4.92 (s, 1H, H_c), 3.28-3.24 (m, 2H, H_d), 2.42-2.38 (m, 2H, H_e), 1.86-1.80 (m, 2H, H_f) ppm.

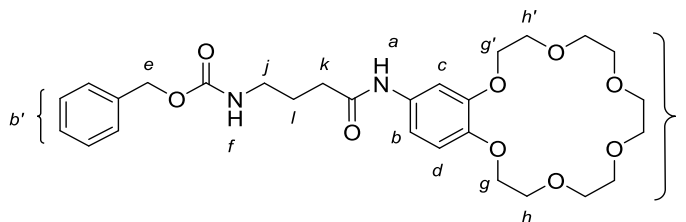
¹³C-NMR [100.6 MHz, 25 °C, CDCl₃] δ : 178.5, 156.6, 136.4, 128.7, 128.4, 128.3, 67.1, 40.3, 31.2, 25.2

IR wavenumber/cm⁻¹: 3325 (m), 3061 (w), 3034 (w), 2933 (m), 1686 (s), 1536 (s), 1451 (s), 1413 (m), 1257 (s), 1210 (s), 1140 (m), 1016 (m), 907 (m), 747 (m), 696 (m)

Elemental Analysis (C₁₂H₁₅NO₄): calcd (%) **C** 60.75, **H** 6.37, **N** 5.90

found (%) **C** 60.72, **H** 6.34, **N** 5.91

5.3.11 Synthesis of Compound 7



To a solution of **6** (420 mg, 1.8 mmol) and 4'-aminobenzo-18-crown-6 (480 mg, 1.5 mmol) in dichloromethane (50 mL) and dimethylformamide (5 mL), *N,N'*-dicyclohexyl-carbodiimide (350 mg, 1.7 mmol) and 4-dimethylaminopyridine (30 mg, 0.25 mmol) were added under a N₂ atmosphere. The reaction mixture was refluxed for 16 hours. The solvent was removed, cold acetone (2 mL) was added to the residue and the solution was filtered to remove residual 4-dimethylaminopyridine and dicyclohexylurea. The filtrate was evaporated and addition of acetone, filtration, and evaporation was repeated three times. Then, the product was dissolved in 2 mL of dichloromethane followed by precipitation in diethyl ether (50 mL). The precipitate was collected to obtain the product as a light-yellow solid.

Yield: 310 mg, 40 %

Mp: 130-132 °C

¹H-NMR [400 MHz, 25 °C, CDCl₃] δ: 8.20 (s, 1H, H_a), 7.40-7.34 (m, 6H, H_{b,b'}), 6.95 (d, 1H, H_c), 6.82 (d, 1H, H_d), 5.11 (s, 2H, H_e), 5.04 (s, 1H, H_f), 4.16-4.11 (m, 4H, H_{g,g'}), 4.91-4.89 (m, 4H, H_{h,h'}), 3.77-3.68 (m, 12H, H_i), 3.32 (m, 2H, H_j), 2.37 (t, 2H, *J*=6.6 Hz, H_k), 1.93-1.86 (m, 2H, H_l) ppm.

¹³C-NMR [100.6 MHz, 25 °C, CDCl₃] δ: 171.2, 157.4, 148.8, 148.5, 145.0, 136.6, 132.8, 128.6, 128.2, 114.3, 112.4, 106.8, 70.8, 70.7, 70.6, 69.7, 69.5, 69.3, 68.7, 66.9, 40.2, 34.6, 26.7 ppm.

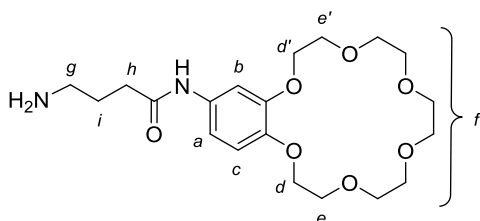
IR wavenumber/cm⁻¹: 3310 (m), 3267 (w), 2935 (m), 2860 (w), 1692 (s), 1653 (s), 1600 (m), 1551 (s), 1517 (s), 1450 (m), 1412 (m), 1266 (s), 1128 (s), 1022 (s), 844 (m)

MALDI-TOF MS *m/z* (%): 546.3 (50) [M]⁺, 569.3 (100) [M+Na]⁺, 585.4 (95) [M+K]⁺

Elemental Analysis ($C_{26}H_{34}N_2O_8 \cdot 0.5H_2O$): calcd (%) **C** 61.04, **H** 6.90, **N** 5.48

found (%) **C** 61.25, **H** 7.08, **N** 5.28

5.3.12 Synthesis of Compound 8



To a solution of compound **7** (230 mg, 0.42 mmol) in MeOH (30 mL), Pd/C (10 %, 36 mg) and HCl (1 M, 0.42 mL) were added, and the reaction was stirred at 25 °C under a H₂ atmosphere for 2 days. Then, the solution was filtered through celite followed by the evaporation of methanol. The crude product was then dissolved in ethyl acetate with 5% triethylamine (25 mL), and this solution was filtered through a short SiO₂ column. The final solution was collected and dried to give the product as a light yellow solid.

Yield: 170 mg, 98 %

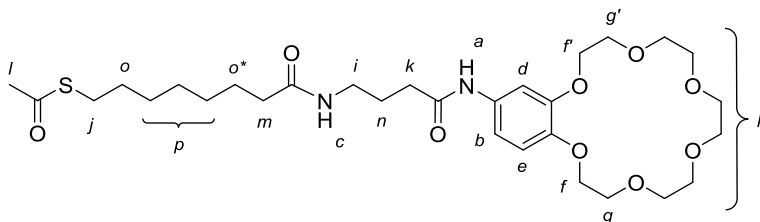
Mp: 134-137 °C

¹H-NMR [400 MHz, 25 °C, D₂O] δ: 7.07 (s, 1H, H_a); 6.96 (m, 1H, H_b); 6.88 (d, 1H, H_c); 4.18 (m, 4H, H_{d,d'}); 3.87 (m, 4H, H_{e,e'}); 3.69-3.65 (m, 12H, H_f); 3.03 (t, 2H, *J*=7.7 Hz, H_g); 2.47 (t, 2H, *J*=7.4 Hz, H_h); 1.98-1.94 (m, 2H, H_i) ppm.

¹³C-NMR [100.6 MHz, 25 °C, D₂O] δ: 173.5, 146.9, 144.3, 129.9, 114.8, 111.8, 107.1, 69.8, 67.2, 38.6, 32.5, 22.8 ppm.

IR wavenumber/cm⁻¹: 3324 (w), 2926 (m), 2852 (m), 1661 (m), 1609 (m), 1547 (m), 1513 (s), 1453 (m), 1223 (s), 1116 (s), 1025 (m), 953 (s), 820 (m)

MALDI-TOF MS *m/z* (%): 413.2 (17) [M+H]⁺, 435.2 (35) [M+Na]⁺, 451.2 (100) [M+K]⁺

5.3.13 Synthesis of Protected Ligand C_{LAc} 

To a solution of **1** (200 mg, 0.9 mmol) in dichloromethane (30 mL) and dimethylformamide (2 mL), *N,N'*-dicyclohexyl carbodiimide (150 mg, 0.73 mmol) and 4-dimethylaminopyridine (15 mg, 0.12 mmol) were added. Compound **8** (100 mg, 0.24 mmol) was added and the reaction mixture was refluxed for 16 hours under a N_2 atmosphere. Then, the solvent was evaporated and cold acetone (2 mL) was added to the residue. The solution was filtered to remove residual 4-dimethylaminopyridine and dicyclohexylurea. The filtrate was evaporated and the addition of acetone, filtration, and evaporation was repeated three times. Then, the product was dissolved in 2 mL of dichloromethane followed by precipitation in diethyl ether (50 mL). The precipitate was collected to afford the product as a light-yellow solid.

Yield: 52 mg, 70 %

Mp: 108-110 °C

1H -NMR [400 MHz, 25 °C, $CDCl_3$] δ : 10.27 (s, 1H, H_a); 7.47 (s, 1H, H_b); 7.43 (s, 1H, H_c); 7.35-7.33 (m, 1H, H_d); 6.58 (d, 1H, H_e); 4.06-3.99 (m, 4H, $H_{f,f'}$); 3.90-3.87 (m, 4H, $H_{g,g'}$); 3.78-3.65 (m, 12H, H_h); 3.33-3.27 (m, 2H, H_i); 2.85-2.79 (m, 2H, H_j); 2.51-2.48 (m, 2H, H_k); 2.31 (s, 3H, H_l); 2.24-2.19 (m, 2H, H_m); 1.90-1.87 (m, 2H, H_n); 1.58-1.52 (m, 4H, $H_{o,o'}$); 1.34-1.27 (m, 6H, H_p) ppm.

^{13}C -NMR [100.6 MHz, 25 °C, D_2O] δ : 196.6, 196.1, 194.3, 148.8, 145.0, 132.9, 114.3, 112.4, 107.2, 70.8, 70.7, 70.6, 69.7, 69.6, 69.4, 68.8, 38.5, 36.8, 34.8, 30.7, 29.5, 29.1, 28.8, 26.5, 25.8 ppm.

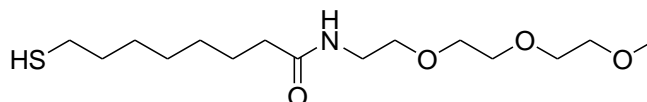
IR wavenumber/ cm^{-1} : 3322 (m), 3072 (w), 2927 (s), 2851 (m), 1639 (m), 1626 (s), 1513 (s), 1428, 1354, 1309, 1229 (s), 1119 (s), 1087 (s), 950, 804 (m).

MALDI-TOF MS m/z %: 613.4 (23) $[M+H]^+$, 635.5 (100) $[M+Na]^+$, 651.5 (21) $[M+K]^+$

Elemental Analysis ($C_{30}H_{50}N_2O_9S \cdot 2H_2O$): calcd (%) **C** 55.52, **H** 8.36, **N** 4.32 **S** 4.94

found (%) **C** 55.23, **H** 7.88, **N** 4.71 **S** 5.13

5.3.14 Deprotection of Ligand TEG_{Ac} under Basic Conditions



Ligand TEG_{Ac} (38 mg, 0.104 mmol) and diisopropylethylamine (2.72 mL, 15.6 mmol) were dissolved in degassed methanol (2.8 mL). The solution was stirred under an argon atmosphere at 25°C for 5 days. The reaction was followed by 1H -NMR spectroscopy by taking a sample with a micro syringe (100 μ L), transferring it to an NMR tube, evaporating the solvent under vacuum, and adding $CDCl_3$. It was observed that deprotection is slow and not completed even after 5 d.

5.3.15 General Procedure of the Deprotection of the Ligands

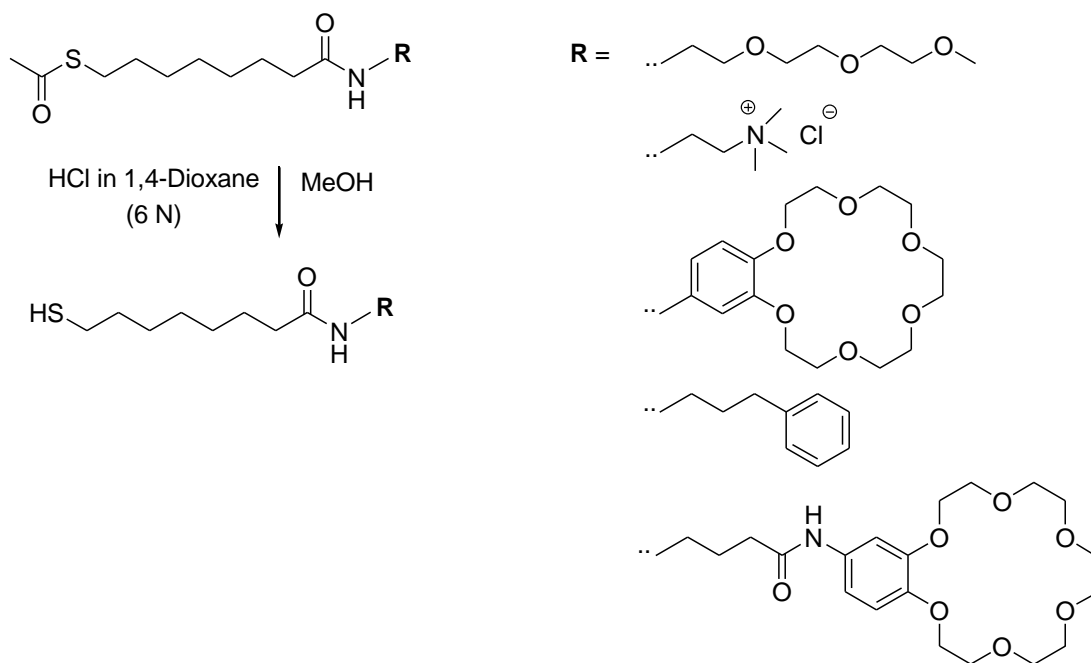
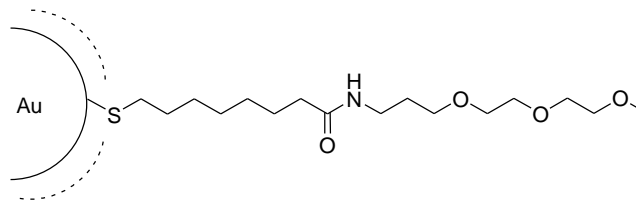


Figure 5.1 Structures of acetyl protected and deprotected ligands

The protected ligands **TEG_{Ac}**, **Q_{Ac}**, **CS_{Ac}**, **P_{Ac}** and **C_{LAc}** (0.2 mmol) were dissolved in degassed methanol (2 mL) in separate vials, and the solutions were purged thoroughly with argon. Afterward, HCl in dry 1,4-dioxane (6 N, 2 mL) was added to each solution and the resulting mixtures were stirred at 25 °C under argon. The reactions were followed by ^1H NMR spectroscopy, as described previously for the deprotection under basic conditions. Progressive disappearance of the methyl signals of the thioacetate groups was observed. After 4 h, each sample was evaporated under vacuum and the thiols thus obtained were kept under argon to prevent disulfide formation. The obtained free thiols were dissolved in degassed methanol under an argon atmosphere prior to the syntheses of the mixed monolayer protected gold nanoparticles.

5.4 Nanoparticle Syntheses

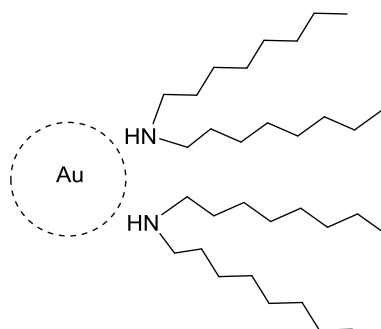
5.1.1 Synthesis of NP TEG without Ligand-Exchange



To a solution of $\text{HAuCl}_4 \cdot 3\text{H}_2\text{O}$ (24.9 mg, 0.075 mmol) in water (14 mL) was added a solution of **TEG** (20 mg, 0.06 mmol) in degassed methanol (7 mL) under a N_2 atmosphere. Afterwards, a freshly prepared solution of NaBH_4 (29.3 mg, 0.77 mol) in water (7 mL) was added dropwise within 1 min and the reaction mixture was stirred for 2 h under inert conditions at 25 °C. Then, the solvents were removed and the obtained nanoparticles were dissolved in 1 mL of dichloromethane. This solution of nanoparticles was added dropwise into cold ether (20 mL). The nanoparticles were collected and purified by dissolving them in methanol and centrifugation through a molecular weight-cutoff (Hydrosart membrane, 5K) tube 4 times. (The centrifugal tubes were rinsed with water several times prior to addition of the nanoparticle solutions to remove impurities and additives such as glycerine and sodium azide.⁴⁹) The nanoparticle layer was collected and dried. The resulting nanoparticles were not completely water soluble but soluble in water/methanol 9:1 (v/v) mixture.

Yield: 12 mg

5.4.2 Synthesis of Dioctylamine-protected Gold Nanoparticles (*NP A*)¹¹⁶



A solution of $\text{HAuCl}_4 \cdot 3 \text{H}_2\text{O}$ (40 mg, 0.12 mmol) in water (15 mL) was mixed with a solution of tetraoctylammonium bromide (2.18 g, 4 mmol) in degassed toluene (100 mL). The yellow aqueous solution turned colorless and the organic layer became reddish-orange. Di-*n*-octylamine (2.78 mL, 9.2 mmol) was added and the mixture was vigorously stirred for 40 min while the color disappeared. Afterwards, a solution of NaBH_4 (37 mg, 0.97 mmol) in H_2O (3 mL) was added within 20 s under vigorous stirring. The solution was stirred for another 3 h. Then, the aqueous layer was separated and the remaining resulting nanoparticle solution was kept under a nitrogen atmosphere for 24 h at 10 °C.

5.4.2 Synthesis of Mixed-Monolayer Protected Gold Nanoparticles¹¹⁶

Deprotected ligands *TEG*, *Q*, *P*, *C_s*, *C_l* were dissolved in degassed methanol (2 mL) separately or as mixtures in the desired ratios (see Table 3.1), and added to the solution of *NP A* (40 mL) under an argon atmosphere in a closed vial. This reaction mixture was stirred for 2 h at 25 °C.

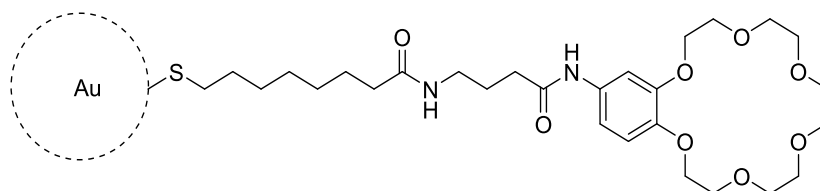
Afterwards, water (2 mL) was added and the nanoparticles were transferred to the aqueous layer by stirring for 30 min. The aqueous layer was separated, the solvent was removed, and the nanoparticles were purified by dissolving them in methanol followed by filtration via centrifugation through a molecular weight cutoff membrane (Hydrosart membrane, 5K). This procedure of dissolving in methanol and filtration by centrifugation was repeated four times in order to obtain pure nanoparticles. (The centrifugal tubes were rinsed with water several times prior to addition of the nanoparticle solutions to remove impurities and additives such as

glycerine and sodium azide¹¹⁷) Afterwards, the layer that contained the nanoparticles was collected and dried and the purity of the particles was controlled by measuring the ¹H NMR spectra of a sample in D₂O. The particles were dried under vacuum for two days. The yields denote the obtained amount of the dried samples (Table 5.1).

Table 5.1 Yields of the nanoparticles

| | Yield (mg) |
|---------------------------|------------|
| NP Q | 17 |
| NP QC_s | 20 |
| NP QP | 15 |
| NP QPC_s | 19 |
| NP QC_L | 23 |
| NP QPC_L | 21 |

5.4.3 Synthesis of Nanoparticle C_L



Deprotected ligand **C_L** (0.2 mmol) was dissolved in degassed methanol (2 mL). This solution (0.4 mL, 0.04 mmol) was added to the solution of **NP A** (40 mL) under an argon atmosphere in a closed vial. This reaction mixture was stirred for 2 h at 25 °C. The nanoparticles precipitated at the bottom of the vial and the supernatant toluene was removed. The nanoparticles were dissolved in methanol for purification by centrifugation through a molecular weight cutoff membrane. This procedure of dissolving in methanol followed by filtration via centrifugation was repeated five times. The resulting nanoparticles are soluble in methanol and water/methanol mixture, 1:1 (v/v) but not in water.

Yield: 12 mg

5.4 General Procedure for Iodine Decomposition^{118, 119}

To a sample of a functionalized nanoparticle (3 mg) in an NMR tube, a solution of iodine (25 mg) in methanol- d_4 (0.5 mL) followed by a stock solution of 2,4,6-trimethoxy-1,3,5-triazine (73 mM, 0.1 mL) in methanol- d_4 were added. The resulting mixture was sonicated for 30 min at 40 °C to decompose the nanoparticles. Afterwards, the ^1H NMR spectrum was recorded and the ratio of the integrals of characteristic signals from the individual ligands were determined by considering the respective number of absorbing protons. In general, at least two signals of each ligand were used to increase the reliability of the results. Specifically, the following signals were considered:

Ligand **Q**: 3.09 ppm (9H), 3.34 ppm (2H)

Ligand **C_S**: 7.20 ppm (1H), 6.90-6.77 ppm (2H), 4.03 ppm (4H), 3.75 ppm (4H)

Ligand **P**: 7.16-7.02 ppm (5H), 1.70 ppm (2H)

Ligand **C_L**: 7.29 ppm (1H), 6.89 ppm (1H), 6.83 ppm (1H), 3.80 ppm (4H), 3.55 ppm (12H).

The integral values for each peak were used to calculate the relative ratios of the respective ligands in the mixed monolayer protected nanoparticles. They were also used to determine the exact amount of ligands and gold atoms in the nanoparticles giving an estimation of the nanoparticle compositions (see Table 3.3).

5.5 DOSY-NMR Spectroscopy and Titrations

DOSY-NMR measurements were performed by using stock solutions of the nanoparticles in D₂O (99.96%). These solutions had a total ligand concentration of 1.9±0.2 mM for all measurements. In Figure 5.2 the amounts of nanoparticles and the values of D₂O to dissolve them are shown. In addition, the amounts of ligands in 0.3 mL of these solutions and the total ligand concentrations in the final solutions are specified.

For the measurements compiled in Table 3.11 a peptide stock solution (12 mM, 3 µL) in D₂O was added to a nanoparticle stock solution (0.3 mL) in an NMR tube. The overall volume of the mixture was made up to 0.5 mL with D₂O, the sample was thoroughly shaken and the DOSY-NMR spectrum recorded.

For the titrations, nine samples were prepared by mixing a nanoparticle stock solution (0.3 mL) in NMR tubes with increasing amounts of a peptide stock solution (3 to 120 µL) in D₂O. All samples were made up to 0.5 mL, shaken thoroughly and the DOSY-NMR spectra were recorded. All measurements were performed at 300 K. After recording the DOSY NMR spectrum of each sample, the diffusion coefficients of the peptides and nanoparticles were determined separately.

The diffusion constants of the nanoparticles (D_{bound}) were determined by taking the average values of diffusion coefficients of nanoparticles of each measurement. The diffusion constant of the peptide (D_{free}) was determined by recording a DOSY-NMR spectrum of the peptide in D₂O in the absence of nanoparticles. Table 5.2 also contains the diffusion coefficients of the peptides determined in these measurements.

Table 5.2 Amounts of nanoparticles and solvents used in the titrations

| NP Q | | |
|------------------------------|--------------------------|--------------------------------|
| m | 45.4 | mg |
| V (D ₂ O) | 12.47 | mL |
| mg NP in 0.3 mL | 1.09 | mg |
| total ligand in 0.3 mL | 9.24 x 10 ⁻⁷ | mol |
| c(lig)tot in sample (0.5 mL) | 1.85 x 10 ⁻³ | M |
| D free | 5.82 x 10 ⁻¹⁰ | m ² s ⁻¹ |
| D bound | 8.05 x 10 ⁻¹¹ | m ² s ⁻¹ |
| NP QP | | |
| m | 27.5 | mg |
| V (D ₂ O) | 7.01 | mL |
| mg NP in 0.3 mL | 1.18 | mg |
| total ligand in 0.3 mL | 9.17 x 10 ⁻⁷ | mol |
| c(lig)tot in sample (0.5 mL) | 1.83 x 10 ⁻³ | M |
| D free | 5.82 x 10 ⁻¹⁰ | m ² s ⁻¹ |
| D bound | 7.46 x 10 ⁻¹¹ | m ² s ⁻¹ |
| NP QCs | | |
| m | 18.2 | mg |
| V (D ₂ O) | 4.44 | mL |
| mg NP in 0.3 mL | 1.23 | mg |
| total ligand in 0.3 mL | 9.10 x 10 ⁻⁷ | mol |
| c(lig)tot in sample (0.5 mL) | 1.82 x 10 ⁻³ | M |
| D free | 5.82 x 10 ⁻¹⁰ | m ² s ⁻¹ |
| D bound | 7.17 x 10 ⁻¹¹ | m ² s ⁻¹ |
| NP QPCs | | |
| m | 10.9 | mg |
| V (D ₂ O) | 2.77 | mL |
| mg NP in 0.3 mL | 1.18 | mg |
| total ligand in 0.3 mL | 9.37 x 10 ⁻⁷ | mol |
| c(lig)tot in sample (0.5 mL) | 1.87 x 10 ⁻³ | M |
| D free | 5.82 x 10 ⁻¹⁰ | m ² s ⁻¹ |
| D bound | 8.00 x 10 ⁻¹¹ | m ² s ⁻¹ |

Table 5.3 summarizes the change of D_{obs} with increasing amount of Gly-Phe observed in the DOSY-NMR measurements.

Table 5.3 Results of DOSY-NMR titrations of **NP Q**, **NP QP**, **NP QPC_s** and **NP QPC_s** with Gly-Phe

| NP Q | | | NP QP | | |
|-------------------|--|--------|-------------------|--|--------|
| C_{Pep} / mM | D_{obs} / $\times 10^{-10}$ $m^2 s^{-1}$ | χ | C_{Pep} / mM | D_{obs} / $\times 10^{-10}$ $m^2 s^{-1}$ | χ |
| 0.072 | 3.93 | 0.377 | 0.036 | 4.32 | 0.297 |
| 0.144 | 4.58 | 0.248 | 0.072 | 4.75 | 0.212 |
| 0.288 | 4.88 | 0.188 | 0.144 | 5.20 | 0.123 |
| 0.567 | 5.17 | 0.131 | 0.288 | 5.64 | 0.035 |
| 0.960 | 5.41 | 0.083 | 0.567 | 5.70 | 0.025 |
| 1.200 | 5.39 | 0.086 | 0.960 | 5.70 | 0.024 |
| 1.440 | 5.46 | 0.073 | 1.440 | 5.66 | 0.033 |
| 2.160 | 5.44 | 0.076 | 2.160 | 5.70 | 0.024 |

| NP QCs | | | NP QPC_s | | |
|-------------------|--|--------|---------------------------|--|--------|
| C_{Pep} / mM | D_{obs} / $\times 10^{-10}$ $m^2 s^{-1}$ | χ | C_{Pep} / mM | D_{obs} / $\times 10^{-10}$ $m^2 s^{-1}$ | χ |
| 0.036 | 3.59 | 0.438 | 0.036 | 1.45 | 0.871 |
| 0.072 | 4.24 | 0.310 | 0.072 | 1.91 | 0.779 |
| 0.144 | 4.40 | 0.279 | 0.144 | 3.02 | 0.558 |
| 0.288 | 4.94 | 0.173 | 0.288 | 3.84 | 0.395 |
| 0.567 | 5.32 | 0.099 | 0.567 | 4.98 | 0.168 |
| 0.960 | 5.38 | 0.087 | 0.960 | 5.43 | 0.079 |
| 1.200 | 5.38 | 0.087 | 1.200 | 5.50 | 0.065 |
| 1.440 | 5.34 | 0.095 | 1.440 | 5.55 | 0.055 |
| 2.160 | 5.45 | 0.073 | 2.160 | 5.60 | 0.045 |

5. Experimental Part

In DOSY-NMR spectra, in which the individual peaks were resolved, mono-exponential fitting of the diffusion decay results was performed by using the TopSpin software to determine the diffusion coefficients (Figure 5.2).¹²⁰ All peaks were taken into account and the diffusion coefficient of the nanoparticle was determined using the graph with the best fit.

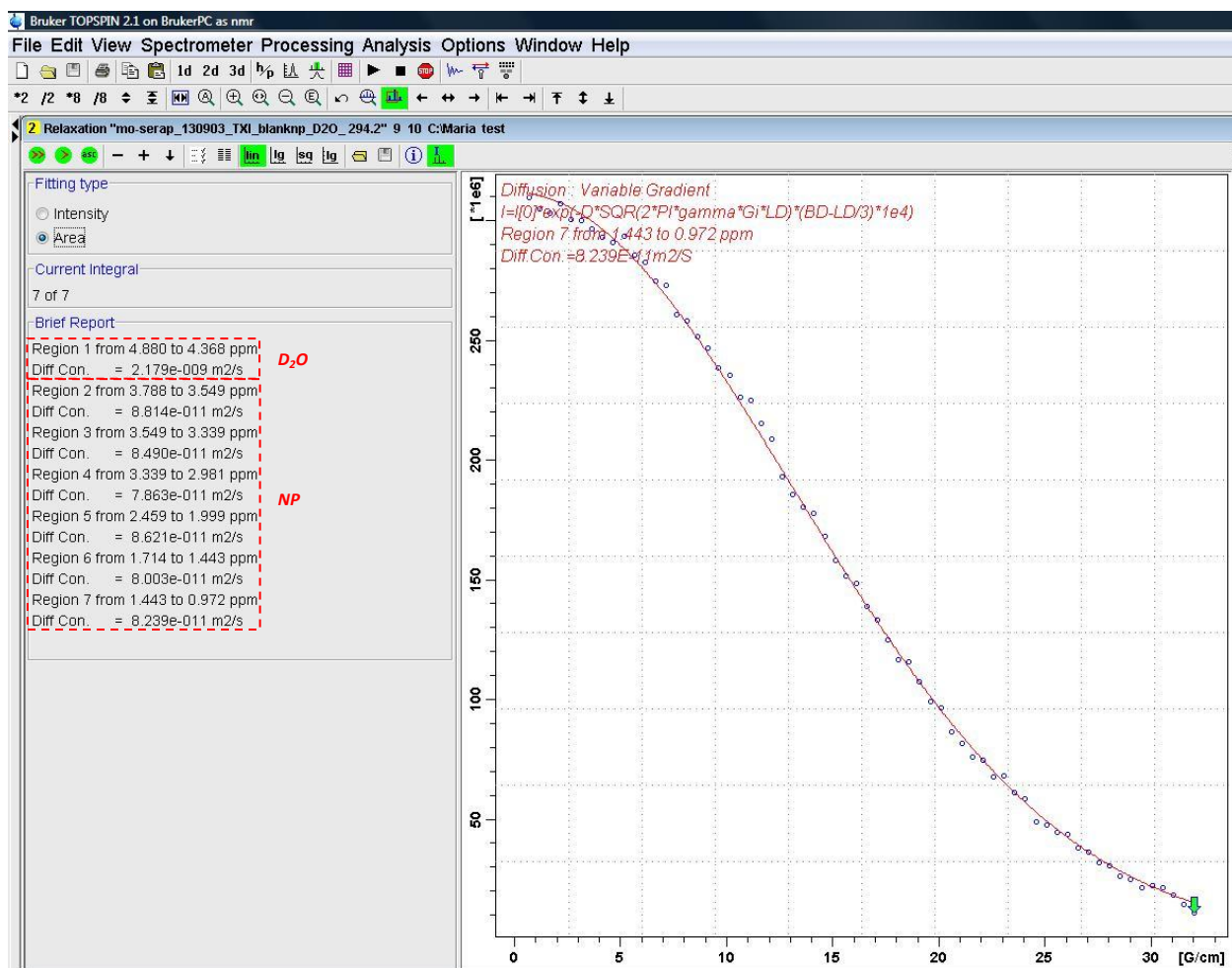


Figure 5.2 Screenshot of TopSpin showing the estimation of the diffusion coefficient of **NP Q**

In spectra containing overlapping peaks multi-exponential fitting was used to resolve the diffusion coefficients. The decay of these signals is described by the Stejskal-Tanner equation (Equation 5.1), where $D_{obs/bound}$ are the diffusion coefficients of the two species, S is the signal

amplitude, δ is the gradient pulse width, γ is the gyromagnetic ratio, g is the gradient amplitude, and Δ' is the diffusion time.¹²¹

$$S = S_{0NP} e^{-D_{bound} \gamma^2 \delta^2 g^2 \Delta'} + S_{0pep} e^{-D_{obs} \gamma^2 \delta^2 g^2 \Delta'} \quad \text{Equation 5.1}$$

In this equation, D_{obs} is the diffusion coefficient of the dipeptide and D_{bound} that of the nanoparticle. The latter can be determined independently.¹²¹ To calculate D_{obs} , the overlapping peaks were processed using TopSpin.

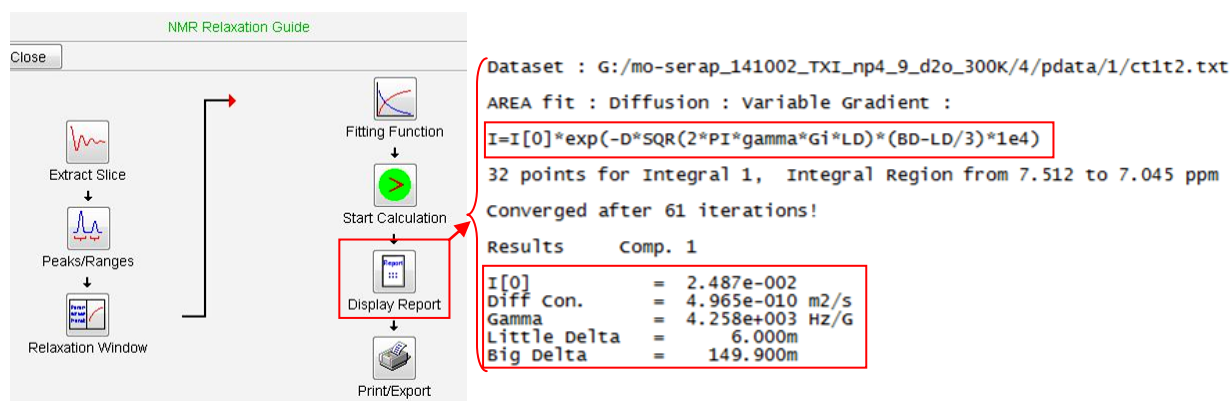


Figure 5.3 Screenshot of the relaxation window obtained from TopSpin and the report extracted from it

Using the parameters obtained from the report of the relaxation window in Figure 5.3, a graph was plotted where x represents the D value that needs to be fitted biexponentially to resolve the individual diffusion coefficients (Figure 5.4). D_{bound} is known from individual measurements. Therefore, D_{obs} could be calculated by using the OriginLab software. There, D_{bound} was denoted as ' $1/t_1$ ' and D_{obs} as ' $1/t_2$ ' in the '*formula**', which is the biexponential formula used by the OriginLab software.

5. Experimental Part

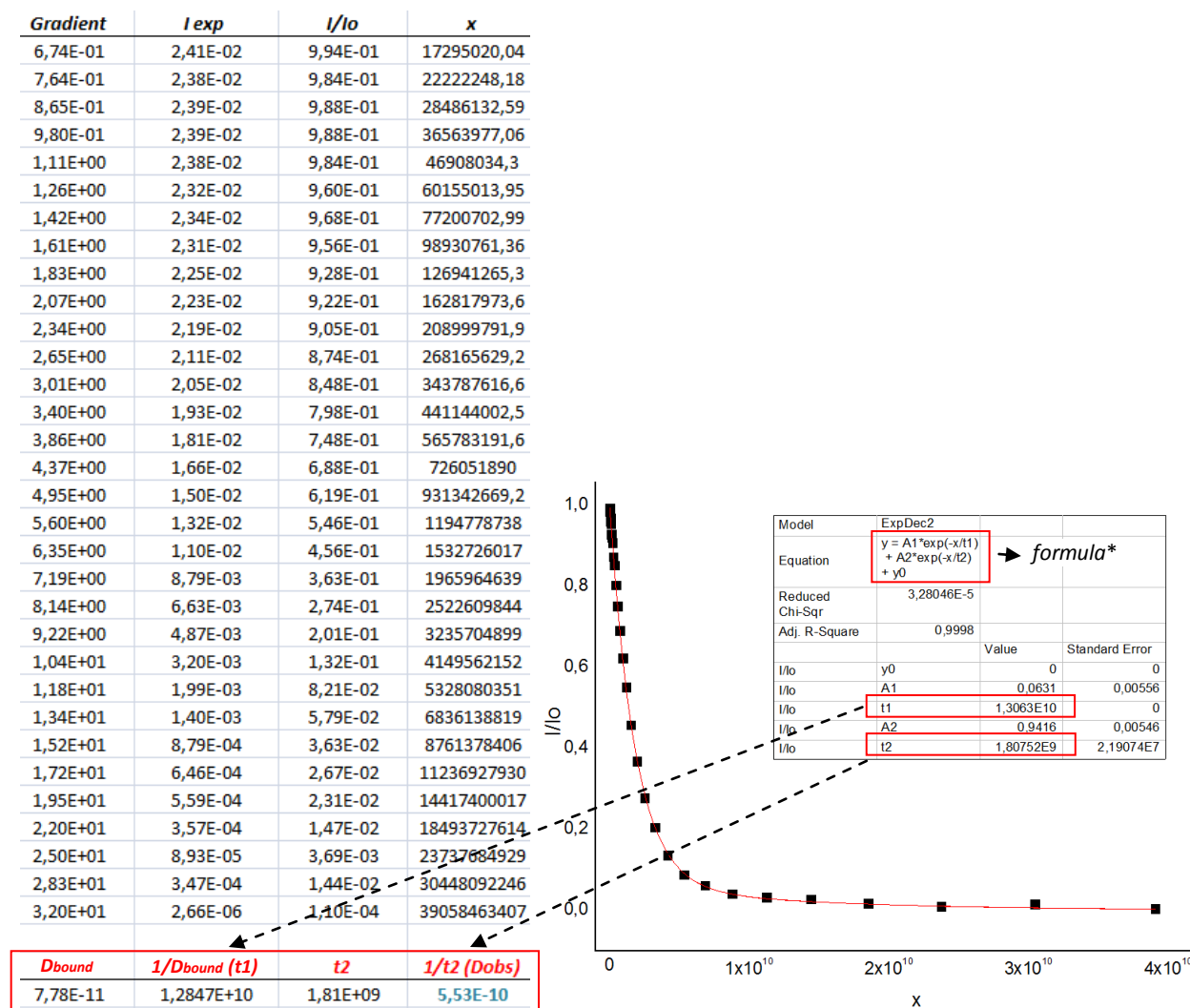


Figure 5.4 Example for the determination of the diffusion coefficients of Gly-Phe (1.2 mM) when binding to **NP QPC_S** ($c(lig_{tot})=1.87$ mM) by the biexponential treatment using OriginLab

5.6 Fluorescence Titration Experiments

For the 'wavelength dependent' measurements, samples were exciting at 295 nm and emission was recorded between 250 and 500 nm. The details of these measurements are summarized in Table 5.4.

Table 5.4 Conditions for 'wavelength dependent' fluorescent intensity measurements

| | |
|---------------------------------------|------------|
| <i>excitation Wavelength</i> | 295 nm |
| <i>emission Wavelength</i> | 363 nm |
| <i>band width (excitation)</i> | 5 nm |
| <i>band width (emission)</i> | 5 nm |
| <i>data pitch</i> | 1 nm |
| <i>scanning speed</i> | 250 nm/min |
| <i>sensitivity</i> | medium |
| <i>start (nm)</i> | 250 nm |
| <i>end (nm)</i> | 500 nm |

Afterwards, 'time dependent' measurements were performed where each sample was scanned for a certain amount of time, and the average value for the fluorescent intensities was measured. Each measurement was performed for 60 seconds with 0.2 seconds between each data point (Table 5.5). During this time the fluorescent intensities of the samples did not decrease significantly due to photo-bleaching.

Table 5.5 Conditions for 'time dependent' fluorescent intensity measurements

| | |
|-------------------------------------|--------|
| <i>excitation Wavelength</i> | 295 nm |
| <i>emission Wavelength</i> | 360 nm |
| <i>band width excitation</i> | 5 nm |
| <i>band width emission</i> | 5 nm |
| <i>resolution</i> | 0.05 s |
| <i>sensitivity</i> | medium |
| <i>measuring time</i> | 60 s |
| <i>data pitch</i> | 0.2 s |

Fluorescent titrations were performed by using nanoparticle stock solutions with similar overall concentrations of surface-bound ligands (1.9 ± 0.2 mM) and Gly-Trp stock solutions

(0.001 M) in HPLC grade water. The amounts of nanoparticles required for the stock solutions was calculated from the previously determined composition of the individual nanoparticles. The amounts of nanoparticles and the respective volumes of H₂O to dissolve them are summarized in Table 5.6.

Table 5.6 Preparation of nanoparticle stock solutions for the fluorescence titration experiments

(*obtained from I₂ decomposition)

| | m (mg) | V (mL) | Total Ligand* (mol / mg of NP) | Total Ligand (Molar) |
|---------------------------|--------|--------|--------------------------------|-----------------------|
| NP Q | 6,2 | 2,69 | $8,61 \times 10^{-7}$ | $1,98 \times 10^{-3}$ |
| NP QP | 10,1 | 4,39 | $8,07 \times 10^{-7}$ | $1,86 \times 10^{-3}$ |
| NP QC_s | 3,6 | 1,40 | $7,36 \times 10^{-7}$ | $1,89 \times 10^{-3}$ |
| NP QPC_s | 5,0 | 2,03 | $8,42 \times 10^{-7}$ | $2,07 \times 10^{-3}$ |
| NP QC_L | 8,7 | 3,39 | $8,04 \times 10^{-7}$ | $2,06 \times 10^{-3}$ |
| NP QPC_L | 3,7 | 1,47 | $8,13 \times 10^{-7}$ | $2,05 \times 10^{-3}$ |

The peptide stock solution was prepared by dissolving Gly-Trp (1.31 mg) in of HPLC grade water (5.01 mL). For the measurements in aqueous NaCl, a stock solution of Gly-Trp with the same concentration (0.001 M) in 3 M aqueous NaCl was prepared.

The titrations were performed by mixing 4.5 μL of the peptide stock solution with increasing amounts of the nanoparticle stock solutions (0-72 μL, Tables 5.7- 5.12) in a quartz cuvette and making up the total volume of each sample to 3 mL with HPLC grade water. The fluorescence intensities of the samples were measured at 360 nm and 25 °C after excitation at 295 nm by using the parameters specified in Table 5.5. Tables 5.7-5.12 summarize the results.

Table 5.7 Results of the fluorescence titration of **NP Q** with Gly-Trp

| | V(NP) / μL | c(lig)tot / M | V(pep) / μL | c(pep) / M | c(lig)tot / c(pep) | I | I ₀ |
|-----------|-----------------------|-------------------------|------------------------|-------------------------|--------------------|------|----------------|
| 1 | 0.0 | 0.00E+00 | 4.5 | 1.50 x 10 ⁻⁶ | 0.00 | 7.57 | 7.57 |
| 2 | 4.5 | 2.98 x 10 ⁻⁶ | 4.5 | 1.50 x 10 ⁻⁶ | 1.98 | 6.82 | 7.15 |
| 3 | 9.0 | 5.95 x 10 ⁻⁶ | 4.5 | 1.50 x 10 ⁻⁶ | 3.96 | 6.26 | 6.80 |
| 4 | 13.5 | 8.93 x 10 ⁻⁶ | 4.5 | 1.50 x 10 ⁻⁶ | 5.95 | 5.83 | 6.45 |
| 5 | 18.0 | 1.19 x 10 ⁻⁵ | 4.5 | 1.50 x 10 ⁻⁶ | 7.93 | 5.36 | 6.22 |
| 6 | 22.5 | 1.49 x 10 ⁻⁵ | 4.5 | 1.50 x 10 ⁻⁶ | 9.91 | 5.06 | 5.90 |
| 7 | 27.0 | 1.79 x 10 ⁻⁵ | 4.5 | 1.50 x 10 ⁻⁶ | 11.89 | 4.62 | 5.46 |
| 8 | 31.5 | 2.08 x 10 ⁻⁵ | 4.5 | 1.50 x 10 ⁻⁶ | 13.88 | 4.33 | 5.18 |
| 9 | 36.0 | 2.38 x 10 ⁻⁵ | 4.5 | 1.50 x 10 ⁻⁶ | 15.86 | 4.09 | 4.86 |
| 10 | 45.0 | 2.98 x 10 ⁻⁵ | 4.5 | 1.50 x 10 ⁻⁶ | 19.82 | 3.52 | 4.19 |
| 11 | 54.0 | 3.57 x 10 ⁻⁵ | 4.5 | 1.50 x 10 ⁻⁶ | 23.79 | 3.04 | 3.60 |
| 12 | 63.0 | 4.17 x 10 ⁻⁵ | 4.5 | 1.50 x 10 ⁻⁶ | 27.75 | 2.56 | 3.12 |
| 13 | 72.0 | 4.76 x 10 ⁻⁵ | 4.5 | 1.50 x 10 ⁻⁶ | 31.72 | 2.19 | 2.64 |

Table 5.8 Results of the for fluorescence titration of **NP QP** with Gly-Trp

| | V(NP) / μL | c(lig)tot / M | V(pep) / μL | c(pep) / M | c(lig)tot / c(pep) | I | I ₀ |
|-----------|-----------------------|-------------------------|------------------------|-------------------------|--------------------|------|----------------|
| 1 | 0.0 | 0 | 4.5 | 1.50 x 10 ⁻⁶ | 0 | 7.40 | 7.40 |
| 2 | 4.5 | 2.78 x 10 ⁻⁶ | 4.5 | 1.50 x 10 ⁻⁶ | 1.86 | 6.75 | 7.08 |
| 3 | 9.0 | 5.57 x 10 ⁻⁶ | 4.5 | 1.50 x 10 ⁻⁶ | 3.71 | 6.15 | 6.84 |
| 4 | 13.5 | 8.35 x 10 ⁻⁶ | 4.5 | 1.50 x 10 ⁻⁶ | 5.57 | 5.65 | 6.42 |
| 5 | 18.0 | 1.11 x 10 ⁻⁵ | 4.5 | 1.50 x 10 ⁻⁶ | 7.42 | 5.06 | 6.06 |
| 6 | 22.5 | 1.39 x 10 ⁻⁵ | 4.5 | 1.50 x 10 ⁻⁶ | 9.28 | 4.61 | 5.56 |
| 7 | 27.0 | 1.67 x 10 ⁻⁵ | 4.5 | 1.50 x 10 ⁻⁶ | 11.13 | 4.37 | 5.28 |
| 8 | 31.5 | 1.95 x 10 ⁻⁵ | 4.5 | 1.50 x 10 ⁻⁶ | 12.99 | 4.03 | 4.89 |
| 9 | 36.0 | 2.23 x 10 ⁻⁵ | 4.5 | 1.50 x 10 ⁻⁶ | 14.85 | 3.67 | 4.53 |
| 10 | 45.0 | 2.78 x 10 ⁻⁵ | 4.5 | 1.50 x 10 ⁻⁶ | 18.56 | 3.13 | 3.96 |
| 11 | 54.0 | 3.34 x 10 ⁻⁵ | 4.5 | 1.50 x 10 ⁻⁶ | 22.27 | 2.52 | 3.15 |
| 12 | 63.0 | 3.90 x 10 ⁻⁵ | 4.5 | 1.50 x 10 ⁻⁶ | 25.98 | 2.13 | 2.67 |
| 13 | 72.0 | 4.45 x 10 ⁻⁵ | 4.5 | 1.50 x 10 ⁻⁶ | 29.69 | 1.70 | 2.16 |

Table 5.9 Results of the fluorescence titration of *NP QCs* with Gly-Trp

| | V(NP) / μL | c(lig)tot / M | V(pep) / μL | c(pep) / M | c(lig)tot / c(pep) | I | I ₀ |
|-----------|-----------------------|-----------------------|------------------------|-----------------------|--------------------|------|----------------|
| 1 | 0.0 | 0 | 4.5 | 1.50×10^{-6} | 0 | 7.41 | 7.41 |
| 2 | 4.5 | 2.81×10^{-6} | 4.5 | 1.50×10^{-6} | 1.87 | 6.91 | 7.12 |
| 3 | 9.0 | 5.62×10^{-6} | 4.5 | 1.50×10^{-6} | 3.74 | 6.34 | 6.96 |
| 4 | 13.5 | 8.43×10^{-6} | 4.5 | 1.50×10^{-6} | 5.62 | 5.74 | 6.58 |
| 5 | 18.0 | 1.12×10^{-5} | 4.5 | 1.50×10^{-6} | 7.49 | 5.34 | 6.05 |
| 6 | 22.5 | 1.41×10^{-5} | 4.5 | 1.50×10^{-6} | 9.36 | 4.73 | 5.69 |
| 7 | 27.0 | 1.69×10^{-5} | 4.5 | 1.50×10^{-6} | 11.23 | 4.08 | 5.28 |
| 8 | 31.5 | 1.97×10^{-5} | 4.5 | 1.50×10^{-6} | 13.11 | 3.88 | 4.87 |
| 9 | 38.0 | 2.37×10^{-5} | 4.5 | 1.50×10^{-6} | 15.81 | 3.37 | 4.56 |
| 10 | 45.0 | 2.81×10^{-5} | 4.5 | 1.50×10^{-6} | 18.72 | 2.84 | 3.82 |
| 11 | 54.0 | 3.37×10^{-5} | 4.5 | 1.50×10^{-6} | 22.47 | 2.30 | 3.16 |
| 12 | 63.0 | 3.94×10^{-5} | 4.5 | 1.50×10^{-6} | 26.21 | 2.09 | 2.65 |
| 13 | 72.0 | 4.50×10^{-5} | 4.5 | 1.50×10^{-6} | 29.96 | 1.98 | 2.36 |

Table 5.10 Results of the fluorescence titration of *NP QPCs* with Gly-Trp

| | V(NP) / μL | c(lig)tot / M | V(pep) / μL | c(pep) / M | c(lig)tot / c(pep) | I | I ₀ |
|-----------|-----------------------|-----------------------|------------------------|-----------------------|--------------------|------|----------------|
| 1 | 0 | 0 | 4.5 | 1.50×10^{-6} | 0 | 7.51 | 7.51 |
| 2 | 4.5 | 3.11×10^{-6} | 4.5 | 1.50×10^{-6} | 2.07 | 6.58 | 6.98 |
| 3 | 9.0 | 6.22×10^{-6} | 4.5 | 1.50×10^{-6} | 4.14 | 5.88 | 6.64 |
| 4 | 13.5 | 9.33×10^{-6} | 4.5 | 1.50×10^{-6} | 6.22 | 5.47 | 6.37 |
| 5 | 18.0 | 1.24×10^{-5} | 4.5 | 1.50×10^{-6} | 8.29 | 4.85 | 6.06 |
| 6 | 22.5 | 1.56×10^{-5} | 4.5 | 1.50×10^{-6} | 10.36 | 4.17 | 5.58 |
| 7 | 27.0 | 1.87×10^{-5} | 4.5 | 1.50×10^{-6} | 12.43 | 3.90 | 5.12 |
| 8 | 31.5 | 2.18×10^{-5} | 4.5 | 1.50×10^{-6} | 14.51 | 3.43 | 4.84 |
| 9 | 38.0 | 2.63×10^{-5} | 4.5 | 1.50×10^{-6} | 17.50 | 2.75 | 4.35 |
| 10 | 45.0 | 3.11×10^{-5} | 4.5 | 1.50×10^{-6} | 20.72 | 2.49 | 3.65 |
| 11 | 54.0 | 3.73×10^{-5} | 4.5 | 1.50×10^{-6} | 24.87 | 1.93 | 3.18 |
| 12 | 63.0 | 4.36×10^{-5} | 4.5 | 1.50×10^{-6} | 29.01 | 1.73 | 2.52 |
| 13 | 72.0 | 4.98×10^{-5} | 4.5 | 1.50×10^{-6} | 33.16 | 1.68 | 2.33 |

Table 5.11 Results of the fluorescence titration of *NP QC_L* with Gly-Trp

| | V(NP) / μL | c(lig)tot / M | V(pep) / μL | c(pep) / M | c(lig)tot / c(pep) | I | I ₀ |
|-----------|-----------------------|-----------------------|------------------------|-----------------------|--------------------|------|----------------|
| 1 | 0 | 0 | 4.5 | 1.50×10^{-6} | 0 | 7.64 | 7.64 |
| 2 | 4.5 | 3.09×10^{-6} | 4.5 | 1.50×10^{-6} | 2.06 | 6.70 | 7.01 |
| 3 | 9.0 | 6.19×10^{-6} | 4.5 | 1.50×10^{-6} | 4.13 | 6.22 | 6.87 |
| 4 | 13.5 | 9.29×10^{-6} | 4.5 | 1.50×10^{-6} | 6.19 | 5.63 | 6.39 |
| 5 | 18.0 | 1.24×10^{-5} | 4.5 | 1.50×10^{-6} | 8.25 | 5.21 | 5.96 |
| 6 | 22.5 | 1.55×10^{-5} | 4.5 | 1.50×10^{-6} | 10.32 | 4.80 | 5.65 |
| 7 | 27.0 | 1.86×10^{-5} | 4.5 | 1.50×10^{-6} | 12.38 | 4.27 | 5.30 |
| 8 | 31.5 | 2.17×10^{-5} | 4.5 | 1.50×10^{-6} | 14.44 | 4.02 | 5.01 |
| 9 | 36.0 | 2.48×10^{-5} | 4.5 | 1.50×10^{-6} | 16.51 | 3.75 | 4.59 |
| 10 | 45.0 | 3.09×10^{-5} | 4.5 | 1.50×10^{-6} | 20.63 | 3.26 | 4.21 |
| 11 | 54.0 | 3.71×10^{-5} | 4.5 | 1.50×10^{-6} | 24.76 | 2.79 | 3.58 |
| 12 | 63.0 | 4.33×10^{-5} | 4.5 | 1.50×10^{-6} | 28.89 | 2.45 | 3.12 |
| 13 | 72.0 | 4.95×10^{-5} | 4.5 | 1.50×10^{-6} | 33.01 | 2.19 | 2.60 |

Table 5.12 Results of the fluorescence titration of *NP QPC_L* with Gly-Trp

| | V(NP) / μL | c(lig)tot / M | V(pep) / μL | c(pep) / M | c(lig)tot / c(pep) | I | I ₀ |
|-----------|-----------------------|-----------------------|------------------------|-----------------------|--------------------|------|----------------|
| 1 | 0 | 0 | 4.5 | 1.50×10^{-6} | 0 | 7.36 | 7.36 |
| 2 | 5.0 | 3.41×10^{-6} | 4.5 | 1.50×10^{-6} | 2.27 | 6.80 | 7.19 |
| 3 | 9.0 | 6.14×10^{-6} | 4.5 | 1.50×10^{-6} | 4.09 | 6.11 | 6.86 |
| 4 | 14.0 | 9.55×10^{-6} | 4.5 | 1.50×10^{-6} | 6.37 | 5.34 | 6.36 |
| 5 | 18.0 | 1.23×10^{-5} | 4.5 | 1.50×10^{-6} | 8.19 | 4.59 | 6.05 |
| 6 | 23.0 | 1.57×10^{-5} | 4.5 | 1.50×10^{-6} | 10.46 | 4.27 | 5.63 |
| 7 | 27.0 | 1.84×10^{-5} | 4.5 | 1.50×10^{-6} | 12.28 | 3.72 | 5.31 |
| 8 | 32.0 | 2.18×10^{-5} | 4.5 | 1.50×10^{-6} | 14.55 | 3.30 | 4.75 |
| 9 | 36.0 | 2.46×10^{-5} | 4.5 | 1.50×10^{-6} | 16.37 | 3.11 | 4.42 |
| 10 | 45.0 | 3.07×10^{-5} | 4.5 | 1.50×10^{-6} | 20.46 | 2.59 | 3.77 |
| 11 | 54.0 | 3.68×10^{-5} | 4.5 | 1.50×10^{-6} | 24.56 | 2.17 | 3.25 |
| 12 | 63.0 | 4.30×10^{-5} | 4.5 | 1.50×10^{-6} | 28.65 | 1.95 | 2.65 |
| 13 | 72.0 | 4.91×10^{-5} | 4.5 | 1.50×10^{-6} | 32.74 | 1.82 | 2.37 |

6. References

1. A. Pastor and E. Martinez-Viviente, *Coord. Chem. Rev.*, 2008, **252**, 2314-2345.
2. C. A. Hunter and H. L. Anderson, *Angew. Chem. Int. Ed.*, 2009, **48**, 7488-7499.
3. J. D. Badjic, A. Nelson, S. J. Cantrill, W. B. Turnbull and J. F. Stoddart, *Acc. Chem. Res.*, 2004, **38**, 723-732.
4. K. E. Sapsford, W. R. Algar, L. Berti, K. B. Gemmill, B. J. Casey, E. Oh, M. H. Stewart and I. L. Medintz, *Chem. Rev.*, 2013, **113**, 1904-2074.
5. S. Chaturvedi and A. K. Mishra, *Front. Med.*, 2016, **3**, 1-18.
6. R. Haag, *Beilstein J. Org. Chem.*, 2015, **11**, 848-849.
7. C. Fasting, C. A. Schalley, M. Weber, O. Seitz, S. Hecht, B. Kokschi, J. Dervede, C. Graf, E.-W. Knapp and R. Haag, *Angew. Chem. Int. Ed.*, 2012, **51**, 10472-10498.
8. M. A. Boles, D. Ling, T. Hyeon and D. V. Talapin, *Nat. Mater.*, 2016, **15**, 141-153.
9. S. A. Alsharif, L. Y. Chen, A. Tlahuice-Flores, R. L. Whetten and M. J. Yacaman, *Phys. Chem. Chem. Phys.*, 2014, **16**, 3909-3913.
10. J. Conde, J. T. Dias, V. Grazú, M. Moros, P. V. Baptista and J. M. d. I. Fuente, *Front. Chem. -Chem. Eng.*, 2014, **2**, 1-27.
11. J. Schill, A. P. H. J. Schenning and L. Brunsveld, *Macromol. Rapid Commun.*, 2015, **36**, 1306-1321.
12. L. H. Tan, H. Xing and Y. Lu, *Acc. Chem. Res.*, 2014, **47**, 1881-1890.
13. K. Saha, S. S. Agasti, C. Kim, X. Li and V. M. Rotello, *Chem. Rev.*, 2012, **112**, 2739-2779.
14. W. Edwards and E. R. Kay, *Chem. Nano. Mat.*, 2016, **2**, 87-98.
15. P. P. Pillai, S. Huda, B. Kowalczyk and B. A. Grzybowski, *J. Am. Chem. Soc.*, 2014, **135**, 6392-6395.
16. L. J. Prins, *Acc. Chem. Res.*, 2015, **48**, 1920-1928.
17. C. P. Shaw, D. A. Middleton, M. Volk and R. Levy, *ACS Nano*, 2012, **6**, 1416-1426.
18. O. Salata, *J. Nanobiotechnol.*, 2004, **2**, 1-6
19. C. Pezzato, S. Maiti, J. L. Chen, A. Cazzolaro, C. Gobbo and L. J. Prins, *Chem. Commun.*, 2015, **51**, 9922-9931.

6. References

20. P. D. Jadzinsky, G. Calero, C. J. Ackerson, D. A. Bushnell and R. D. Kornberg, *Science*, 2007, **318**, 30-433.
21. Y. Xue, X. Li, H. Li and W. Zhang, *Nat. Commun.*, 2014, **5**, 1-9.
22. M. Boeckl and D. Graham, *Mater. Matters*, 2006, **1.2**, 3.
23. L. H. Dubois, *Annu. Rev. Phys. Chem.*, 1992, **43**, 437-463.
24. J. Nam, N. Won, J. Bang, H. Jin, J. Park, S. Jung, S. Jung, Y. Park and S. Kim, *Adv. Drug Delivery Rev.*, 2013, **65**, 622-648.
25. G. L. Nealon, B. Donnio, R. Greget, J.-P. Kappler, E. Terazzib and J.-L. Gallani, *Nanoscale*, 2012, **4**, 5244-5258.
26. R. Levy, N. T. K. Thanh, R. C. Doty, I. Hussain, R. J. Nichols, D. J. Schiffrin, M. Brust and D. G. Fernig, *J. Am. Chem. Soc.*, 2004, **126**, 10076-10084.
27. P. Ionita, A. Volkov, G. Jeschke and V. Chechik, *Anal. Chem.*, 2008, **80**, 95-106
28. M. J. Hostetler, A. C. Templeton and R. W. Murray, *Langmuir*, 1999, **15**, 3782-3789.
29. H. Häkkinen, *Nat. Chem.*, 2012, **4**, 443-455.
30. H. K. Bisoyia and S. Kumar, *Chem. Soc. Rev.*, 2011, **40**, 306-319.
31. J. Turkevich, P. C. Stevenson and J. Hillier, *Discuss. Faraday Soc.*, 1951, **11**, 55-75.
32. G. Frens, *Nat. Phys. Sci.*, 1973, **241**, 20-22.
33. A. D. McFarland, C. L. Haynes, C. A. Mirkin, R. P. V. Duyne and H. A. Godwin, *J. Chem. Educ.*, 2004, **81**, 544A.
34. M. Brust, M. Walker, D. Bethell, D. J. Schiffrin and R. Whyman, *Chem. Commun.*, 1994, **7**, 801-802.
35. W. P. Wuelfing, S. M. Gross, D. T. Miles and R. W. Murray, *J. Am. Chem. Soc.*, 1998, **120**, 12696-12697.
36. E. Oh, K. Susumu, R. Goswami and H. Mattoussi, *Langmuir*, 2010, **10**, 7604-7613.
37. F. Manea, C. Bindoli, S. Polizzi, L. Lay and P. Scrimin, *Langmuir*, 2008, **24**, 4120-4124.
38. C. Gentilini, F. Evangelista, P. Rudolf, P. Franchi, M. Lucarini and L. Pasquato, *J. Am. Chem. Soc.*, 2008, **130**, 15678-15682
39. R. C. V. Lehn and A. Alexander-Katz, *Soft Matter*, 2015, **11**, 3165-3175.

6. References

40. H.-Y. Lee, S. H. R. Shin, L. L. Abezgauz, S. A. Lewis, A. M. Chirsa, D. D. Danino and K. J. M. Bishop, *J. Am. Chem. Soc.*, 2013, **135**, 5950-5953.
41. S. Rana, Y.-C. Yeh and V. M. Rotello, *Curr. Opin. Chem. Biol.*, 2010, **14**, 828-834.
42. S. Rana, A. Bajaja, R. Mouta and V. M. Rotello, *Adv. Drug Deliv. Rev.*, 2012, **2**, 200-216.
43. J. I. Cutler, E. Auyeung and C. A. Mirkin, *J. Am. Chem. Soc.*, 2012, **134**, 1376-1391.
44. M. De, S. Rana, H. Akpınar, O. R. Miranda, R. R. Arvizo, U. H. F. Bunz and V. M. Rotello, *Nat. Chem.*, 2009, **1**, 461-465.
45. G. Pieters, A. Cazzolaro, R. Bonomi and L. J. Prins, *Chem. Commun.*, 2012, **48**, 1916-1918.
46. B. Perrone, S. Springhetti, F. Ramadori, F. Rastrelli and F. Mancin, *J. Am. Chem. Soc.*, 2013, **135**, 11768-11771.
47. A. A. Shemetov, I. Nabiev and A. Sukhanova, *ACS Nano*, 2012, **6**, 4585-4602.
48. L. Pasquato, P. Pengob and P. Scrimin, *J. Mater. Chem.*, 2004, **14**, 3481-3487.
49. C. C. You, M. De, G. Han and V. M. Rotello, *J. Am. Chem. Soc.*, 2005, **127**, 12873-12881.
50. M. Dai, J. A. Frezzo, E. Sharma, R. Chen, N. Singh, C. Yuvienco, E. Caglar, S. Xiao, A. Saxena and J. K. Montclare, *J. Nanomed. Nanotechnol.*, 2016, **7**, 1-7.
51. Y. Zhao, K. Thorkelsson, A. J. Mastroianni, T. Schilling, J. M. Luther, B. J. Rancatore, K. Matsunaga, H. Jinnai, Y. Wu, D. Poulse, J. M. J. Fréchet, A. P. Alivisatos and T. Xu, *Nat. Mater.*, 2009, **8**, 979-985
52. D. Zaramella, P. Scrimin and L. J. Prins, *J. Am. Chem. Soc.*, 2012, **134**, 8396-8399.
53. F. Manea, F. B. Houillon, L. Pasquato and P. Scrimin, *Angew. Chem. Int. Ed.*, 2004, **43**, 6165-6169.
54. G. Zaupa, C. Mora, R. Bonomi, L. J. Prins and P. Scrimin, *Chem. Eur. J.*, 2011, **17**, 4879-4889.
55. M. Diez-Castellnou, F. Mancin and P. Scrimin, *J. Am. Chem. Soc.*, 2014, **136**, 1158-1161.
56. A. Bayir, B. J. Jordan, A. Verma, M. A. Pollier, G. Cookeb and V. M. Rotello, *Chem. Commun.*, 2006, 4033-4035.
57. A. K. Boal and V. M. Rotello, *J. Am. Chem. Soc.*, 2000, **122**, 734-735.
58. R. A. Sperling, P. R. Gil, F. Zhang, M. Zanella and W. J. Parak, *Chem. Soc. Rev.*, 2008, **37**, 1896-1908.

6. References

59. M.-V. Salvia, G. Salassa, F. Rastrelli and F. Mancin, *J. Am. Chem. Soc.*, 2015, **137**, 11399-11406.
60. A. C. Templeton, M. J. Hostetler, C. T. Kraft and R. W. Murray, *J. Am. Chem. Soc.*, 1998, **120**, 1906-1911.
61. O. Uzun, A. Verma, S. Chen, A. Centrone and F. Stellacci, *Chem. Commun.*, 2008, 196-198.
62. A. Arduini, D. Demuru, A. Pochini and A. Secchi, *Chem. Commun.*, 2005, 645-647.
63. R. S. Macomber, *J. Chem. Educ.*, 1992, **69**, 375-378.
64. P. Thordarson, *Chem. Soc. Rev.*, 2011, **40**, 1305-1323.
65. D. Zaramella, P. Scrimin and L. J. Prins, *J. Am. Chem. Soc.*, 2012, **134**, 8396-8399.
66. R. Bonomi, A. Cazzolaro and L. J. Prins, *Chem. Commun.*, 2011, **47**, 445-447.
67. M. De, O. R. Miranda, S. Ranaa and V. M. Rotello, *Chem. Comm.*, 2009, 2157-2159.
68. C. Johnson, *Prog. Nucl. Magn. Reson. Spectrosc.*, 1999, **34**, 203-256.
69. A. Pastor and E. Martinez-Viviente, *Coord. Chem. Rev.*, 2008, **252**, 2314-2345.
70. T. M. Hermans, M. A. Broeren, N. Gomopoulos, P. v. d. Schoot, M. v. Genderen, N. A. Sommerdijk, G. Fytas and E. W. Meijer, *Nat. Nanotechnol.*, 2009, **4**, 721-726.
71. R. Gomes, A. Hassinen, A. Szczygiel, Q. Zhao, A. Vantomme, J. C. Martins and Z. Hens, *J. Phys. Chem. Lett.*, 2011, **2**, 145-152.
72. X. Zhang, M. R. Servos and J. Liu, *J. Am. Chem. Soc.*, 2012, **134**, 7266-7269.
73. M. A. Hossain and H.-J. Schneider, *J. Am. Chem. Soc.*, 1998, **120**, 11208-11209.
74. P. Pengo, S. Polizzi, M. Battagliarin, L. Pasquato and P. Scrimin, *J. Mater. Chem.*, 2003, **13**, 2471-2478.
75. H. Hill, J. Millstone, M. Banholzer and C. A. Mirkin, *ACS Nano*, 2009, **3**, 418-424.
76. S. Ahmed and S. L. Wunder, *Langmuir*, 2009, **25**, 3682-3691.
77. K. B. Cederquist and C. D. Keating, *ACS Nano*, 2009, **3**, 256-260.
78. M. I. Bethencourt, L.-O. Srisombat, P. Chinwangso and T. R. Lee, *Langmuir*, 2009, **25**, 1265-1271.
79. C. Mayer, *Annu. Rep. NMR Spectrosc.*, 2005, **55**, 205-258.
80. Y. Cohen, L. Avram and L. Frish, *Angew. Chem. Int. Ed.*, **44**, 2005, 520-554.

6. References

81. D. V. Leff, P. C. Ohara, J. R. Heath and W. M. Gelbart, *J. Phys. Chem.*, 1995, **99**, 7036-7041.
82. M. J. Hostetler, J. E. Wingate, C.-J. Zhong, J. E. Harris, R. W. Vachet, M. R. Clark, D. Londono, S. J. Green, J. J. Stokes, G. D. Wignall, G. L. Glish, M. D. Porter, N. D. Evans and R. W. Murray, *Langmuir*, 1998, **14**, 17-30.
83. R. S. Macomber, *J. Chem. Educ.*, 1992, **69**, 375-378.
84. K. Niwa, S. Toda, K. Fuwa and H. Haraguchi, *Agric. Biol. Chem.*, 1977, **41**, 1287-1294.
85. C.S. Johnson, *Prog. Nucl. Magn. Reson. Spectrosc.*, 1999, **34**, 203-256.
86. M. Nilsson, M. A. Connel, A. L. Davis and G. A. Morris, *Anal. Chem.*, 2006, 3040-3045.
87. J. R. Lakowicz, Principles of Fluorescence Spectroscopy, *Springer Science&Business Media*, 2006.
88. I. Berlman, Handbook of Fluorescence Spectra of Aromatic Molecules, *Academic Press, New York*, 1971.
89. K. Sakakibara, L. A. Joyce, T. Mori, T. Fujisawa, S. H. Shabbir, J. P. Hill, E. V. Anslyn and K. Ariga, *Angew. Chem., Int. Ed.*, 2012, **51**, 9643-9646.
90. S. L. Wiskur, H. Ait-Haddou, J. J. Lavigne and E. V. Anslyn, *Acc. Chem. Res.*, 2001, **34**, 963-972.
91. M. Kitamura, S. H. Shabbir and E. V. Anslyn, *J. Org. Chem.*, 2009, **74**, 4479-4489.
92. H. S. Jeong, S. M. Choi, H. W. Kim, J. W. Park, H. N. Park, S. M. P. S. K. Jang, Y. M. Rhee and B. H. Kim, *Mol. BioSyst.*, 2013, **9**, 948-951.
93. T. Minami, Y. Liu, A. Akdeniz, P. Koutnik, N. A. Esipenko, R. Nishiyabu, Y. Kubo and P. A. Jr., *J. Am. Chem. Soc.*, 2014, **136**, 11396-11401.
94. B. T. Nguyen and E. V. Anslyn, *Coord. Chem. Rev.*, 2006, **250**, 3118-3127.
95. S. Jeon, W. Y. Kang, C. K. Song and J. S. Park, *Dyes Pigm.* 2012, **93**, 1544-1548.
96. K. A. Kang, J. Wang, J. B. Jasinski and S. Achilefu, *J. Nanobiotechnol.*, 2011, **9**, 1-13.
97. E. Dulkeith, A. C. Morteani, T. Niedereichholz, T. A. Klar and J. Feldmann, *Phys. Rev. Lett.*, 2002, **89**, 1-4.
98. X. Liu, H. T. Ngo, Z. Ge, S. J. Butler and K. A. Jolliffe, *Chem. Sci.*, 2013, **4**, 1680-1686.
99. T.-C. Liang and H.-C. Lin, *J. Mater. Chem.*, 2009, **19**, 4753-4763.

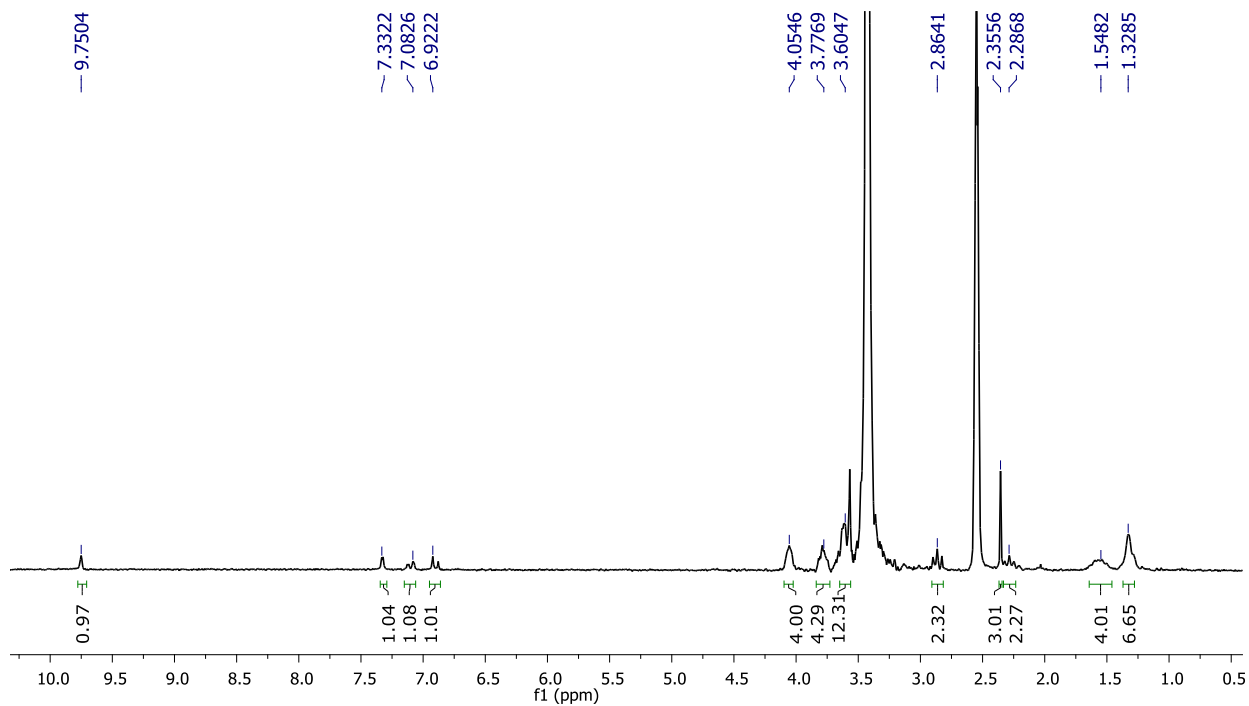
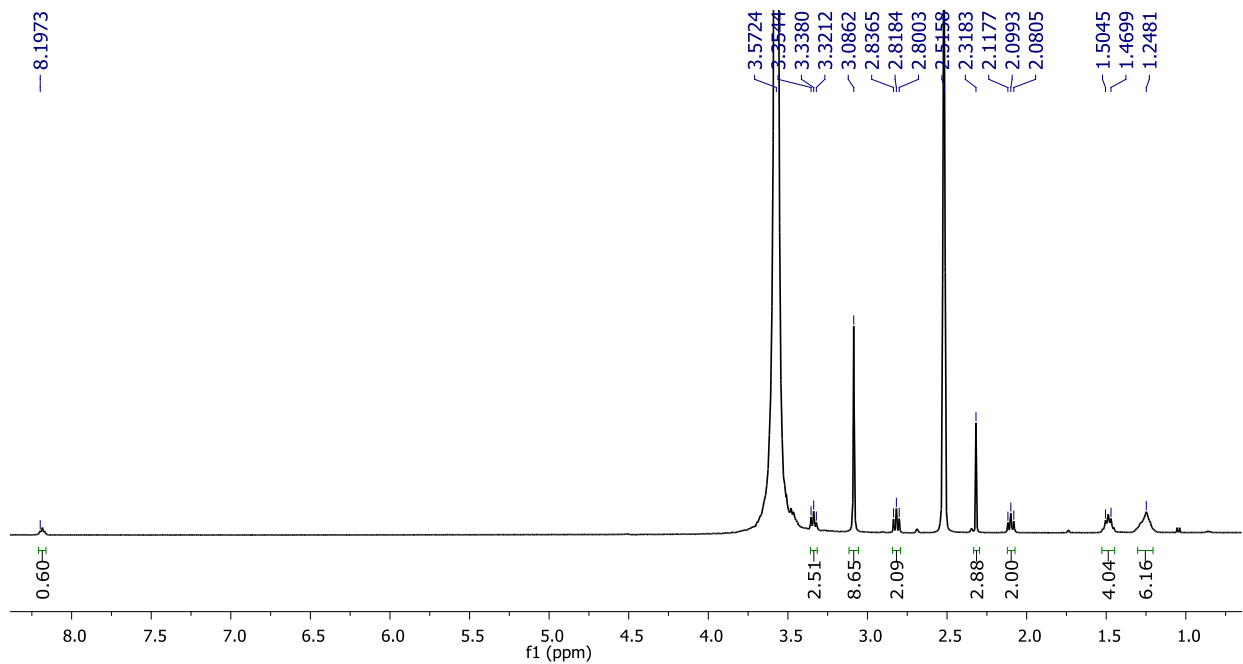
6. References

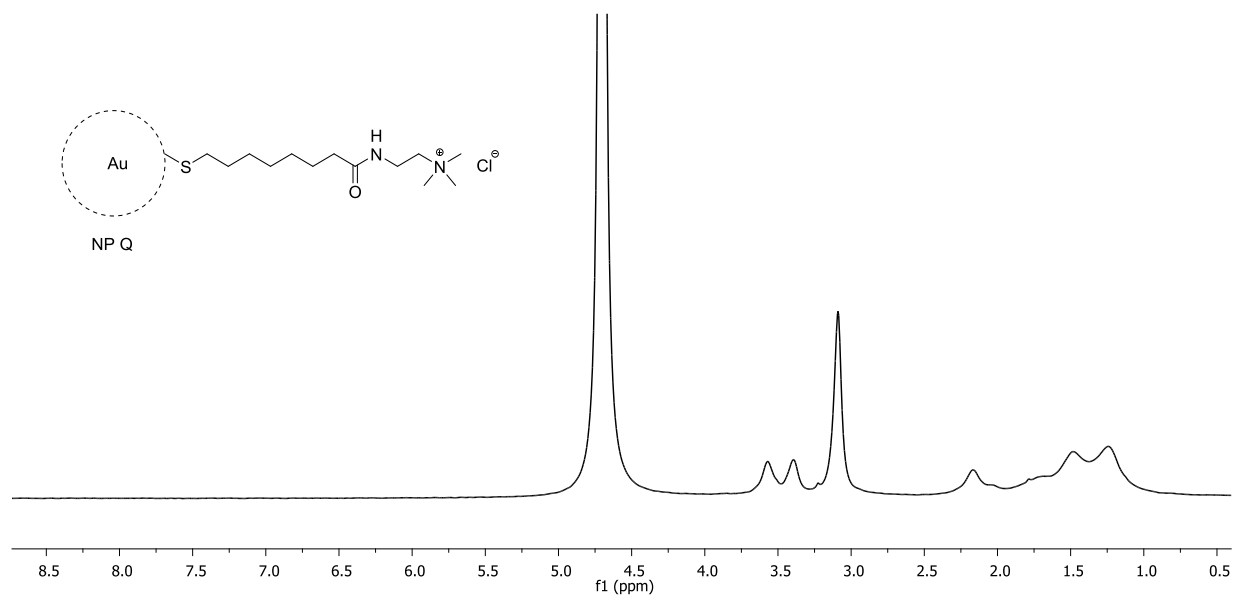
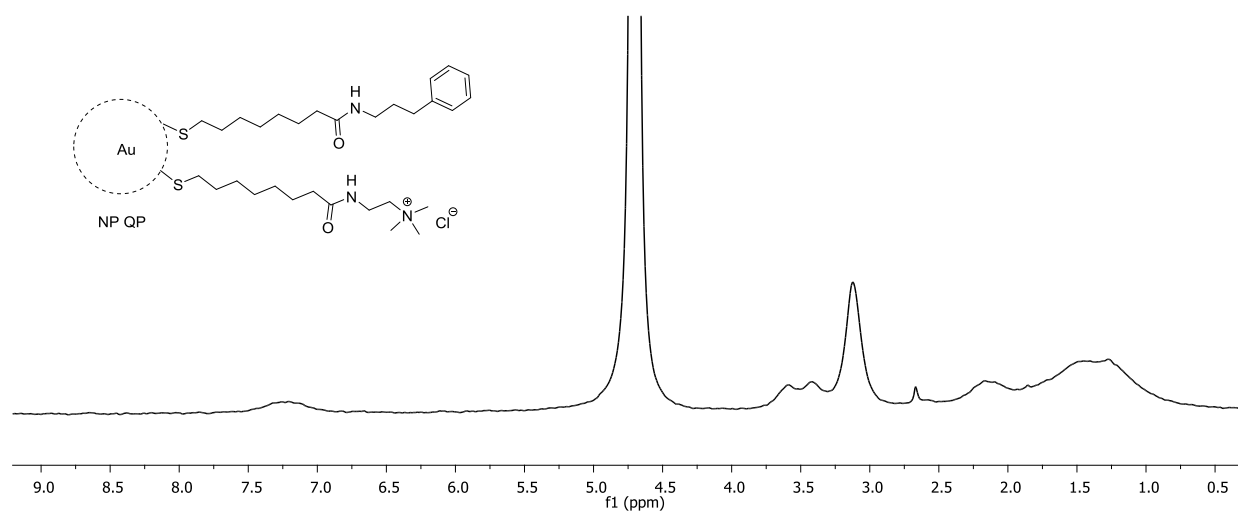
100. O. S. Wolfbeis, *Chem. Soc. Rev.*, 2015, **44**, 4743-4768.
101. A. E. Prigodich, P. S. Randeria, W. E. Briley, N. J. Kim, W. L. Daniel, D. A. Giljohann and C. A. Mirkin, *Anal. Chem.*, 2012, **4**, 2062-2066.
102. S. Yapar, M. Oikonomou, A. Velders and S. Kubik, *Chem. Commun.*, 2015, **51**, 14247-14250.
103. R. J. Sime, *The Langmuir Adsorption Isotherm, Physical Chemistry: Methods, Techniques, Experiments*, Philadelphia 1990.
104. K. Y. Foo and B. Hameed, *Chem. Eng. J.*, 2010, **156**, 2-10.
105. M. D. LeVan and T. Vermeulen, *J. Phys. Chem.*, 1981, **85**, 3247-3250.
106. S. H. Brewer, W. R. Glomm, M. C. Johnson, M. K. Knag and S. Franzen, *Langmuir*, 2005, **21**, 9303-9307.
107. X. Zhang, M. R. Servos and J. Liu, *Langmuir*, 2012, **28**, 3896-3902.
108. R. D. Ross and R. K. Roeder, *J. Biomed. Mater. Res., Part A*, 2011, **99**, 58-66.
109. Y. Han, P. Nowak, M. Colomb-Delsuc, M. P. Leal and S. Otto, *Langmuir*, 2015, **31**, 12658-12663.
110. P. Nowak, M. Colomb-Delsuc, S. Otto and J. Li, *J. Am. Chem. Soc.*, 2015, **137**, 10965-10969.
111. S. G. Martin and L. J. Prins, *Chem. Comm.*, 2016, **52**, 9387-9390.
112. S. Maiti and L. J. Prins, *Chem. Comm.*, 2015, **51**, 5714-5716.
113. E. R. Kay, *Chem. Eur.J.*, 2016, **22**, 10706-10716.
114. F. d. Sala and E. R. Kay, *Angew. Chem. Int. Ed.*, 2015, **54**, 4187-4191
115. P. Pengo, S. Polizzi, M. Battagliarin, L. Pasquato and P. Scrimin, *J. Mater. Chem.*, 2003, **13**, 2471-2478. *Angew. Chem. Int. Ed.*, 2015, **127**, 4261-4265
116. F. Manea, C. Bindoli, S. Polizzi, L. Lay and P. Scrimin, *Langmuir*, 2008, **24**, 4120-4124.
117. Vivaspin 15R, Technical data and Operating Instructions, *Vivaproducts*, 1998-2016, 85030-515-89.
118. C. Templeton, M. J. Hostetler, C. T. Kraft and R. W. Murray, *J. Am. Chem. Soc.*, 1998, **120**, 1906-1911.
119. L. Sun, R. M. Crooks and V. Chechik, *Chem. Commun.*, 2001, 359-360.

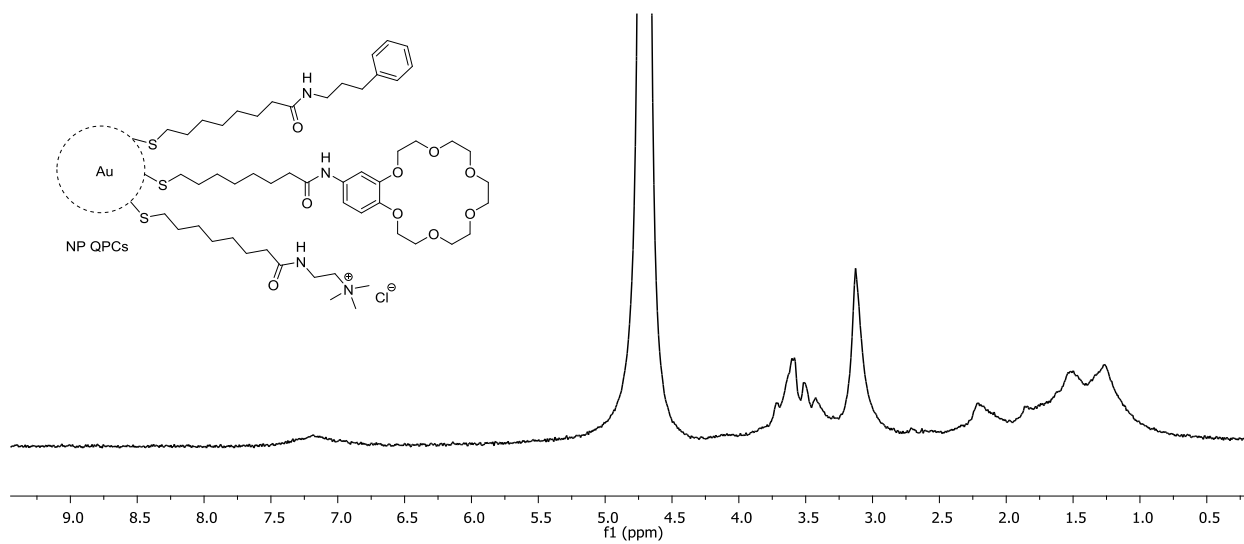
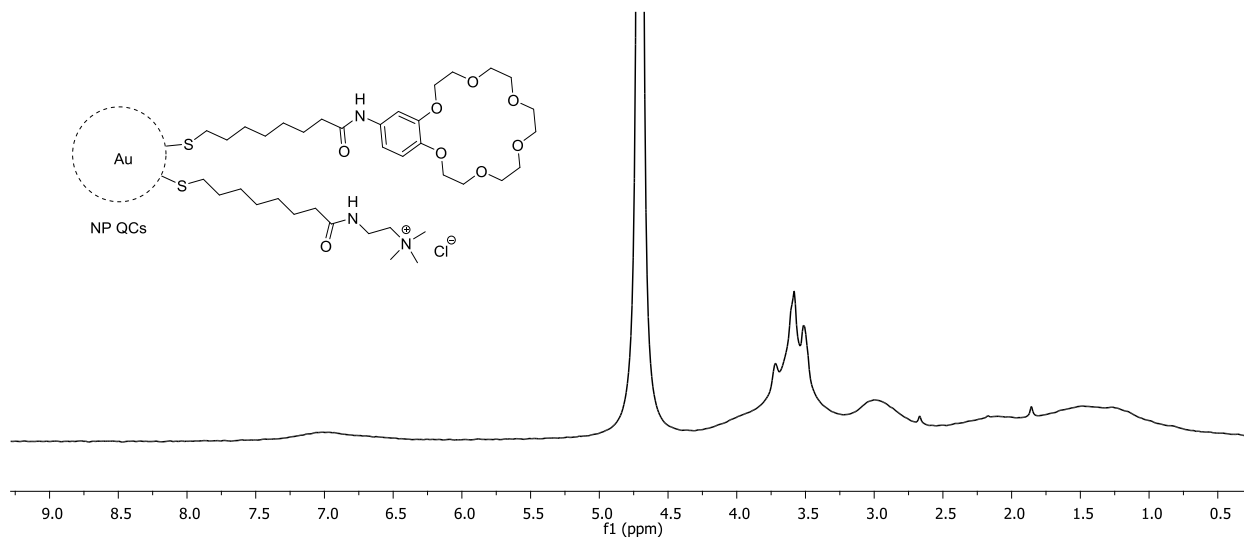
6. References

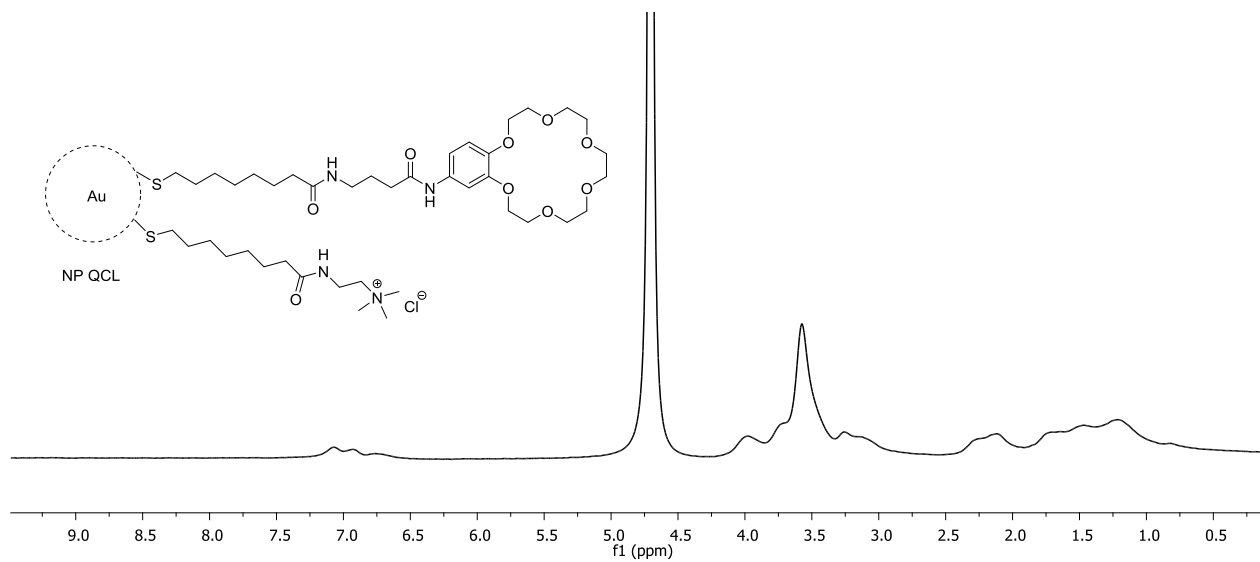
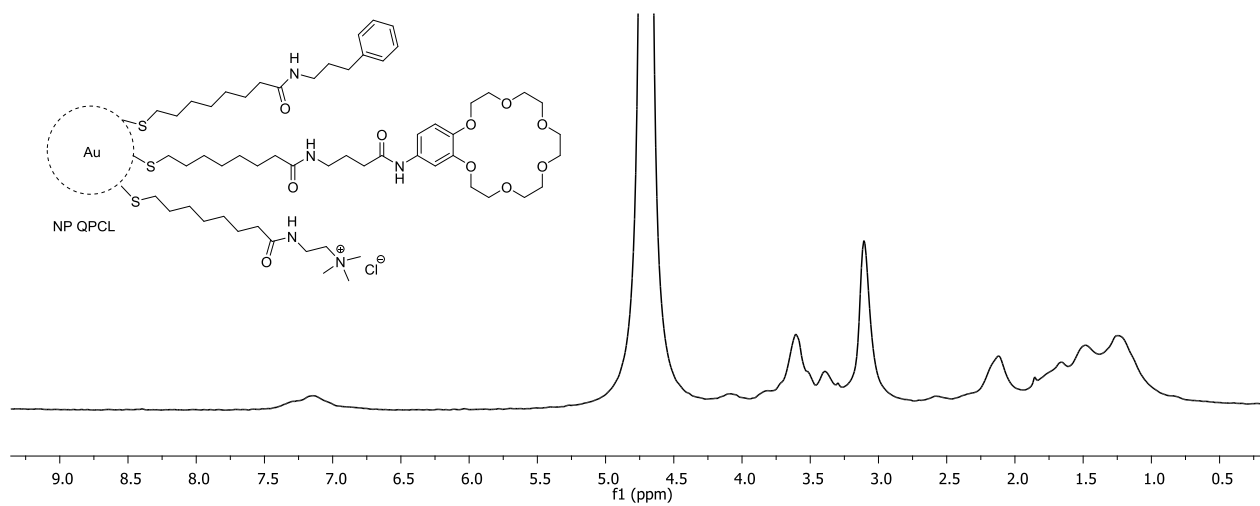
120. R. Kerssebaum and G. Salnikov, DOSY and Diffusion by NMR, *Bruker GmbH*, 2002-2006, **2.0.0**.
121. M. Nilsson, M. A. Connell, A. L. Davis and G. A. Morris, *Anal. Chem.*, 2006, **78**, 3040-3045.

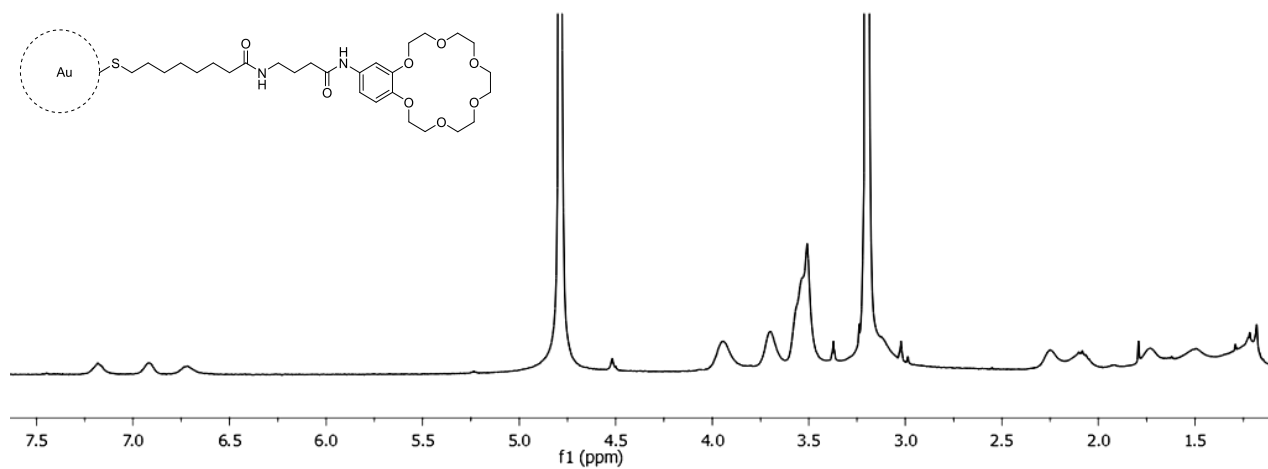
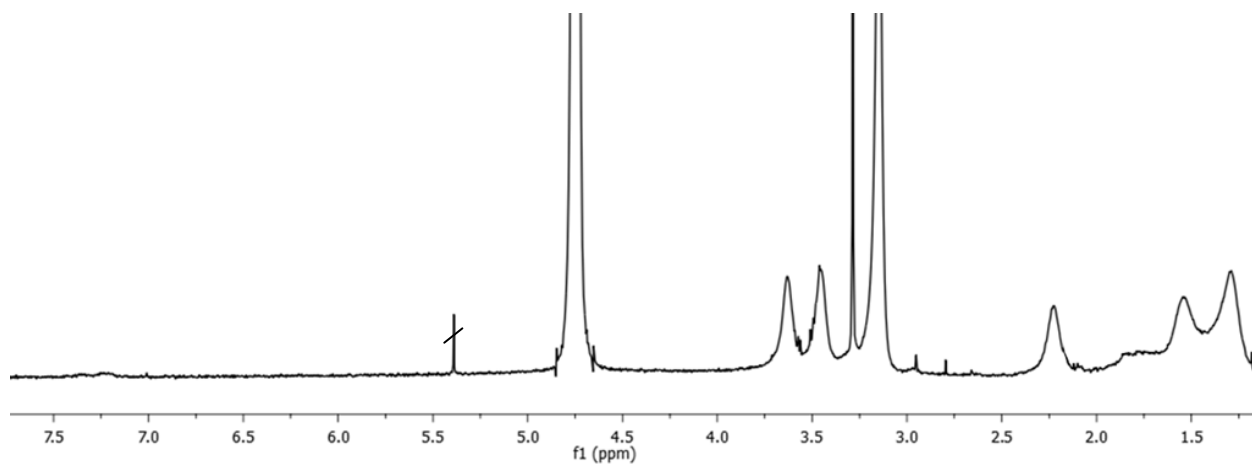
7. Appendix



Figure 7.3 $^1\text{H-NMR}$ spectrum of **NP Q** in D_2O Figure 7.4 $^1\text{H-NMR}$ Spectrum of **NP QP** in D_2O



Figure 7.7 $^1\text{H-NMR}$ Spectrum of **NP QCL** in D_2O Figure 7.8 $^1\text{H-NMR}$ Spectrum of **NP QPCl** in D_2O

Figure 7.9 1H -NMR Spectrum of $NP C_L$ in D_2O Figure 7.10 1H -NMR Spectrum of $NP QPC_{S-a}$ in D_2O

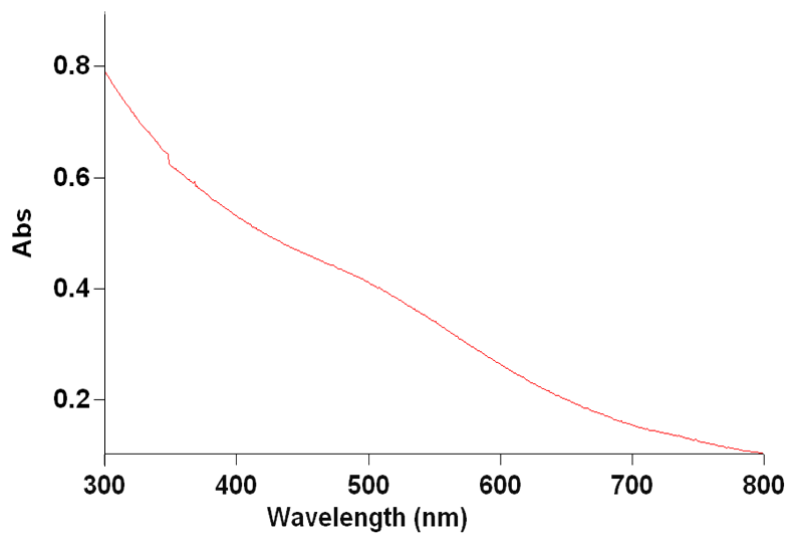


Figure 7.11 UV-Vis spectrum of **NP QC₅** in H₂O

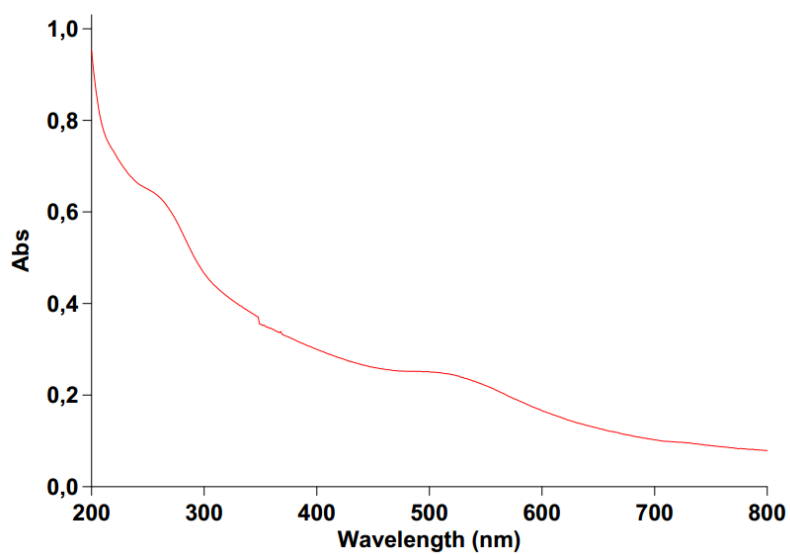
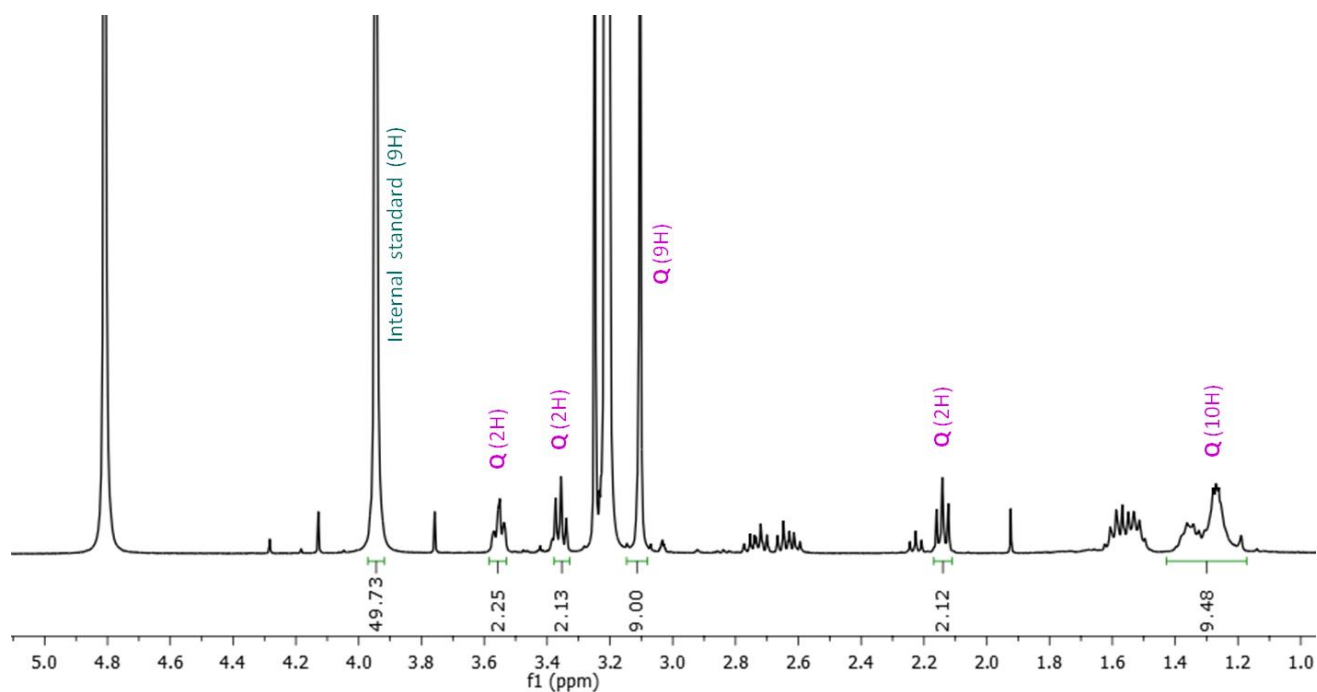
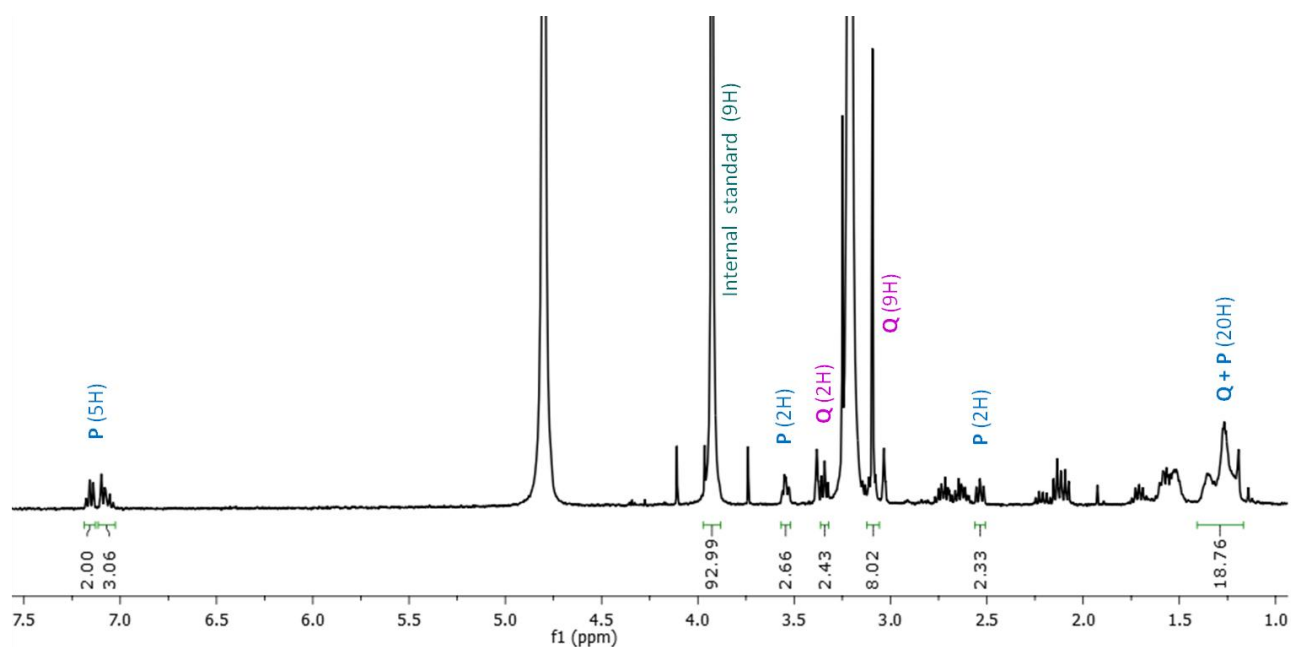
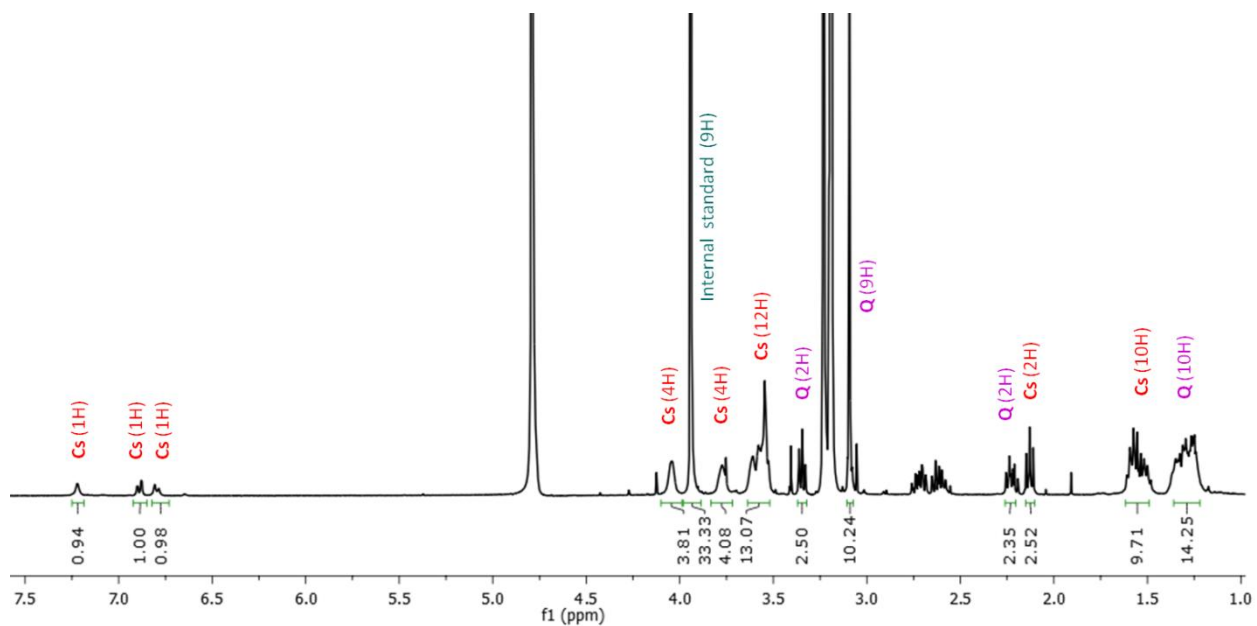
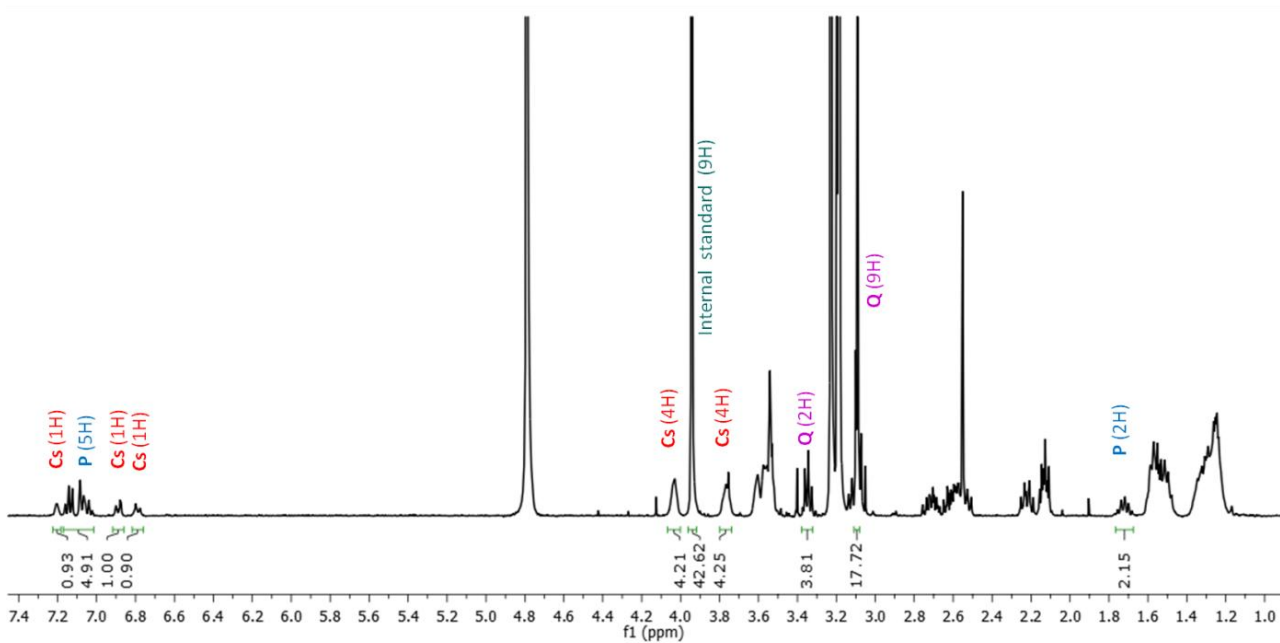
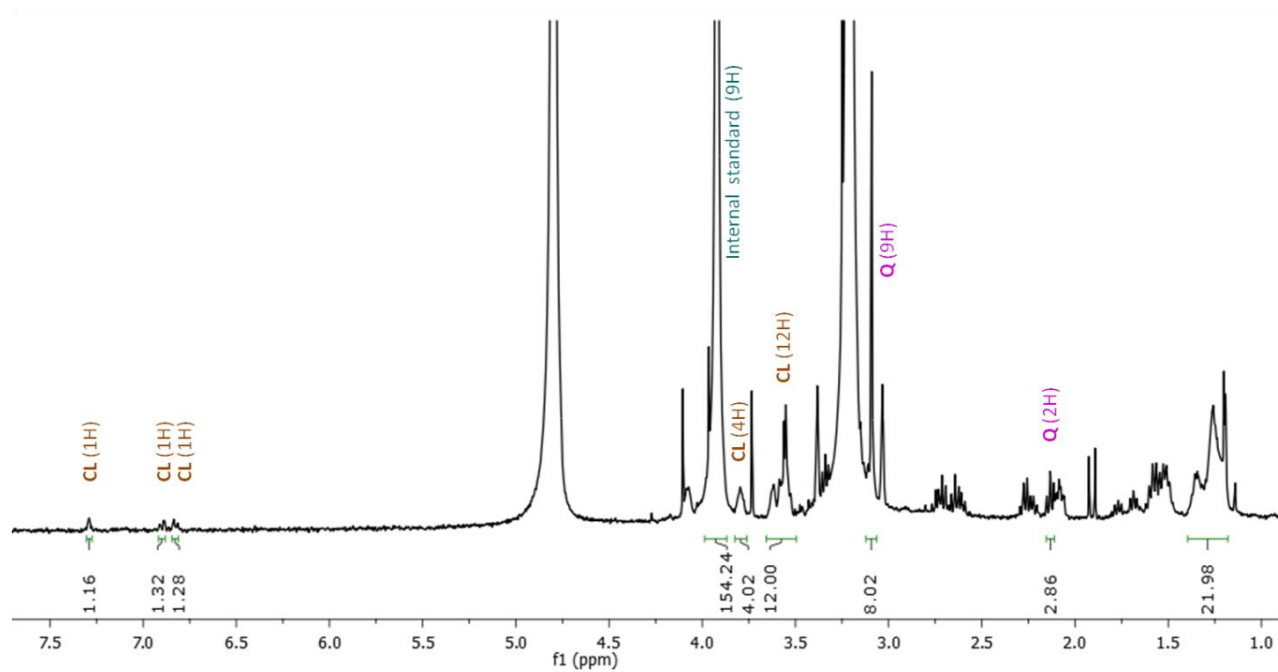
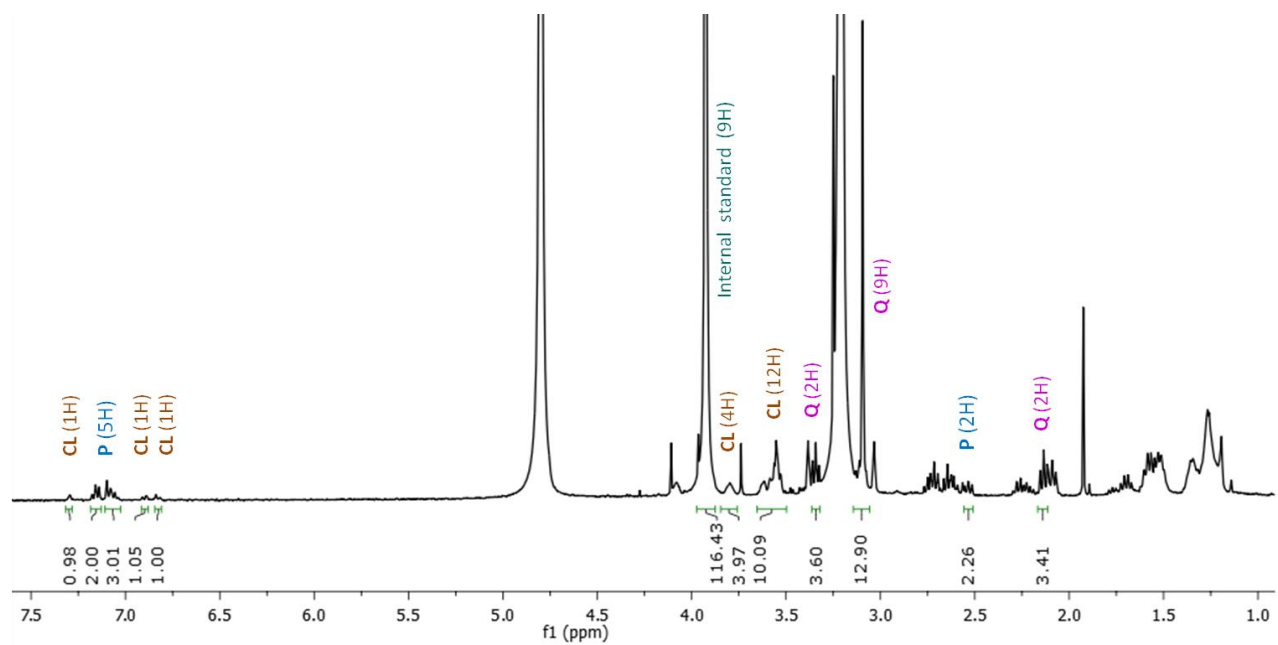
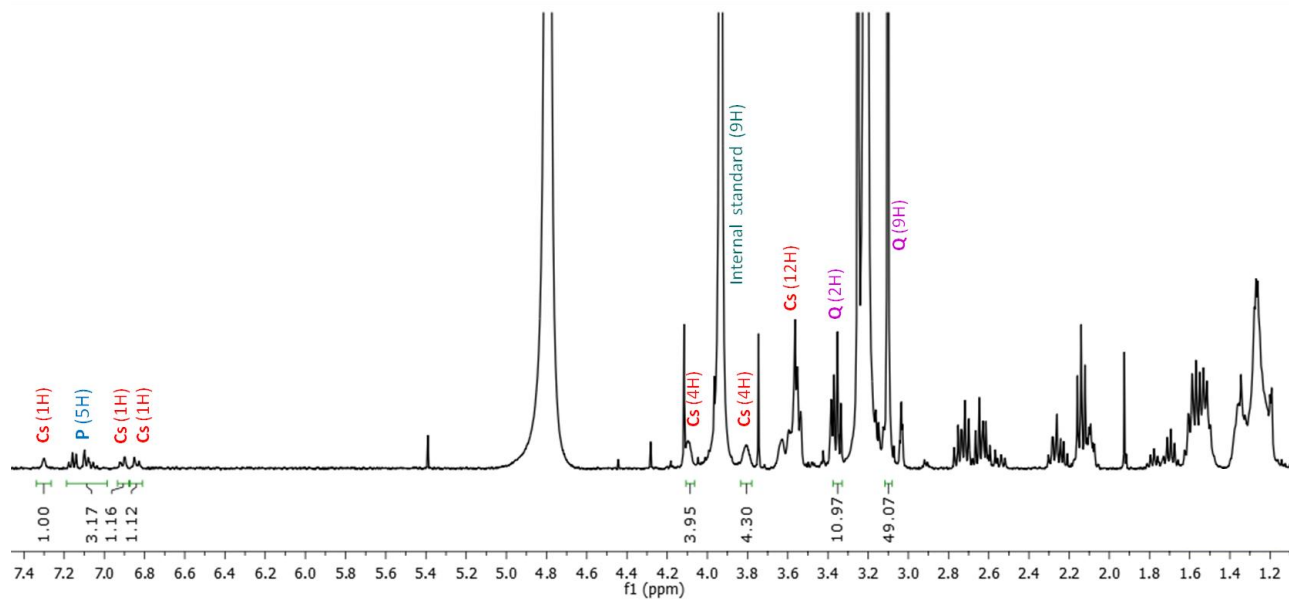


Figure 7.12 The UV-Vis spectrum of **NP C_L** in H₂O

7.1 $^1\text{H-NMR}$ Spectra of Nanoparticle Solutions After Iodine DecompositionFigure 7.13 $^1\text{H-NMR}$ Spectrum of **NP Q** in MeODFigure 7.14 $^1\text{H-NMR}$ Spectrum of **NP QP** in MeOD

Figure 7.15 ¹H-NMR Spectrum of *NP QC*₅ in MeODFigure 7.16 ¹H-NMR Spectrum of *NP QPC*₅ in MeOD

Figure 7.17 ¹H-NMR Spectrum of **NP QCL** in MeODFigure 7.18 ¹H-NMR Spectrum of **NP QPCl** in MeOD

Figure 7.19 $^1\text{H-NMR}$ Spectrum of NP QPC_{S-a} in MeOD

7.2 Results of the Iodine Decomposition Experiments

| NPQ | | | |
|-----------------------------------|----------|---------------------|------|
| amount of nanoparticle | 0,80 | mg | |
| molar amount of internal standard | 3,74E-06 | mol | |
| ∫ internal standard (9H) | 5,68 | per H | |
| ∫ Q | 1,05 | per H | |
| ∫ P | 0,00 | per H | |
| ∫ Cs | 0,00 | per H | |
| Molar amount Q | 6,89E-07 | mol | |
| Molar amount P | 0 | mol | |
| Molar amount Cs | 0 | mol | |
| total molar amount of ligands | 6,89E-07 | mol | |
| Mw Au | 196,96 | g mol ⁻¹ | |
| Mw Q | 295,89 | g mol ⁻¹ | 100% |
| Mw P | 292,46 | g mol ⁻¹ | 0% |
| Mw Cs | 484,63 | g mol ⁻¹ | 0% |
| amount Q | 0,20 | mg | |
| amount P | 0 | mg | |
| amount Cs | 0 | mg | |
| amount Au | 0,60 | mg | |
| # Au/# Lig | 4,40 | | |
| total molar amount of ligands | 8,61E-07 | mol/mg NP | |

| NPQ | | |
|-------------------------------|--------|--------------------------|
| NP radius | 0,95 | nm |
| NP diameter | 1,90 | nm |
| # Au atoms in nanoparticle | 211 | |
| # surface Au atoms | 122 | |
| # ligands on surface | 53 | |
| coverage (# Lig/# surface Au) | 43,3% | |
| Mw Au | 196,96 | g mol ⁻¹ |
| Mw Q | 295,89 | g mol ⁻¹ 100% |
| Mw P | 292,46 | g mol ⁻¹ 0% |
| Mw Cs | 484,63 | g mol ⁻¹ 0% |
| # Au/# Lig | 4,40 | |
| # ligands on surface | 48 | |
| coverage (# Lig/# surface Au) | 39,3% | |

Figure 7.20 Iodine decomposition of **NP Q** and gold/ligand ratio calculation

| NPQP | | |
|-----------------------------------|----------|-------------------------|
| amount of nanoparticle | 0,90 | mg |
| molar amount of internal standard | 3,74E-06 | mol |
| ∫ internal standard (9H) | 10,33 | per H |
| ∫ Q | 0,95 | per H |
| ∫ P | 1,06 | per H |
| ∫ Cs | 0,00 | per H |
| Molar amount Q | 3,44E-07 | mol |
| Molar amount P | 3,82E-07 | mol |
| Molar amount Cs | 0 | mol |
| total molar amount of ligands | 7,26E-07 | mol |
| Mw Au | 196,96 | g mol ⁻¹ |
| Mw Q | 295,89 | g mol ⁻¹ 47% |
| Mw P | 292,46 | g mol ⁻¹ 53% |
| Mw Cs | 484,63 | g mol ⁻¹ 0% |
| amount Q | 0,10 | mg |
| amount P | 0,11 | mg |
| amount Cs | 0 | mg |
| amount Au | 0,69 | mg |
| # Au/# Lig | 4,80 | |
| total molar amount of ligands | 8,07E-07 | mol/mg NP |

| NPQP | |
|-------------------------------|--------------------------------|
| NP radius | 1,30 nm |
| NP diameter | 2,60 nm |
| # Au atoms in nanoparticle | 541 |
| # surface Au atoms | 246 |
| # ligands on surface | 99 |
| coverage (# Lig/# surface Au) | 40,3% |
| Mw Au | 196,96 g mol ⁻¹ |
| Mw Q | 295,89 g mol ⁻¹ 47% |
| Mw P | 292,46 g mol ⁻¹ 53% |
| Mw Cs | 484,63 g mol ⁻¹ 0% |
| # Au/# Lig | 4,80 |
| # ligands on surface | 113 |
| coverage (# Lig/# surface Au) | 45,8% |

Figure 7.21 Iodine decomposition of **NPQP** and gold/ligand ratio calculation

| NPQCs | | |
|-----------------------------------|----------|-------------------------|
| amount of nanoparticle | 1,50 | mg |
| molar amount of internal standard | 1,87E-06 | mol |
| f internal standard (9H) | 3,77 | per H |
| f Q | 1,17 | per H |
| f P | 0,00 | per H |
| f Cs | 1,05 | per H |
| Molar amount Q | 5,82E-07 | mol |
| Molar amount P | 0 | mol |
| Molar amount Cs | 5,20E-07 | mol |
| total molar amount of ligands | 1,10E-06 | mol |
| Mw Au | 196,96 | g mol ⁻¹ |
| Mw Q | 295,89 | g mol ⁻¹ 53% |
| Mw P | 292,46 | g mol ⁻¹ 0% |
| Mw Cs | 484,63 | g mol ⁻¹ 47% |
| amount Q | 0,17 | mg |
| amount P | 0 | mg |
| amount Cs | 0,25 | mg |
| amount Au | 1,08 | mg |
| # Au/# Lig | 4,96 | |
| total molar amount of ligands | 7,35E-07 | mol/mg NP |

| NPQCs | | |
|-------------------------------|--------|-------------------------|
| NP radius | 1,25 | nm |
| NP diameter | 2,50 | nm |
| # Au atoms in nanoparticle | 481 | |
| # surface Au atoms | 226 | |
| # ligands on surface | 92 | |
| coverage (# Lig/# surface Au) | 40,6% | |
| Mw Au | 196,96 | g mol ⁻¹ |
| Mw Q | 295,89 | g mol ⁻¹ 53% |
| Mw P | 292,46 | g mol ⁻¹ 0% |
| Mw Cs | 484,63 | g mol ⁻¹ 47% |
| # Au/# Lig | 4,96 | |
| # ligands on surface | 97 | |
| coverage (# Lig/# surface Au) | 43,0% | |

Figure 7.22 Iodine decomposition of **NP QCs** and gold/ligand ratio calculation

| NPQPCs | | |
|-----------------------------------|----------|-------------------------|
| amount of nanoparticle | 2,20 | mg |
| molar amount of internal standard | 1,87E-06 | mol |
| f internal standard (9H) | 3,99 | per H |
| f Q | 1,88 | per H |
| f P | 1,01 | per H |
| f Cs | 1,06 | per H |
| Molar amount Q | 8,83E-07 | mol |
| Molar amount P | 4,72E-07 | mol |
| Molar amount Cs | 4,97E-07 | mol |
| total molar amount of ligands | 1,85E-06 | mol |
| Mw Au | 196,96 | g mol ⁻¹ |
| Mw Q | 295,89 | g mol ⁻¹ 48% |
| Mw P | 292,46 | g mol ⁻¹ 25% |
| Mw Cs | 484,63 | g mol ⁻¹ 27% |
| amount Q | 0,26 | mg |
| amount P | 0,14 | mg |
| amount Cs | 0,24 | mg |
| amount Au | 1,56 | mg |
| # Au/# Lig | 4,27 | |
| total molar amount of ligands | 8,42E-07 | mol/mg NP |

| NPQPCs | |
|-------------------------------|--------------------------------|
| NP radius | 0,95 nm |
| NP diameter | 1,90 nm |
| # Au atoms in nanoparticle | 211 |
| # surface Au atoms | 122 |
| # ligands on surface | 53 |
| coverage (# Lig/# surface Au) | 43,3% |
| Mw Au | 196,96 g mol ⁻¹ |
| Mw Q | 295,89 g mol ⁻¹ 48% |
| Mw P | 292,46 g mol ⁻¹ 25% |
| Mw Cs | 484,63 g mol ⁻¹ 27% |
| # Au/# Lig | 4,27 |
| # ligands on surface | 49 |
| coverage (# Lig/# surface Au) | 40,4% |

Figure 7.23 Iodine decomposition of *NP QPC_S* and gold/ligand ratio calculation

| NPQCL | | |
|-----------------------------------|----------------------------|-----|
| amount of nanoparticle | 0,55 mg | |
| molar amount of internal standard | 3,74E-06 mol | |
| f internal standard (9H) | 17,14 per H | |
| f Q | 0,99 per H | |
| f P | 0,00 per H | |
| f Cs | 1,00 per H | |
| Molar amount Q | 2,15E-07 mol | |
| Molar amount P | 0 mol | |
| Molar amount Cs | 2,19E-07 mol | |
| total molar amount of ligands | 4,34E-07 mol | |
| Mw Au | 196,96 g mol ⁻¹ | |
| Mw Q | 295,89 g mol ⁻¹ | 50% |
| Mw P | 292,46 g mol ⁻¹ | 0% |
| Mw CL | 569,7 g mol ⁻¹ | 50% |
| amount Q | 0,06 mg | |
| amount P | 0 mg | |
| amount CL | 0,12 mg | |
| amount Au | 0,36 mg | |
| # Au/# Lig | 4,22 | |
| total molar amount of ligands | 7,90E-07 mol/mg NP | |

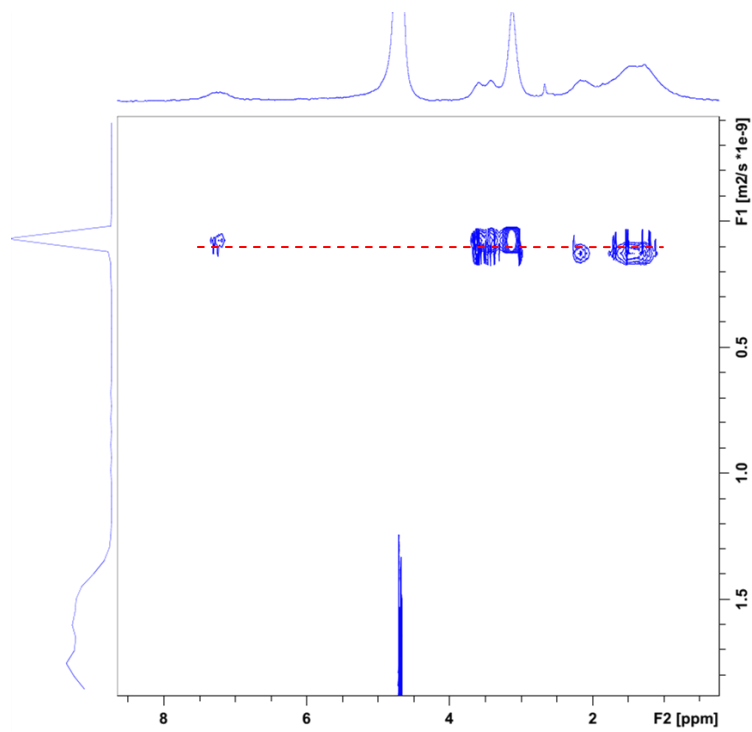
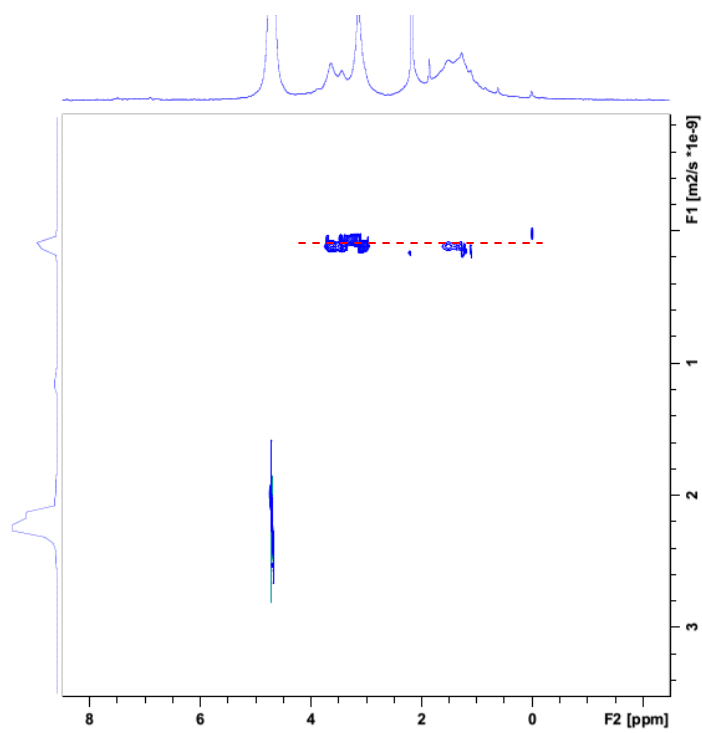
| NPQCL | | |
|-------------------------------|--------|-------------------------|
| NP radius | 0,98 | nm |
| NP diameter | 1,96 | nm |
| # Au atoms in nanoparticle | 232 | |
| # surface Au atoms | 131 | |
| # ligands on surface | 56 | |
| coverage (# Lig/# surface Au) | 43,0% | |
| Mw Au | 196,96 | g mol ⁻¹ |
| Mw Q | 295,89 | g mol ⁻¹ 50% |
| Mw P | 292,46 | g mol ⁻¹ 0% |
| Mw CL | 569,73 | g mol ⁻¹ 50% |
| # Au/# Lig | 4,11 | |
| # ligands on surface | 56 | |
| coverage (# Lig/# surface Au) | 43,0% | |

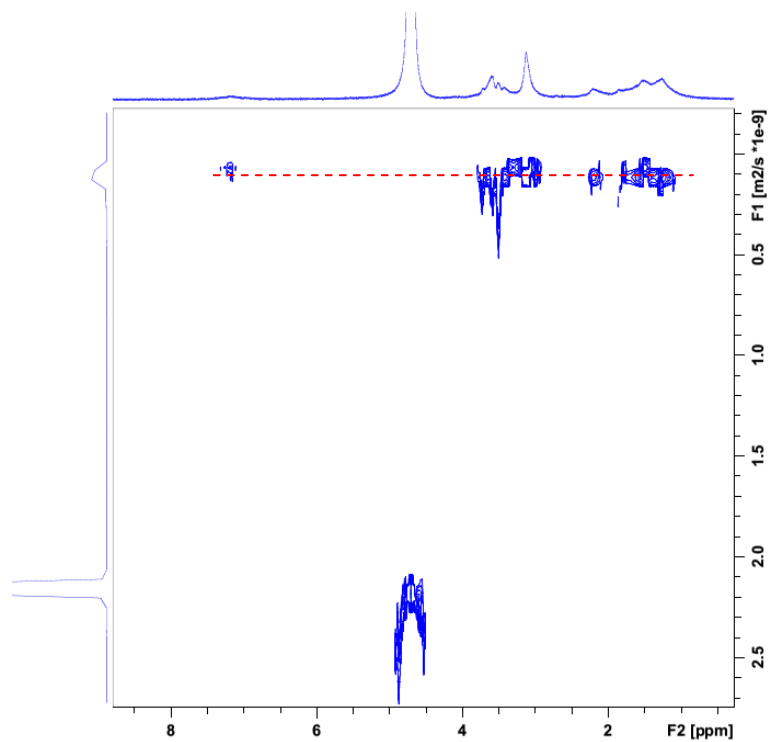
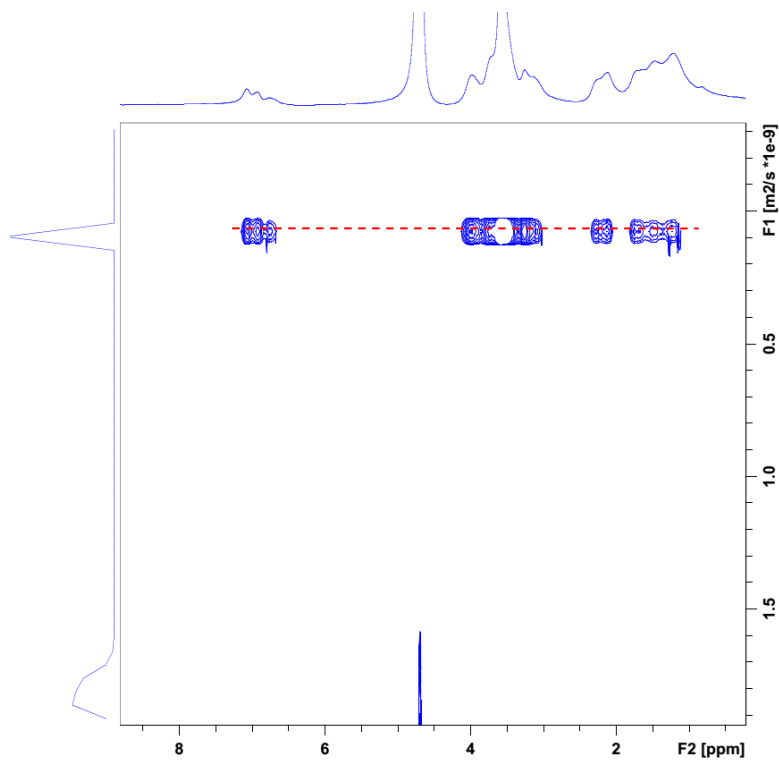
Figure 7.24 Iodine decomposition of **NP QCL** and gold/ligand ratio calculation

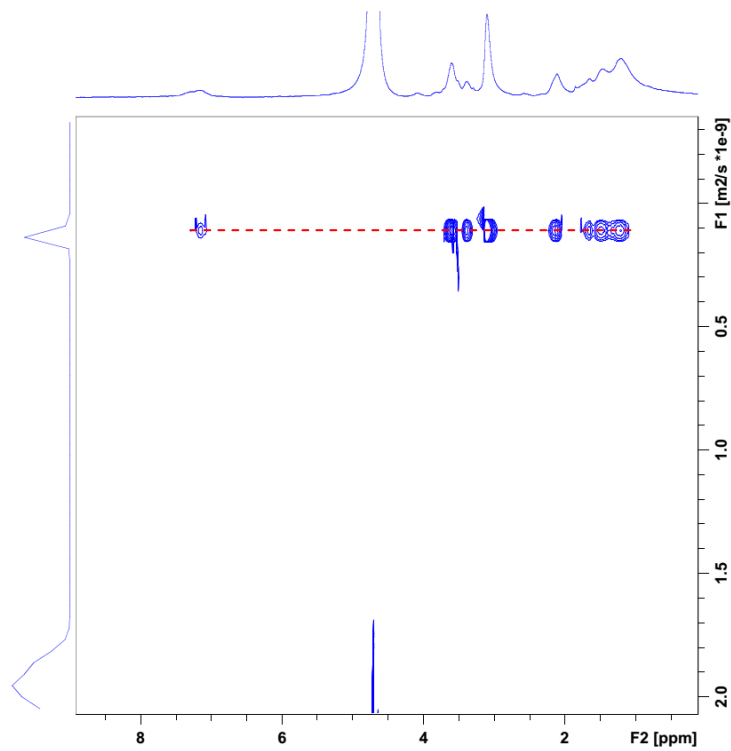
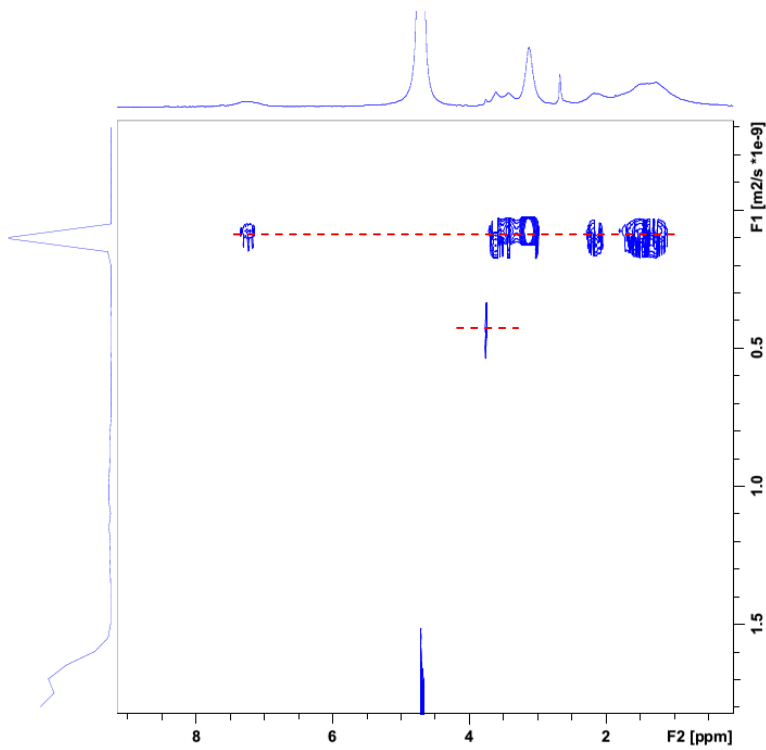
| NPQPCL | | |
|-----------------------------------|----------|-------------------------|
| amount of nanoparticle | 1,25 | mg |
| molar amount of internal standard | 3,74E-06 | mol |
| ∫ internal standard (9H) | 12,94 | per H |
| ∫ Q | 1,42 | per H |
| ∫ P | 1,04 | per H |
| ∫ Cs | 1,00 | per H |
| Molar amount Q | 4,09E-07 | mol |
| Molar amount P | 3,00E-07 | mol |
| Molar amount Cs | 2,89E-07 | mol |
| total molar amount of ligands | 9,99E-07 | mol |
| Mw Au | 196,96 | g mol ⁻¹ |
| Mw Q | 295,89 | g mol ⁻¹ 41% |
| Mw P | 292,46 | g mol ⁻¹ 30% |
| Mw CL | 569,73 | g mol ⁻¹ 29% |
| amount Q | 0,12 | mg |
| amount P | 0,09 | mg |
| amount CL | 0,16 | mg |
| amount Au | 0,88 | mg |
| # Au/# Lig | 4,46 | |
| total molar amount of ligands | 7,99E-07 | mol/mg NP |

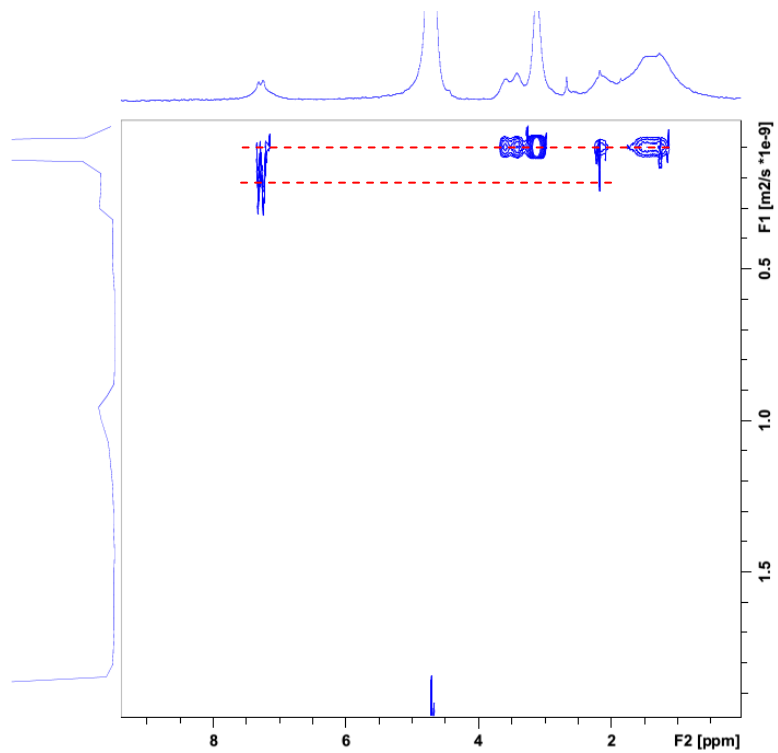
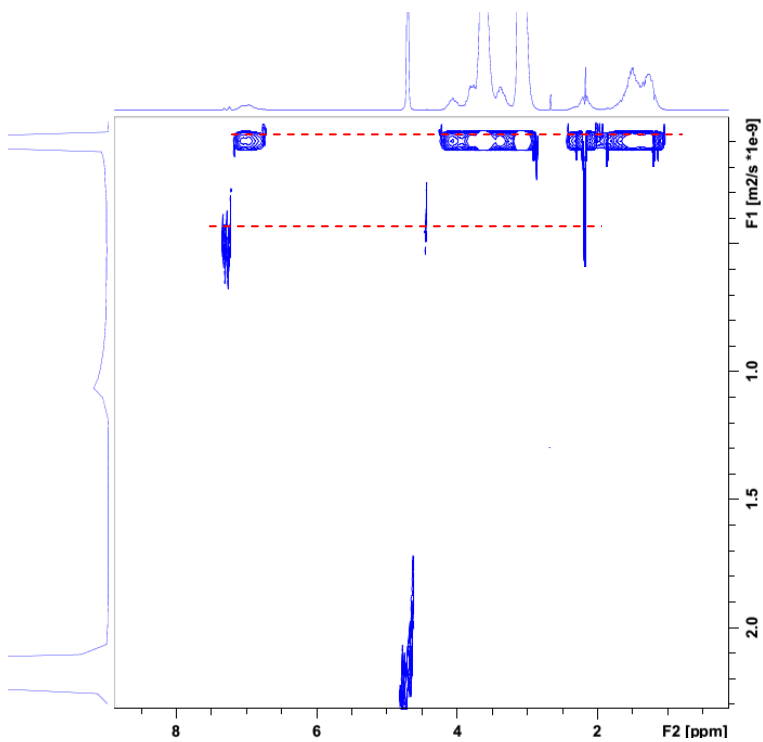
| NPQPCL | | |
|-------------------------------|--------|-------------------------|
| NP radius | 0,99 | nm |
| NP diameter | 1,98 | nm |
| # Au atoms in nanoparticle | 239 | |
| # surface Au atoms | 134 | |
| # ligands on surface | 58 | |
| coverage (# Lig/# surface Au) | 42,9% | |
| Mw Au | 196,96 | g mol ⁻¹ |
| Mw Q | 295,89 | g mol ⁻¹ 41% |
| Mw P | 292,46 | g mol ⁻¹ 30% |
| Mw CL | 569,73 | g mol ⁻¹ 29% |
| # Au/# Lig | 4,35 | |
| # ligands on surface | 55 | |
| coverage (# Lig/# surface Au) | 40,9% | |

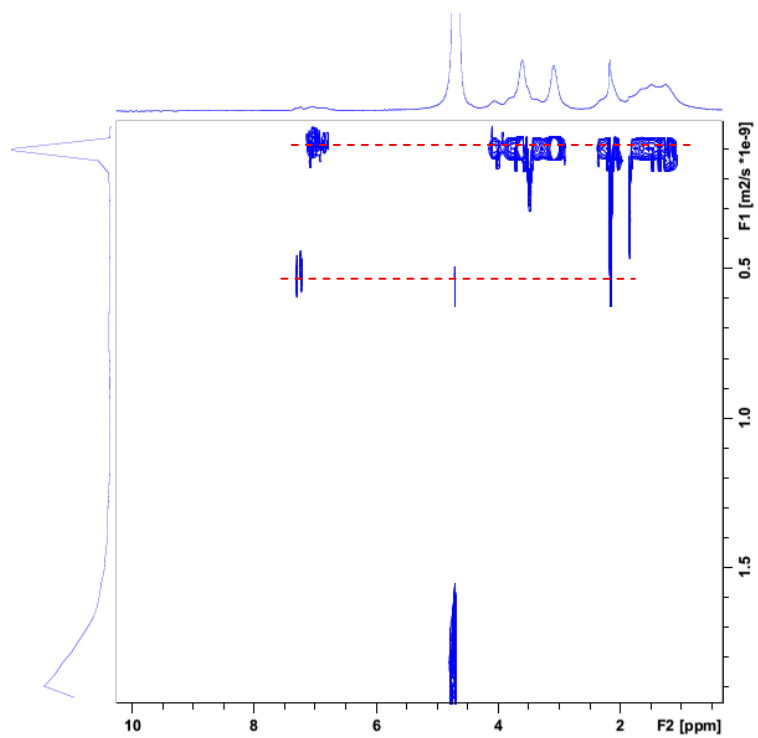
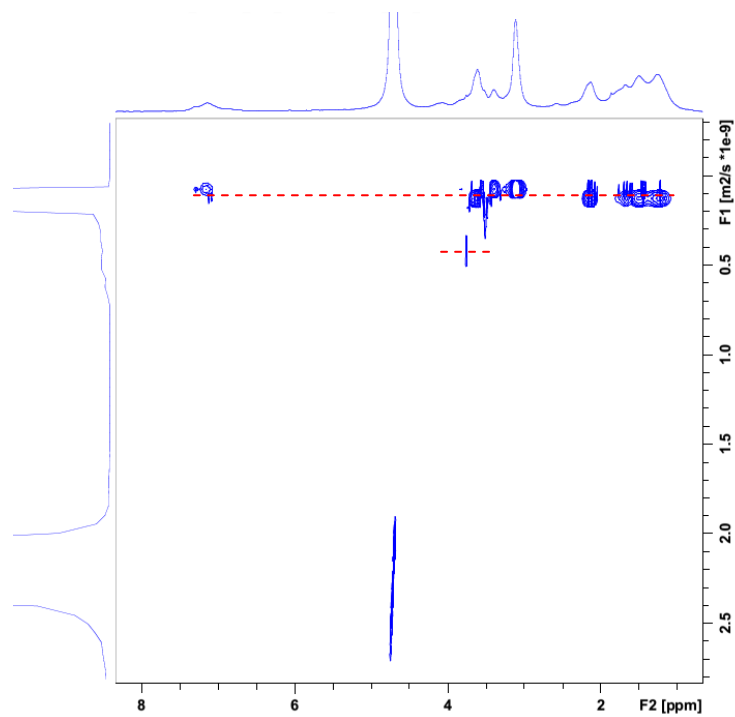
Figure 7.25 Iodine decomposition of *NP QPC_L* and gold/ligand ratio calculation

Figure 7.26 2D DOSY-NMR map of **NP QP**Figure 7.27 2D DOSY-NMR map of **NP QC₅**

Figure 7.28 2D DOSY-NMR map of *NP QPC₅*Figure 7.29 2D DOSY-NMR map of *NP QCL*

Figure 7.30 2D DOSY-NMR map of **NP QPC_L**Figure 7.31 2D DOSY-NMR map of **NP QP** and Gly-Gly mixture

Figure 7.32 2D DOSY-NMR map of **NP QP** and Gly-Phe mixtureFigure 7.33 2D DOSY-NMR map of **NP QPC₅** and Gly-Phe mixture

Figure 7.34 2D DOSY-NMR map of **NP QC_L** and Gly-Phe mixtureFigure 7.35 2D DOSY-NMR map of **NP QPC_L** and Gly-Gly mixture

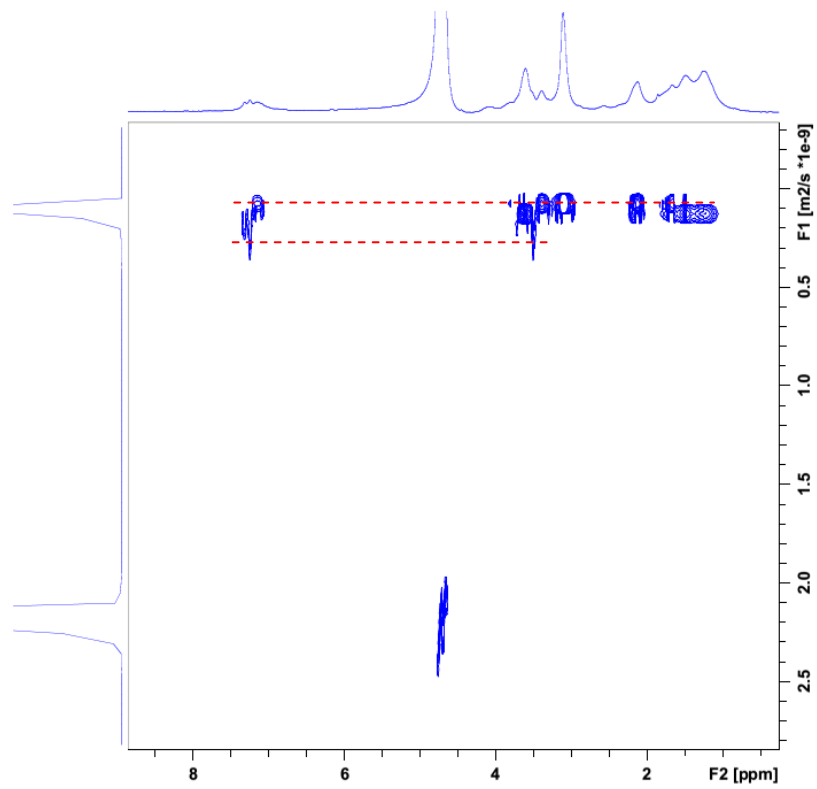
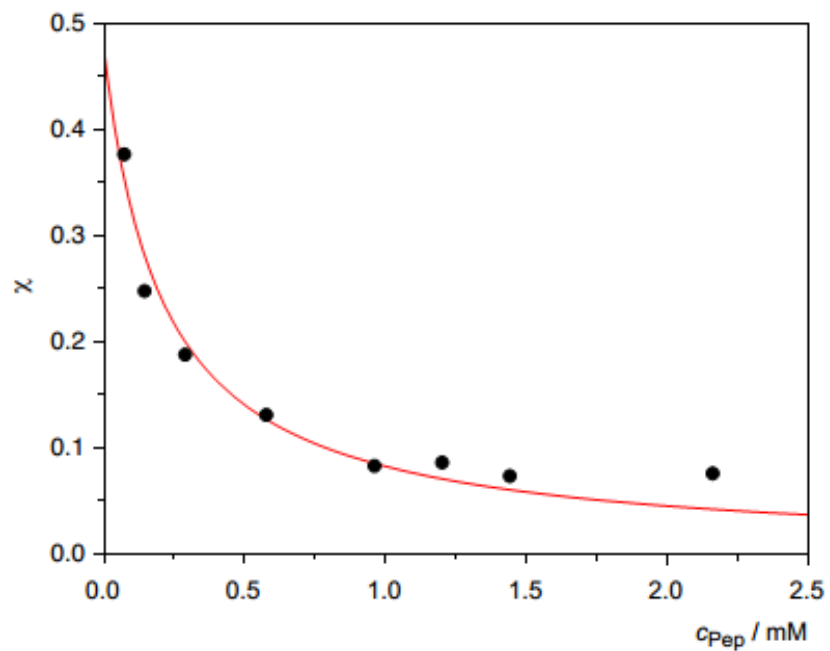
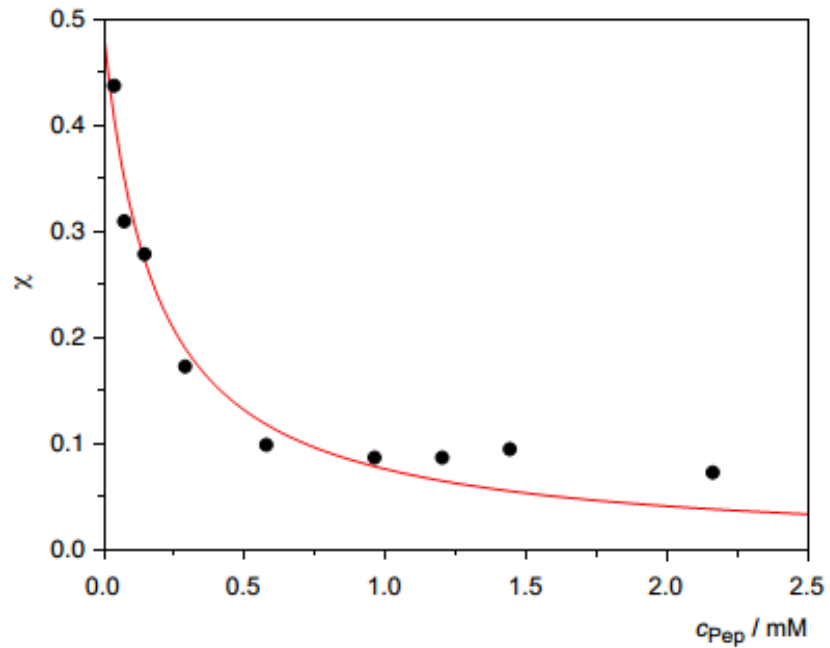


Figure 7.36 2D DOSY-NMR map of **NP QPC_L** and Gly-Phe mixture

Figure 7.37 Langmuir isotherm of the titration of Gly-Phe with **NP Q**Figure 7.36 Langmuir isotherm of the titration of Gly-Phe with **NP QC₅**

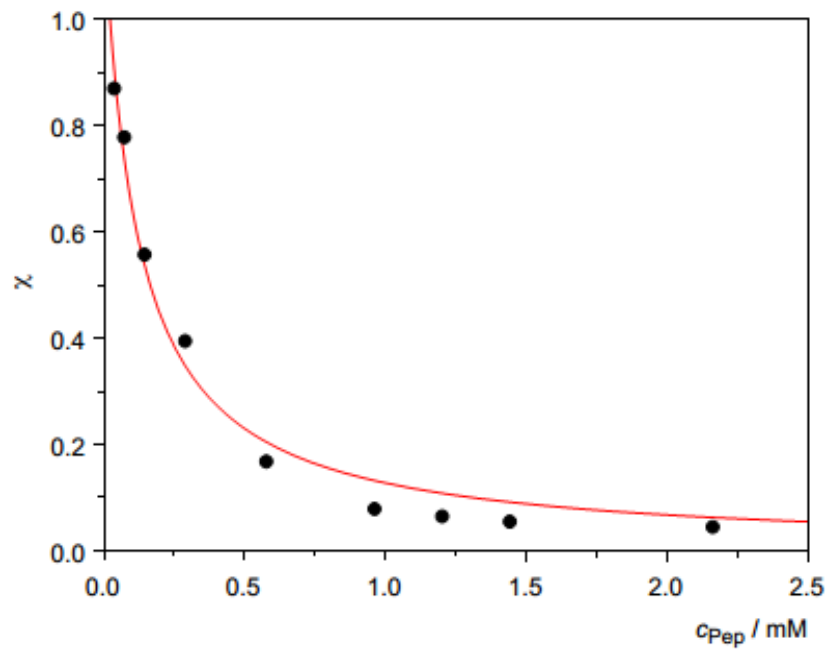


Figure 7.37 Langmuir isotherm of the titration of Gly-Phe with **NP QPC₅**

Curriculum Vitae

Serap Yapar

EDUCATION

- 09.2011-08.2016 Ph.D. in Chemistry, Organic Chemistry Department, TU Kaiserslautern, Germany
"Novel Water Soluble Gold Nanoparticles for Peptide Recognition"
- 09.2011-09.2014 Early-Stage Researcher (ESR) in DYNAMOL- Marie Curie Initial Training Network
- 08.2008-07.2010 MSc. in Chemistry, Bogazici University, Istanbul, Turkey
"Synthesis and Microcontact Molding of Functionalizable Hydrogels"
- 09.2004-08.2008 BS. in Chemistry, Bogazici University, Istanbul, Turkey
- 09.2003-06.2004 Bogazici University School of Foreign Languages, English Proficiency for Undergraduate Programs, Istanbul, Turkey
- 09.2000-06.2003 Ibrahim Hakki Science High School, Erzurum, Turkey

LIST OF PUBLICATIONS

- S. Kaga, S. Yapar, E. M. Gecici, R. Sanyal, "Photo-Patternable 'Clickable' Hydrogels: 'Orthogonal' Control over Fabrication and Functionalization" *Macromolecules*, 2015, 48 (15), 5106-5115.
- S. Yapar, M. Oikonomou, A. Velders, S. Kubik, "Dipeptide Recognition in Water Mediated by Mixed Monolayer Protected Gold Nanoparticles", *Chemical Communucations*, 2015, 51, 14247-14250.